

IN-SITU DEFECT DETECTION USING ACOUSTIC VIBRATION MONITORING
FOR ADDITIVE MANUFACTURING PROCESSES

A Thesis
presented to
the Faculty of California Polytechnic State University,
San Luis Obispo

In Partial Fulfillment
of the Requirements for the Degree
Master of Science in Industrial Engineering

by
Ali Harake
June 2022

© 2022

Ali Harake

ALL RIGHTS RESERVED

COMMITTEE MEMBERSHIP

TITLE: In-Situ Defect Detection using Acoustic Vibration
Monitoring for Additive Manufacturing Processes

AUTHOR: Ali Harake

DATE SUBMITTED: June 2022

COMMITTEE CHAIR: Xuan Wang, Ph.D.
Professor of Industrial and Manufacturing Engineering

COMMITTEE MEMBER: Tali Freed, Ph.D.
Professor of Industrial and Manufacturing Engineering,
Graduate Coordinator - IME

COMMITTEE MEMBER: Daniel Waldorf, Ph.D.
Professor of Industrial and Manufacturing Engineering,
Department Chair - IME

ABSTRACT

In-Situ Defect Detection using Acoustic Vibration Monitoring for Additive

Manufacturing Processes

Ali Harake

The world of additive manufacturing revolves around speed and repeatability. Inherently, the process of 3D printing is plagued with variability that fluctuates with every material and parameter modification. Without proper qualification standards, processes can never become stable enough to produce parts that may be used in aerospace, medical, and construction industries. These industries rely on high quality metrics in order to protect the lives of those who may benefit from them. To establish trust in a process, all points of variation must be controlled and accounted for every part produced. In instances where even the best process controls are enacted, there still may be situational unknowns that can cause detrimental defects, often on micron scales.

Through in-situ monitoring techniques, such as visual or acoustic monitoring, a secondary level of quality assessment can be performed. This type of real time monitoring solution can be used in a variety of ways to help reduce scrap rate, increase overall quality, and improve the mechanical characteristics of a newly developing material. In this proposal, a goal was set to develop a system that can be a low-cost alternative to a comparable acoustic monitoring system. This design is meant to be a low fidelity concept that can alert a user of any potential anomalies within a build by detecting spikes in acoustic emissions.

The overall success of this experiment is set on two conditions. First, the new low-cost system should be mountable on various types of machines. Second, this system should demonstrate some level of equivalency to a similar system. These two situations were successfully met as the system was able to provide indications of anomalies present within a build. The system was calibrated and tuned to be able to measure signals on a SLM 125 running 316L powder. Minor modifications to the code and system can make it adaptable to different types of equipment such as CNC's, bandsaws, casting processes, and other advanced manufacturing equipment. The model can be attenuated to support higher or lower frequencies as well as different types of acoustic sensors, which demonstrates the vast potential that this system can provide for detecting different types of defects.

Keywords: Additive manufacturing, In-situ monitoring, Acoustic vibration

ACKNOWLEDGMENTS

This adventure would not have been possible without the endless support and effort provided by my advisor Dr. Xuan Wang. I appreciate all the late nights and early mornings guiding me on not only my project, but the functionality of our additive machine. This project has been an extension of my learning and has continuously challenged me, all while reinforcing my strong appreciation for additive manufacturing, I would also like to thank my thesis committee consisting of Dr. Dan Waldorf and Dr. Tali Freed who both helped shape the essence of this project through their various classes and support. Finally, I'd like to thank my family, friends, and coworkers for their endless support and motivation.

TABLE OF CONTENTS

	Page
LIST OF TABLES	viii
LIST OF FIGURES	ix
CHAPTER	
1. Introduction.....	1
1.1 Problem Description.....	2
1.2 Background	3
1.2.1 Additive Manufacturing	3
1.2.2 Defects.....	4
1.2.3 Cal Poly SLM 125 Overview	7
1.3 Current State.....	9
1.4 Literature Review	11
1.5 Acoustic Sensors	17
1.6 Analysis Methodology	22
2. Experimental Setup and Design.....	23
2.1 Design and Build of Experimental Setup.....	23
2.1.1 Arduino Design and Layout	23
2.1.2 Raspberry Pi Build + Integration.....	25
2.1.3 Setup Onto SLM 125.....	26
2.2 Software Setup of Sensor	28
2.3 Cost Comparison of Systems	30
2.4 Test Coupon Design and Print Parameters.....	32

2.5 Original Testing Plan and Pivot	33
3. Coupon Builds and Data Collection Analysis	35
3.1 Build 1 and Build 2	35
3.2 Build 3	39
3.3 Build 4	44
3.4 Build 5	48
3.5 Build 6	58
4. Defect Detection Analysis	68
4.1 Calibration Builds	68
4.2 Acoustic Analysis.....	68
4.3 Image Analysis	71
4.4 Experimental Setup Evaluation.....	71
5. Conclusion	72
5.1 Analysis Summary	72
5.2 Future Recommendations.....	73
5.3 Conclusion.....	74
References.....	76
 APPENDICES	
A. Arduino Code	82
B. Full Size Images of Frequency Plots	84

LIST OF TABLES

Table	Page
1.1 Most common LPBF defects	5
1.2 Overview of in-situ process sensing approaches in PBF	7
2.1 Existing commercial AM in-situ monitoring systems	30
2.2 Cost Analysis for acoustic vibration setup.....	31
2.3 Chess print parameters used in printing coupons for the majority of this experiment.....	33

LIST OF FIGURES

Figure	Page
1.1 Simplified PBF printing process	4
1.2 Ishikawa process input/output diagram	5
1.3 SLM solutions 125 HL at Cal Poly	8
1.4 SLM 125 build chamber with build coordinate system and gas flow direction	9
1.5 SLM in-situ image analysis	10
1.6 Basic setup of acoustic monitoring on a LPBF machine	12
1.7 Diagram of in-situ monitoring using optical imagery for PBF Process.....	14
1.8 Point cloud data points example	16
1.9 Diagram showing how a diaphragm and backplate create a capacitor	18
1.10 Diagram showing the inner workings of a dynamic microphone	19
1.11 Inner workings of a piezoelectric sensor	20
1.12 Electret condenser microphone inner workings.....	21
1.13 Devmo LM393 electret sensor module.....	21
2.1 Fritzing diagram of Devmo sound sensor to Arduino connection.....	24
2.2 Arduino Mega 2560 signal converter connected to Devmo sound sensor.....	24
2.3 Arduino (Left), Devmo sound sensor (Middle), and Raspberry Pi (Right).....	25
2.4 Image showing mounting positions of sound sensor and Arduino	26
2.5 Image showing mounting location of Raspberry Pi (Top side of SLM 125).....	27
2.6 Monitor setup to visually analyze data and interface with Raspberry Pi.....	27
2.7 Snippet of Arduino code that converts the signal into an understandable frequency.....	28
2.8 Datalogger that pulls all information output from the Arduino's serial monitor in real time.....	29

2.9	Sensors/DAQ equipment purchased for a previous experiment to measure anomalies within the build chamber (Coria 2017).....	32
2.10	Modified DOE coupon, designed to fail at red outlined areas.....	34
3.1	Build 1 frequency vs. print time plot (11-03-2021).....	36
3.2	Build 2 frequency vs. print time plot (12-15-2021).....	36
3.3	Descriptive statistical analysis for homemade system using Minitab – Build 1....	37
3.4	Descriptive statistical analysis for homemade system using Minitab - Build 2	38
3.5	1 sample sign test using Minitab - Build 1	38
3.6	Completed Build 3 with parts on build plate (Welding coupons, rings, and benchys)	39
3.7	Build 3 frequency vs. print time lot (01-20-2022).....	40
3.8	Enhanced image of welding coupons, emphasizing the delamination between the part and support structures	40
3.9	Image of the first few layers of build 3 in which the support structures in front of the welding coupons were overexposed due to an issue in preprocessing	42
3.10	Build 3 frequency vs. print time zoomed in during 0-8 minutes (01-20-22).....	42
3.11	Descriptive statistical analysis for homemade system using Minitab - Build 3	43
3.12	1 sample sign test using Minitab - Build 3	43
3.13	Build 4 thin-walled pressure vessels test coupons.....	44
3.14	Zoomed in image on intersection between hex and main body showing discoloration and potential leak points	45
3.15	Build 4 frequency vs. print time plot (02-22-22).....	46
3.16	Build 4 frequency vs. print time zoomed in during 0-9 minutes (02-22-22).....	47
3.17	Build 4 frequency vs. print time zoomed in during 830-860 minutes (02-22-22)	47
3.18	Descriptive statistical analysis for homemade system using Minitab - Build 4	48

3.19	Build 5 tensile coupons printed at a 45° angle.....	49
3.20	Build 5 frequency vs. print time plot (02-24-22).....	50
3.21	Build 5 frequency vs. print time zoomed in during 0-27 minutes (02-24-22).....	51
3.22	Build 5, Layer 5 Initial exposure burn with limited powder on bed.....	51
3.23	Build 5, Layer 17 sharp protrusions present creating shadows behind them.....	52
3.24	Build 5, Layer 36 first signs of rake deterioration with streak appearing.....	52
3.25	Damaged rubber recoater blade indicated by the lines filled with powder.....	53
3.26	Build 5 frequency vs. print time zoomed in during 53-83 minutes (02-24-22).....	54
3.27	Build 5, Layer 131 multiple streaks present outlined in red showing locations that the recoated blade has been damaged	54
3.28	Build 5, Layer 153 distinct protrusions present near areas of streaking.....	55
3.29	Build 5 frequency vs. print time zoomed in during 1397-1430 minutes (02-24-22)	56
3.30	Build 5, Layer 2289 evident streaking and melted material protrusion from build plate.....	56
3.31	Side shot of Build 5 highlighting quality of build with minor discoloration at overhang.....	57
3.32	Descriptive statistical analysis for homemade system - Build 5 using Minitab	58
3.33	Kistler DAQ system (Left), Mounting location under build plate for accelerometers and sound monitor (Right).....	59
3.34	Build 6 benchys and rings comparison with Kistler System (3-14-22).....	60
3.35	Picture of overhang failure on non-supported roof.....	60
3.36	Build 6 frequency vs. print time plot (03-14-22).....	62
3.37	Build 6 sensitivity vs. print time plot (03-14-22)	62
3.38	Build 6, Layer 47 prominent streaking visible in the middle of build plate	63
3.39	Build 6, Layers 91 and 92 illustrating streaking in multiple areas of the build as well as material protrusions from the powder	63

3.40	Build 6. Layers 790 and 791 streaks are more uniform in size and spread out throughout the build, there appears to be more areas of material protrusion	64
3.41	Build 6, Layers 812-813 minor anomaly detected, these layers appear to be the lower end of the benchy roof	64
3.42	Descriptive statistical analysis for homemade system - Build 6 using Minitab	66
3.43	Descriptive statistical analysis for Kistler system - Build 6 using Minitab.....	66
3.44	Mann-Whitney nonparametric test - Build 6 using Minitab.....	67
4.1	Frequency response plot using Discrete Fourier Transform analysis.....	69

1. Introduction

Additive manufacturing (AM) is an ever-growing field with opportunities that reach beyond our known world. Materials have evolved to compete with current wrought products and the influence fueling this growth can be spread across most industries. 3D printing is much more than growing prototypes and tools; it has expanded to couple strength with unique and complex designs to create parts with optimal strength to weight ratios.

One of the most critical issues encountered in complex geometries and optimized parts is the potential for defects within the microstructure of the part. Defects are often discovered during post-inspection or during sudden failure of a part during operation. This is quite costly, not only from a monetary standpoint, but also from a time perspective. The opportunities to catch potential critical failure defects are crucial to the success of AM in future industries, such as mass transit, space exploration, and commercial aviation. Current defect detection protocol takes place post-print and requires trained eyes coupled with costly equipment. This process can be nearly eliminated with the introduction of an in-process monitoring solution that is able to parse and process the data to create a timeline of potential defect development. With further work, this technique can grow to encompass many different types of machines and materials. From previous students at Cal Poly, there are initial studies and data that will support my current project, where the main focus is on the collection and interpretation of the data as it comes out of the sensors through the utilization of a low-cost alternative to image processing.

1.1 Problem Description

In-situ defect detection is a challenging and costly process that can be unreliable without proper calibration and in-depth testing. As commercial manufacturing begins to adopt the productivity of AM, more complex and unique shapes will be desired and the need for automated monitoring will grow. The universal goal of any in-situ monitoring system is to create a fool-proof system that can accurately analyze and alert a user of potential defects present during part production. The goal of this thesis project is to achieve creating this fool-proof system within reasonable accuracy and cost. By utilizing pre-existing acoustic and accelerometer data present on Cal Poly's SLM 125, the aim is to develop a system that can correctly interpret the acoustic data emitted by the machine and interpret it into user friendly visual models.

With the massive amount of data that can be generated by these types of sensors, the main challenge is the accuracy of the visual models and their ability to aid the user in understanding the current conditions of the print. The obvious answer may be to use a powerful computer that has this capability, but the overall goal of the project is to be able to import the technology to any industry by ensuring utility by most types of available computer systems on/off network. Successful implementation of this technology requires a product that is low cost, easy to set up, and modular for different printer systems and materials.

1.2 Background

1.2.1 Additive Manufacturing

The world of AM has grown to encompass much more than the term “3D Printing” can even begin to describe. AM is the next revolutionary technology that will disrupt how we look upon construction, aerospace, medicine, and the future. As the technology has evolved, the complexity of parts has progressed exponentially. Components are increasingly becoming vital for critical infrastructure, such as HVAC, aerospace, and life systems.

To begin to fully appreciate what AM can accomplish, it is crucial to first understand the entire process behind producing a part. First, there will be need for a printed part, whether it is for efficiency’s sake or that specific part cannot be produced by any other means. The operator must start by producing a 3D part file utilizing a design software. The operator will then need to convert this file into a stereolithography file (STL). The STL file is composed of surface level triangles of chosen resolution, that can be imported and interpreted across most software packages. Once the STL file is created, the operator will need to import the file into the selected “slicing” software, which can be machine-specific. This software is now responsible for separating the file into many different layers as well as defining the parameters for the build, such as orientation, resolution, support, and power. Once the file is complete it can now be transferred over to the machine to begin printing. To maintain consistency, all the work covered in this thesis is focused on defining the process for a Powder Bed Fusion (PBF) machine, specifically in the metal printing genre. A PBF machine utilizes one or more energy sources to melt

metallic powder together to effectively grow parts. An example of the process can be seen in Figure 1.1 (TWI-Global 2022).

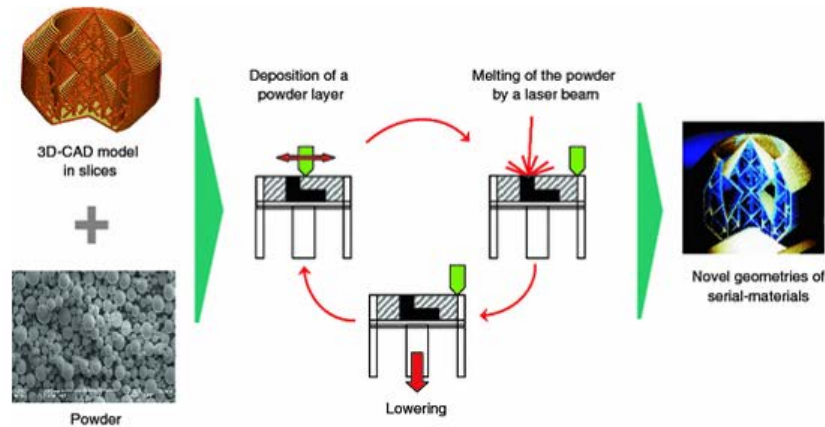
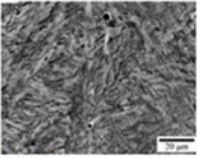
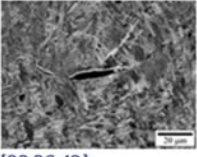
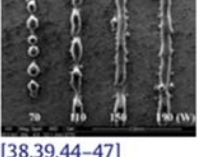
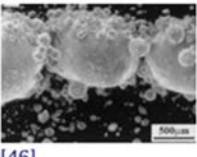
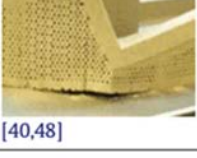


Figure 1.1: Simplified PBF printing process

1.2.2 Defects

One of the major issues in AM is the potential for defects to be present within a grown part. Defects can range in size from the micro to macro scale and are defined as an imperfection in the microstructure of a printed part. Most imperfections can be seen on the surface and are not usually the main concern; some of the important types of defects that can cause catastrophic failure include warpage, microcracking, voids, and layer delamination. With the slightest deviation from the ideal parameter for a given material, a defect is possible and depending on the severity of the deviation can greatly affect the type and size of the flaw. A good explanation of potential defects and their presumed causes can be seen in Table 1.1 and Figure 1.2 (Everton et al. 2016; Wang, 2019). By current inspection methods, defects are not detected until after a part has been completed and pulled from the build plate. This process can waste valuable time, money, and effort for a nonconforming part.

Table 1.1: Most common LPBF defects

Material discon.	Photo	Description
(Gas) pores	 [33,36]	Entrapped gas pores within the bulk of the material. Material dependent.
(Elongated) pores	 [33,36,43]	Lack of fusion pores in between layers of the AM process.
Balling	 [38,39,44-47]	Molten material is not a flat layer, but instead creates large spherically shaped particles on the surface.
Unfused powder	 [46]	The melt pool varies in size and unfused powder is present.
Cracking	 [40,48]	Cracks can be within the component or more commonly, a disconnection of the part from the baseplate is seen.

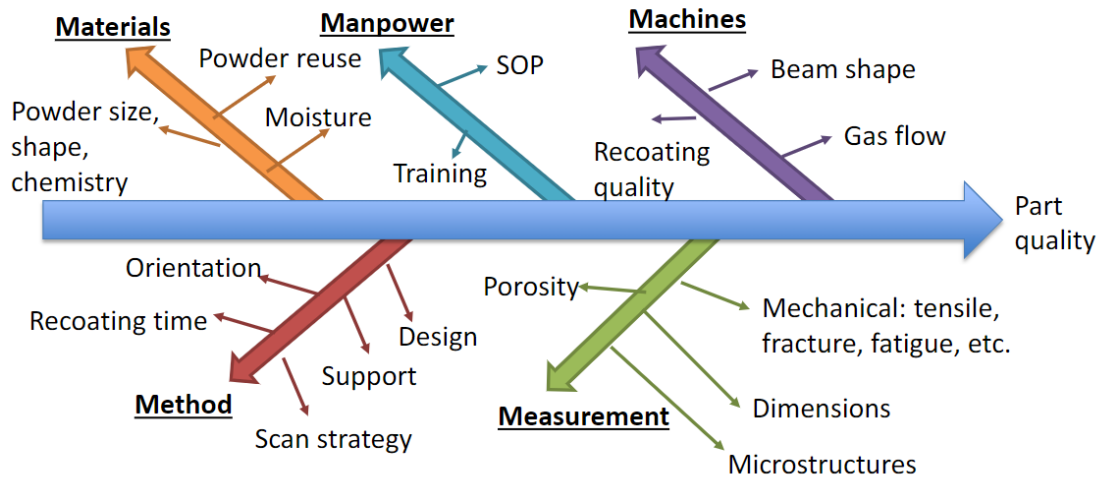


Figure 1.2: Ishikawa process input/output diagram

Cracks and warpage are two of the more visible defects that can be categorized in an AM part. Warpage can come about in a multitude of ways on a part or even on a build plate. Most often, warpage can happen between the interface of a part and the build plate. The edges of a part may appear to peel away from the plate as the part cools, ultimately causing damage to the recoater. Cracks can occur when a large area of a part is cooling. The shrinkage rate can become so great that the lower segments of the part may begin to shear. An overview of different in-situ process sensing approaches can be seen in Table 1.2 which also explains the different types of defects that can be detected (McCann et al., 2021). Ideally, there will be an audible ping when a part cracks that the sensor can pick up during the print. If a part warps and begins to collide with the recoater, a rhythmic ping should be heard when the recoater makes passes to spread powder. Unfortunately, these defects cannot be seen during most prints as the parts are submerged in powder. Since these issues happen while a part is cooling, the part is usually too deep in powder for traditional photo analysis software to pick up. The next best method is listening to the high frequency pings that these anomalies can create and trying to categorize those for different materials and machines.

Table 1.2: Overview of in-situ process sensing approaches in PBF

Principle	Coaxial	Recognisable type of defects	Vertical size [μm]	Horizontal size [μm]	Ref.	Notes
Ultrasonic Testing	–	Porosity	40	–	[27, 28]	Qualitative, but potential for calibration against known porosities.
Acoustic Emission Spectroscopy	–	Balling, Overheating, Porosity, Cracking	–	–	[29, 30]	More suited for qualitative process monitoring.
Optical Imaging	On/Off	Powder Bed Irregularities, Overheating	–	–	[31, 32]	Can be used for thermal measurements depending on detector.
Optical Emission Spectroscopy	On/Off	Overheating, Porosity	–	–	[33]	Commonly used in other advanced manufacturing techniques such as plasma deposition.
Optical Tomography		Balling, Surface Roughness, Dimensional Accuracy, Powder Bed Irregularities, Lack-of-fusion defects	–	–	[34, 35]	Suitable for sub-surface defect detection.
X-Ray Tomography		Porosity	–	–	[36, 37]	Less developed for in-situ AM applications than other tomographic methods.
Optical Coherence Tomography	On/Off	Porosity	20	50	[38]	Can examine powder bed, core part regions or bending defects on part. Limited to surface analysis.
Pyrometry	On/Off	Overheating	–	–	[39]	Suitable for single or multiple point measurements in the build area. Total scan area depending on optical setup.
Infrared Imaging	On/Off	Overheating	–	> 600 × 600	[40]	Can be scaled to entire build areas with reduction in spatial resolution.

1.2.3 Cal Poly SLM 125 Overview

At California Polytechnic State University – San Luis Obispo, or Cal Poly for short, the Industrial Engineering department operates and maintains a SLM Solutions 125 HL, shown in Figure 1.3. This machine was donated to Cal Poly by Lawrence Livermore National Lab in 2017 and its primary purpose is to aid research and senior projects. The SLM 125 features a 125mm x 125mm x 125mm build envelope, which is enclosed in an airtight, argon purged chamber during builds. As seen in Figure 1.4, the build chamber features a powder recoater in the +Y direction that recoats powder after each layer by moving in the -Y direction and then back to its home position (Swartz, 2019). The build plate moves down with each new layer to accommodate for the parts' growth while the argon continuously flows in a laminar fashion across the X axis throughout the build. The build plate can also be set to heat up to a max temperature of 200 °C by the operator depending on what is being printed. Through the SLM software all the print settings can be monitored and output through a .csv file. The printing media that is used is stainless

steel 316L powder from SLM solutions. It is loaded into a top hopper approximately 22kg at a time and is recycled through an in-house sieving unit. There is a laser unit that provides the heat source for melting the powder. This laser can reach a maximum power of 400 W. To create a perfect part, many parameters may need to be manipulated and set during each build. These parameters may include: laser power, layer height, build plate temp, scan speed, fill pattern, hatching distance, etc. Another important feature of this printer is the camera within the build chamber. This camera is normally used to analyze the powder coverage across the build plate by taking pictures after the recoater has moved and just before the laser begins to scan. These images are saved after each build and can be used for outside analysis such as defect or error analysis during a build.



Figure 1.3: SLM solutions 125 HL at Cal Poly

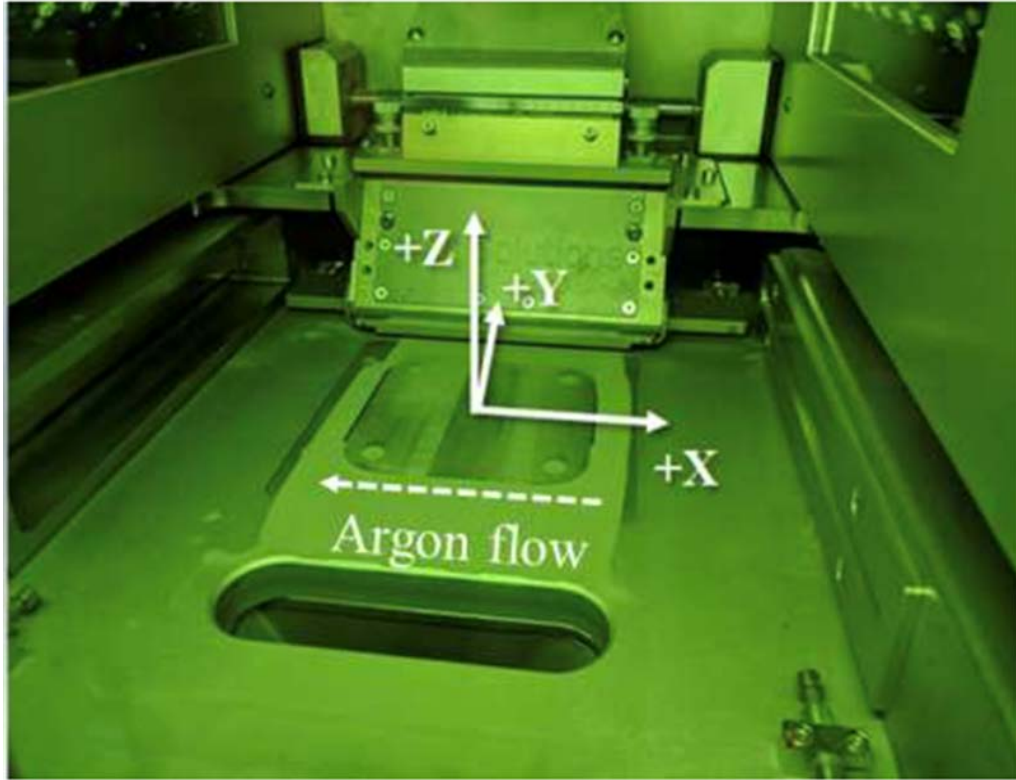


Figure 1.4: SLM 125 build chamber with build coordinate system and gas flow direction

1.3 Current State

The current state of in-situ defect detection is growing rapidly. In the past few years, OEM's have begun to implement and develop monitoring equipment that can be utilized inside of the build chamber of their machines. Most of the products that are offered today are based solely on the use of optical imagery analysis, which has its own unique benefits and challenges. Visual systems rely on expensive cameras and processors that can interpret large amounts of images quickly. The amount of data being stored can become an issue in terms of storage and analysis which also contributes to the overall cost of the system. However, visual systems do provide great illustrations of exactly what is happening during a build. These cameras can be optimized to pick up temperatures to map hot spots as well as track different trajectory of ejecta occurring during laser scans.

A few OEM manufacturers that currently produce in-situ monitoring type systems include: Concept Laser (QM), EOS (EOSTATE), Renishaw (InfiniAM), and SLM (Additive Quality). A sample GUI of SLM's version can be seen in Figure 1.5, which illustrates a user-friendly visual system that determines anomalies (EOS, 2021). These systems vary in effectiveness and cost; however, they are built to integrate with their respective OEM. There are obvious drawbacks to using a system tied exclusively to one machine OEM, with one being differing quality and data provided with each system. An alternative to using an OEM system is to integrate a machine agnostic system developed by outside companies. A few currently on the market that are advertised toward universal implementation include: PlasmO (Deepobserver), Open Additive (AMSense), and Sigma Labs (PrintRite3D). These systems are adaptable to different types of machine setups and processes while keeping a universal data processing algorithm. The benefits of this model can range from large cost savings to simplified systems that can work with a multitude of industries.

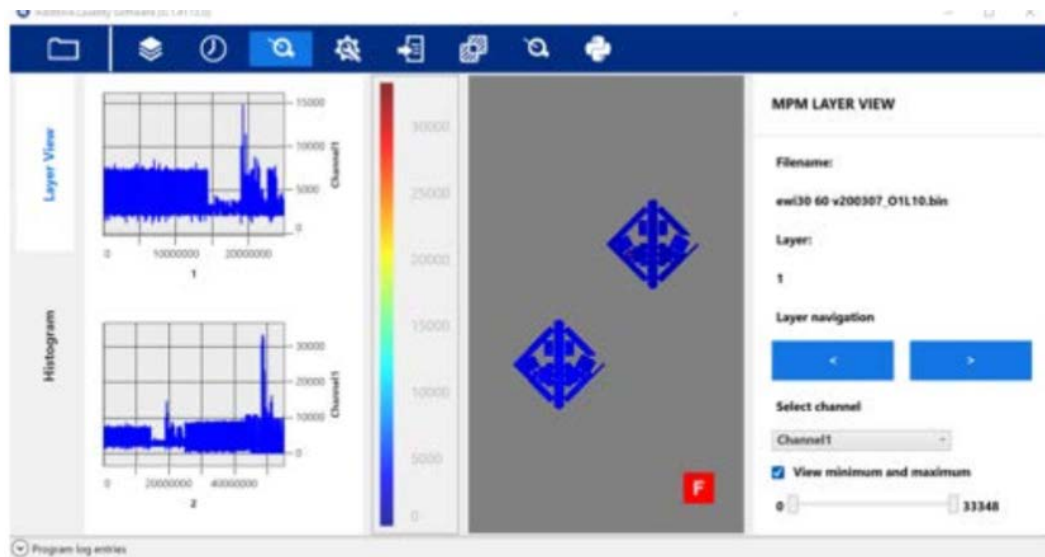


Figure 1.5: SLM in-situ image analysis

1.4 Literature Review

A comprehensive investigation was conducted on various similar topics within both industry and the academic realm. The papers that were examined pertain to systems that conduct acoustic, optical, and statistical analysis of additively manufactured parts and the defects generated during build.

The collection of data that currently takes place on the SLM 125 includes accelerometer and acoustic emission information. Acoustic emission (AE) is the radiation of acoustic waves in solids when a material undergoes irreversible changes in its structure. This phenomenon is quite unique, and the frequency of acoustic waves can be correlated to the type of material being used. This type of data collection can easily and quickly determine defects such as warpage, delamination, and cracking. Quantitative information about temporal-local behavior has been found to explain the signal from features in the surface, which shows that it is a good signal analysis technique (Sadowsky, 1994). However, the data can be quite noisy and require a large sample size coupled with automated data interpretation to develop usable models. In an article by Shevchik et al., acoustic signals were collected and separated into different groups that could be easily fed into a neural network for processing and training (Shevchik, 2018). The type of data that can be collected and processed using acoustic sensors is small, manageable, and easily scalable to improve resolution. There have been many innovations in applying active and/or passive AE sensors to monitor AM processes. Using convolutional neural networks to interpret the data which has led to patent applications for their future uses (Shevchik et. Al, 2019). The possibilities of utilizing AE

for data interpretation are only just beginning to be understood for use in AM processes. A simple setup of acoustic monitoring set up on LPBF machine can be seen in Figure 1.6 (Shevchik et al., 2019).

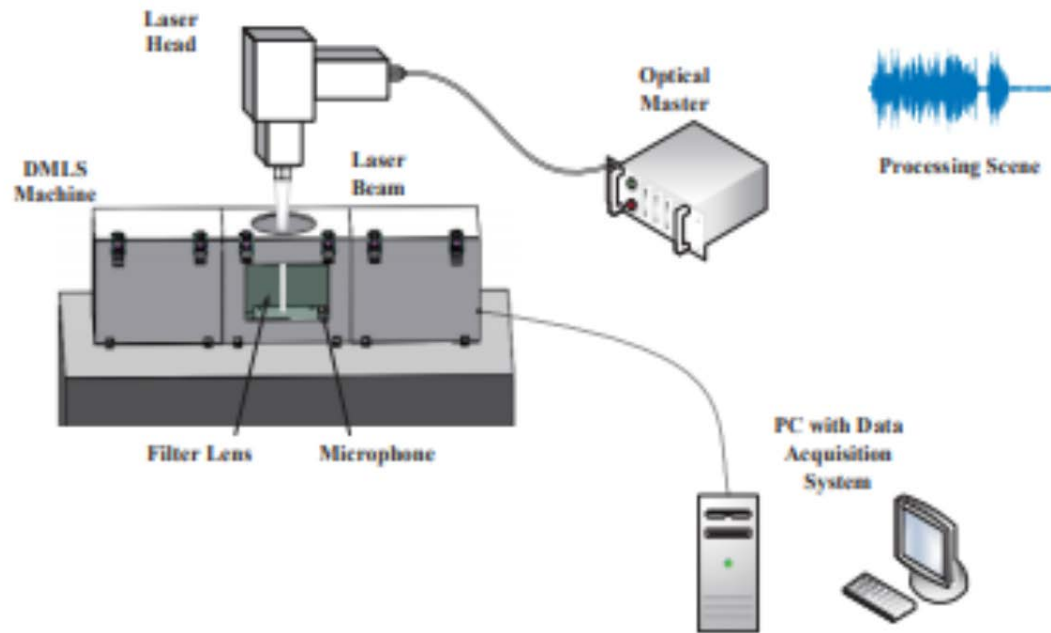


Figure 1.6: Basic setup of acoustic monitoring on a LPBF machine

In one study, AE was used during the lifetime of an AM part and the results demonstrated that it was possible to localize the main areas of discrepancy much more reliably and quickly than traditional methods (Strantza et al., 2017). By introducing AE technology earlier, an engineer is more likely to catch issues at a much cheaper phase of the overall AM process and increase overall throughput of part manufacturing. Neural networks are a unique technique that can be coupled with many processes to predict and detect useful information. They are currently being used throughout many industries to sift through data to predict the proper parameters necessary to produce specific types of parts under different loading conditions (Koeppel et al., 2018). Developing a single one-

size-fits all neural network is not reasonable or possible with the current technological boom of AM. With such knowledge, a neural net must be positioned to assist the user in a variety of ways. One way that machine learning (ML) could be used is to develop a feedback control to assist in adjusting input voltages, such as in experiments conducted using liquid metal jet printing (Wang et al., 2018). As ML continues to expand into more technological areas, there may someday be whole systems that are capable of running autonomously, adapting and growing to the surrounding conditions to protect, develop, and expand.

Another type of in-situ monitoring technique that is becoming increasingly popular is the use of optical imagery and thermal tomography. By incorporating at least one camera into the build process, a user can track important periods of time within a build and correlate potential defects to visual snapshots. A diagram of an optical imagery camera setup on a PBF machine can be seen in Figure 1.7 (Li et al., 2018). For increased throughput and traceability, being able to track and maintain a record of all parts printed as well as their exact as-printed image is quite valuable. In an article by Craeghs et al. (2012), the researchers illustrate the benefits of presenting the melt pool visuals by 'mapping' the melt pool data in space, on the X-Y plane. Visual interpretation of data is quite useful for the engineer as it provides easy to read maps of where a defect may exist and how big this potential defect may be. To couple visual data interpretation with live feedback would take an immensely powerful system/processing power as the data being output by a visual feed cannot be compressed while still maintaining its resolution. One challenge to utilizing optical imaging for in-situ monitoring is assuming that the calibration of your sensors is accurate in reference to non-contact temperature monitoring

(Grasso & Colosimo, 2017). Without proper calibration and testing, the data cannot be trusted and becomes overall useless to the user. There are many checks and balances that must be incorporated into the in-situ process to allow for some level of confidence in each batch of data taken.

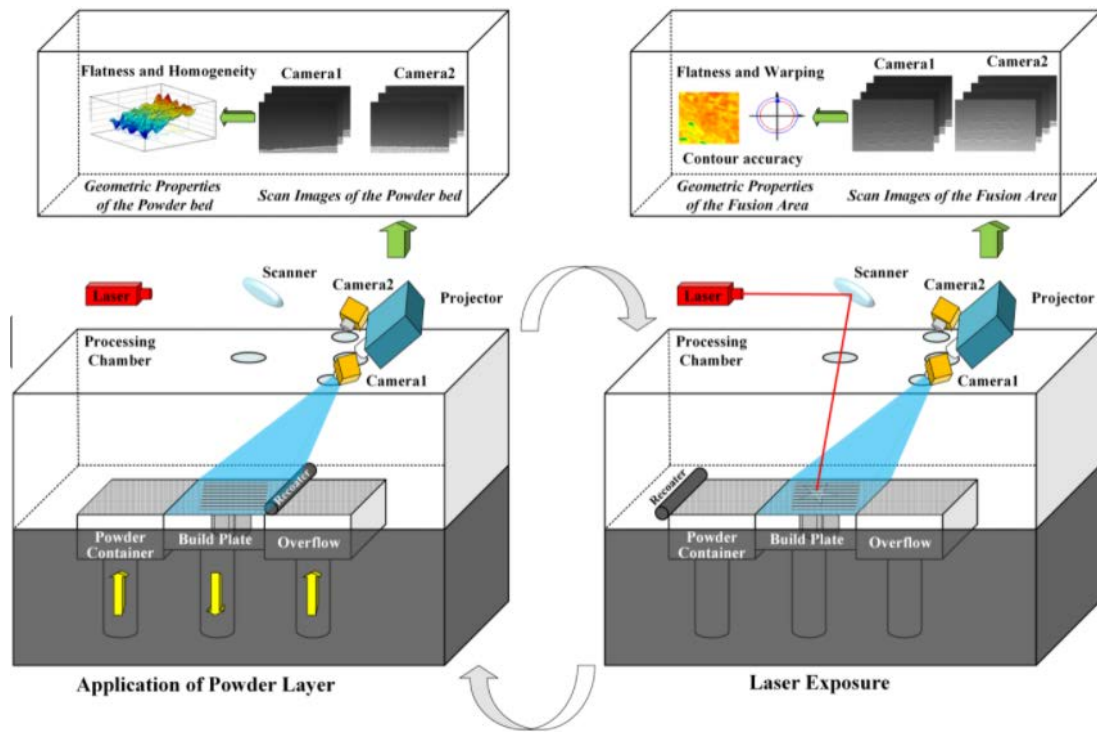


Figure 1.7: Diagram of in-situ monitoring using optical imagery for PBF Process

With all the data being produced from the user's preferred choice of in-situ monitoring solution, data management becomes difficult. Data interpretation and manipulation go hand-in-hand with the data management side of in-situ monitoring. All the sensors, cameras, and programs can produce terabytes of data that must be quickly interpreted and viewed. There are many solutions to this problem, with one of the main

ones being ML and artificial intelligence (AI). There are many different types of ML techniques, and these can be adopted to track and alert as certain issues arise during the AM process. One type of ML technique is properly named unsupervised ML, which can be used to characterize the geometric accuracy of a part by examining the point cloud data from a particular build (Zhu et al., 2020). An example of the potential of point cloud datapoints is shown in Figure 1.8, which demonstrates the level of detail that can be seen with a limited number of data points that correlate an image into a 3D figure (Grans, 2020). Allowing a system to characterize accuracy of parts unassisted is a true testament to the potential future of in-situ as well as data analytics. The real potential in ML is the ability to continuously learn and develop by incorporating AI. Another type of ML technique is supervised learning. This type of learning relies on a labeled set of training data, which provides examples of input values and the correct corresponding outputs (Razvi et al., 2019). This is the approach that most users take as it can be much faster and can be conducted with a smaller sample size of data. Renken et al. (2017) showed that an adapted self-learning program was successful in transferring information back and forth to continuously self-learn. Allowing a program to continually learn and develop is extremely important in the world of in-situ monitoring and AM. It needs to be able to keep up with the ever-growing field while maintaining a high level of accuracy and dependability.

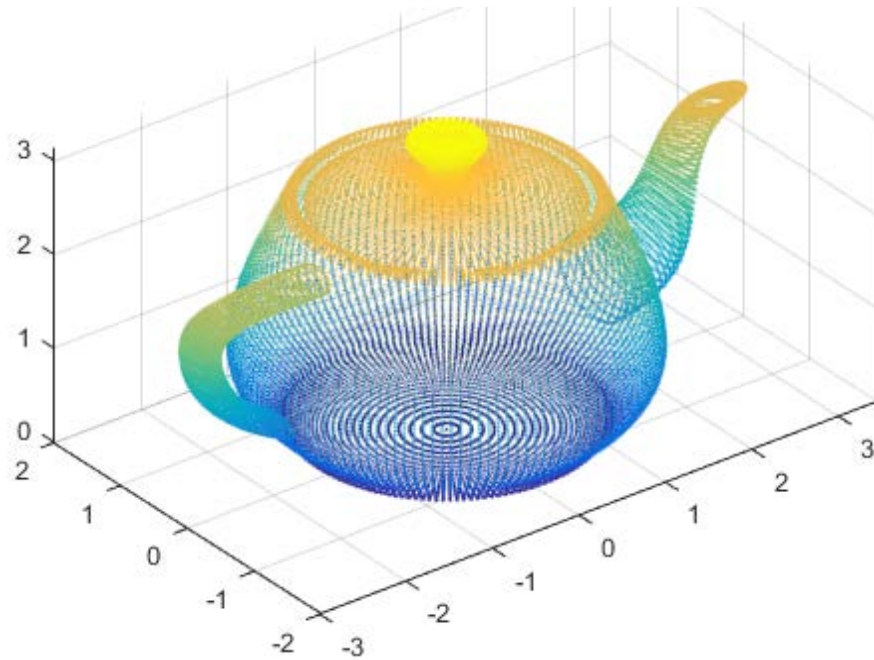


Figure 1.8: Point cloud data points example

ML and AI can take place over a variety of platforms whether it be local or cloud based. Many systems benefit from the flexibility of operating on the cloud because it can be accessed from remote areas; however, military customers prefer to keep local servers inaccessible by the outside world. Each technique comes with its own benefits and through online process monitoring there appears to be a valid approach to utilize multiple servers to detect anomalies in real time even with large datasets (Khazadeh et al., 2018). Using a cluster of servers, the data can be processed in real time. This is a great improvement to current techniques which require truncating the information so that it can be processed in a timely fashion. As AM becomes more data-intensive, the growth projected directly benefits the future of innovation through the increased knowledge in the design for AM (Ko et al., 2020). Expanding the AM potential to more designers, engineers, and non-technical collaborators is overall very beneficial to the resilience and

growth of AM. Zhang et al. (2017) were able to develop process maps that could introduce roughness into a powder layer that offsets the uneven temperature distribution of a build. With innovations like these, the possibilities are endless for what can be achieved using AM technology enhancements.

For an in-situ process to be most useful, it must have easy-to-interpret results, quick and manageable results allowing for live feedback, and low maintenance/cheap equipment that can be used universally on different machines. To truly reach a point where in-situ monitoring can be seen as revolutionary, a system would also need to develop an optimal scan strategy on a layer-by-layer approach using pre-existing data essentially predicting the optimal parameters for any type of future build (Carter et al., 2014).

1.5 Acoustic Sensors

During the research phase, a few options were considered in terms of acoustic sensors. Acoustics can be classified as the study of sound, including its production, transmission, and effects. There are many factors that can affect what type of sound or frequency a sensor is able to register. The basis of this experiment depends on the idea that when a defect occurs a distinct ping or frequency change is present. Some considerations that ultimately impacted the final decision in sensor choice were cost, effectiveness, availability, and difficulty of setup. There are a few types of sensors that were explored including: condenser, dynamic, piezoelectric, and electret acoustic sensors.

Condenser microphones operate on an electrostatic principle, using charged metal plates to help generate sound. (Tsing, 2020) These microphones depend on sound

waves hitting a diaphragm, and capacitance is formed when the distance between the two plates changes. This variation in spacing can be used to generate an electrical signal corresponding to the sound produced. A diagram depicting the basic workings of a condenser sensor can be seen in Figure 1.9 (“Condenser Microphone”, 2022). Condensers are beneficial because they register flat and wide ranges of frequencies and have a petite design. However, these sensors are more complex than traditional sensors and tend to be affected by differing temperatures and humidity. In summary, condenser microphones are more expensive and do not operate well in situations of high sound pressures; thus, they are not the best choice for this experiment.

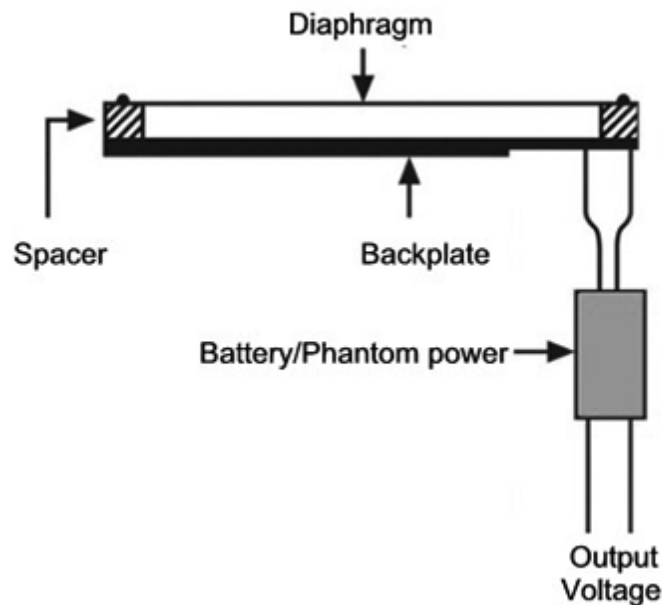


Figure 1.9: Diagram showing how a diaphragm and backplate create a capacitor

Dynamic microphones are the most common type of microphone technology. They consist of a thin metallic diaphragm that is attached to a coil of wire. As the diaphragm vibrates the coil a magnet produces a magnetic field that generates the electrical signal in correspondence to the sound produced. A diagram illustrating the inner workings of a dynamic style microphone can be seen in Figure 1.10 (“Dynamic Microphones”, 2022). This type of microphone is rugged and able to handle high sound pressure levels while providing good sound quality. Unfortunately, this type of sensor consists of a heavy diaphragm as well as a limiting design due to the wire coil that constrains the frequency response of the microphone. Due to the limits imposed by this type of sensor in conjunction with its limits on high-frequency content it was not chosen for this project.

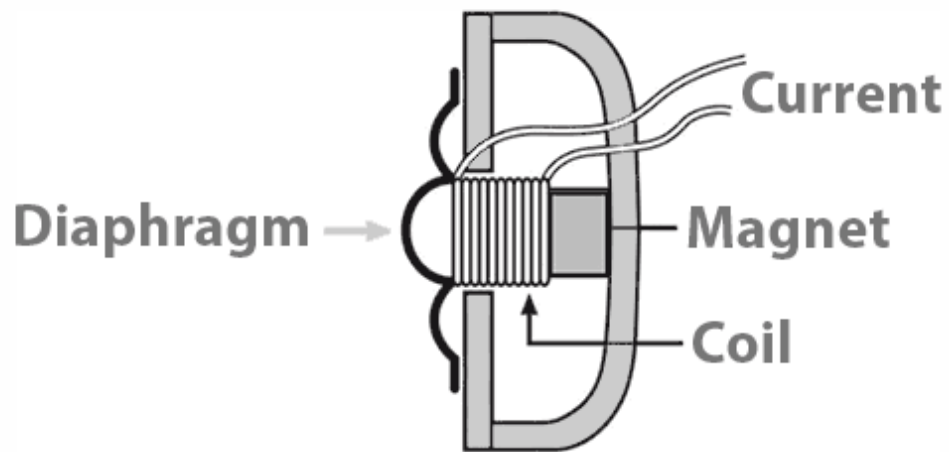


Figure 1.10: Diagram showing the inner workings of a dynamic microphone

Piezoelectric sensors work by measuring a voltage across a piezoelectric element generated by an applied pressure. When a force is applied to a piezoelectric diaphragm, a voltage proportional to the pressure is created. A visualization of the inner workings of a

piezoelectric sensor can be seen Figure 1.11 (Avnet, 2021). This pressure can take the form of sound waves, force, pressure, and frequencies. These types of sensors are good at measuring small changes in pressure, even in high pressure situations. A downside is that these sensors are limited to operating below temperatures of 120°C. Also, the high impedance output of this type of sensor means that the circuit is sensitive to noise caused by poor connections, movement, and RF interference. For these reasons, this type of sensor was strongly considered but was not chosen for this design.

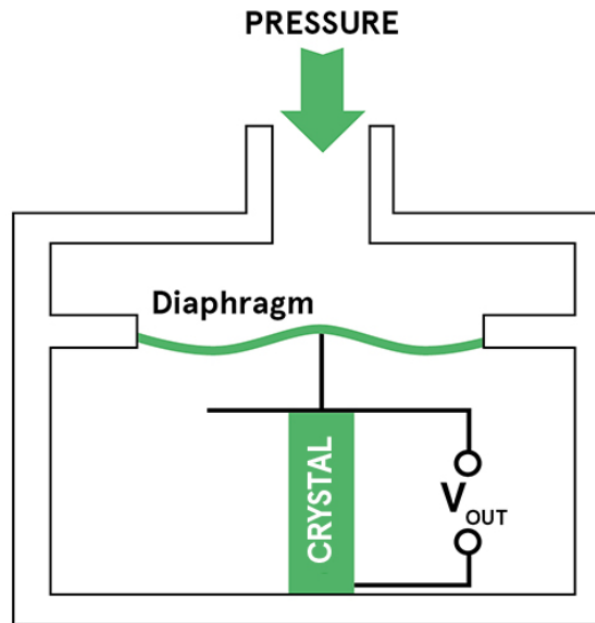


Figure 1.11: Inner workings of a piezoelectric sensor

Electret microphones utilize a diaphragm that has a fixed surface charge spaced close to a conductive plate. This close distance creates a capacitor within the air gap; as the voltage across the capacitor varies, the value of capacitance changes due to the pressure waves created by the sound moving across the electret diaphragm. Since there is a static charge embedded within an electret, this type of sensor eliminates the need for a

polarizing voltage to operate successfully. A diagram of this type of sensor and the inner workings is shown in Figure 1.12 (ECM, 2021). Electret condenser microphones are most commonly found in telephones, global positioning systems (GPS), and hearing aids. They can be used for high frequency acoustic measuring, while maintaining a high caliber of protection from elements like dust and moisture. This is ideal for the current parameters of our experiment, so the chosen sensor for this project was an electret condenser microphone. The chosen sensor was a Devmo LM393 module, as seen in Figure 1.13.

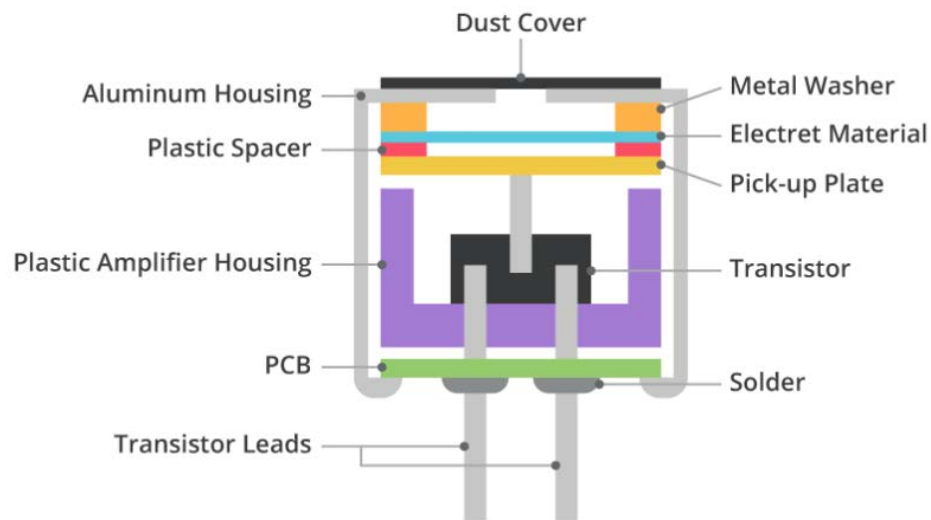


Figure 1.12: Electret condenser microphone inner workings

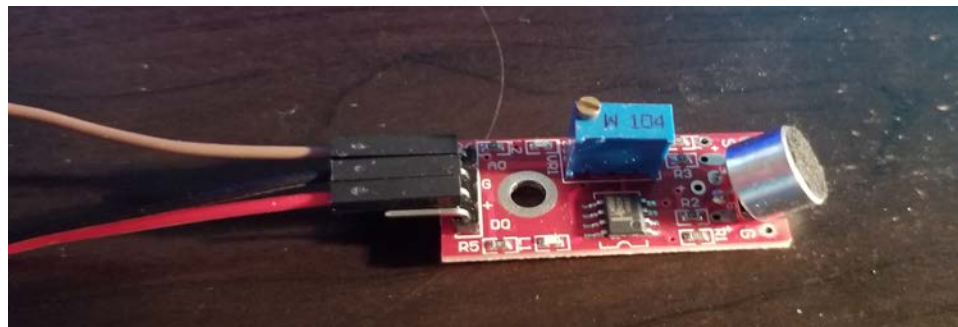


Figure 1.13: Devmo LM393 electret sensor module

1.6 Analysis Methodology

To begin, the analysis acoustic data was first collected along with the corresponding images taken during the build. The electret condenser setup recorded signal data that had to be converted into understandable frequencies. This was done using a Fast Fourier Transform (FFT) technique within the Arduino controller. With the acoustic data collected, the data was processed through a python script and organized through placement into a stable array as well as generated into a visual graph. This quick interpretation yielded potential areas of concern that could be addressed. The goal is to be able to correlate these anomalies with the image data taken with the internal SLM camera. If these areas can show situations of defect starting points, then it can be further investigated through sectioning or visual inspection.

FFT is an important analysis tool that assists in the conversion of a signal from the electret condenser to a spectral component that provides the frequency of the wavelengths in the air. The reason that FFT was used instead of the standard Fourier transform is due to the fact that FFT is fast while maintaining both efficiency and accuracy. In mathematical terms, the FFT reduces the number of computations needed for a problem of size Y from $X(Y^2)$ to $X(Y \log Y)$. (Warhammer et al., 2007) Since FFT can do everything a normal discrete Fourier transform can with greater efficiency and speed, FFT was chosen to be used to convert the input signal into comprehensible frequencies that can be processed quickly. For the simplicity of this experiment, time domain measurements were taken using the acoustic sensor and actively converted into frequency domain measurements by using the FFT process. The peak frequency was then taken and plotted on a graph to determine anomalies within a build.

2. Experimental Setup and Design

2.1 Design and Build of Experimental Setup

The data collection portion of this experiment relies on a constant feed of data pulled from a sound sensor and ultimately relayed back to a processing device. This sound sensor to processing device interface is crucial to develop a proper system of data analysis tools. The goal of the project is to be able to produce a defect detection device using readily available products at affordable prices. The benefits to having such a low-cost system could outweigh the decrease in accuracy from using low-cost parts.

2.1.1 Arduino Design and Layout

The current design incorporates the use of an Arduino Mega 2560 coupled with a Devmo LM393 electret sensor connected together using male to female jumper wires. A Fritzing diagram can be seen in Figure 2.1, which illustrates the necessary inputs from the Arduino that the sensor needs. In order for the sensor to output data through the A0 analog connection, it requires a 5v input and a grounding wire to operate properly. The sensor is activated through code within the Arduino. The code will be explained in more detail in section 2. The two components are housed in separate 3D printed enclosures which will then be mounted onto the SLM 125. These two components can be seen together in Figure 2.2. These components collect the data and process it, it is then fed into a Raspberry Pi which organizes the data and then uploads it to a OneDrive folder where it is then ready for processing.

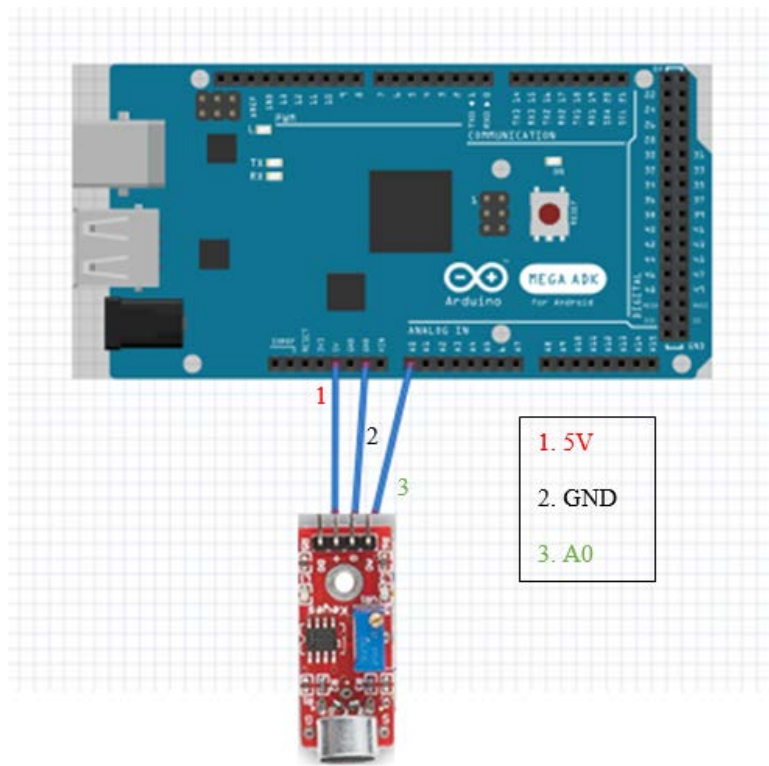


Figure 2.1: Fritzing diagram of Devmo sound sensor to Arduino connection

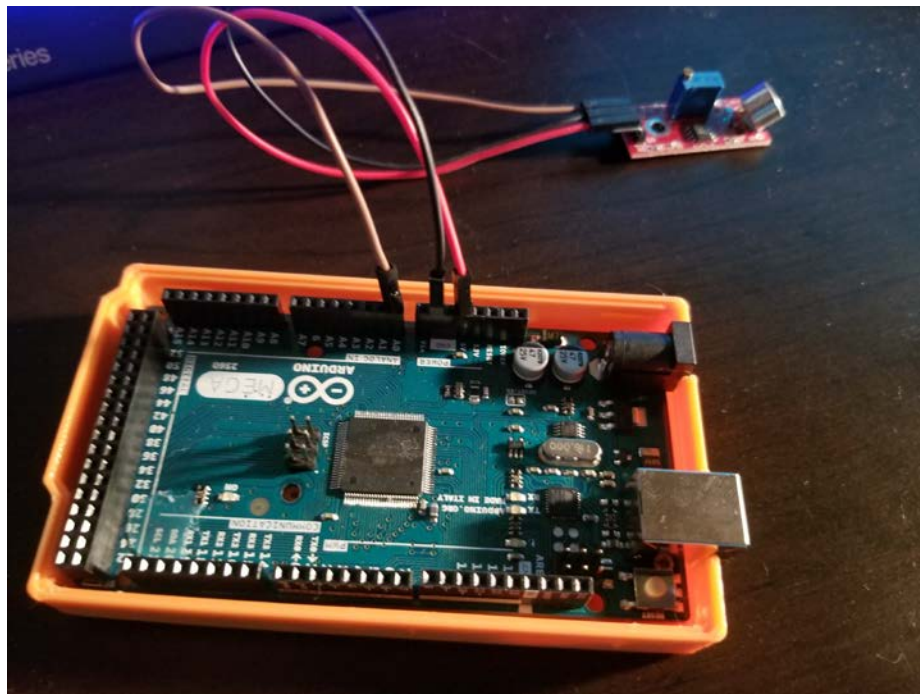


Figure 2.2: Arduino Mega 2560 signal converter connected to Devmo sound sensor

2.1.2 Raspberry Pi Build + Integration

The data collection and organization portion of this experiment is handled by a Raspberry Pi 3. This device is a low cost, miniature computer that can be connected to Wi-Fi or ethernet. The versatility that this connectivity provides opens up the possibilities for companies to keep their information internal to their servers or visible to the open web. The reason for connecting the Arduino to a Raspberry Pi is to both create a smaller footprint for the device as well as enable the Arduino to solely focus on deciphering the data, while the Raspberry Pi can handle the majority of the processing/interpretation. The Raspberry Pi is secured in a 3D printed enclosure and connected to Arduino using a USB A to USB B connector. The 3 main components (Arduino, Sensor, and Raspberry Pi) can be seen in Figure 2.3. These three components are then mounted onto the additive machine of choice in a position that is close enough to the build chamber to pick up the different frequencies that may occur during the build.



Figure 2.3: Arduino (Left), Devmo sound sensor (Middle), and Raspberry Pi (Right)

2.1.3 Setup Onto SLM 125

The sound sensor assembly is attached to the SLM 125 using Velcro strips so that it can be removed for updates or maintenance. Each piece is secured in a strategic location that will not interfere with the operation of the machine nor any doors that may need to be opened periodically. The wires are temporarily taped to prevent any potential to be accidentally pulled. Figure 2.4 shows the location of the sound sensor and the accompanying Arduino. This location is the closest to the build chamber while still being outside of the chamber, in an ideal situation the sensor would be within the chamber and away from outside noise pollution. Some fine tuning will be necessary to create an average ambient noise frequency, in order for the sensor to be able to detect anomalies. Figure 2.5 illustrates the chosen mounting position for the Raspberry Pi on the topside of the machine. In Figure 2.6 the monitor setup can be seen off to the side of the machine. These components connected in series make up the entirety of the monitoring system.



Figure 2.4: Image showing mounting positions of sound sensor and Arduino



Figure 2.5: Image showing mounting location of Raspberry Pi (Top side of SLM 125)



Figure 2.6: Monitor setup to visually analyze data and interface with Raspberry Pi

2.2 Software Setup of Sensor

An important part of this experiment is developing the architecture for the sensor to be able to record the frequencies and then process the data to determine the current state of the build. The sound sensor is activated by the Arduino and a script is run to take a certain number of signal samples and then pick the peak value to report back to the serial monitor. This peak value is converted into a recognizable frequency value that can be analyzed further. The Arduino code utilizes the FFT previously discussed by incorporating premade Arduino libraries. A sample of the code for the Arduino can be seen in Figure 2.7, while the entirety of the code can be seen in Appendix A.

```
*/
#include "arduinoFFT.h"

#define SAMPLES 128 //SAMPLES-pt FFT. Must be a base 2 number. Max 128 for Arduino Uno.
#define SAMPLING_FREQUENCY 4000 //Ts = Based on Nyquist, must be 2 times the highest expected frequency.

arduinoFFT FFT = arduinoFFT();

unsigned int samplingPeriod;
unsigned long microseconds;
unsigned long myTime;

double vReal[SAMPLES]; //create vector of size SAMPLES to hold real values
double vImag[SAMPLES]; //create vector of size SAMPLES to hold imaginary values

void setup()
{
  Serial.begin(115200); //Baud rate for the Serial Monitor
  samplingPeriod = round(1000000*(1.0/SAMPLING_FREQUENCY)); //Period in microseconds
}
void loop()
{
  /*Sample SAMPLES times*/
  for(int i=0; i<SAMPLES; i++)
  {
    microseconds = micros(); //Returns the number of microseconds since the Arduino board began running the current script.

    vReal[i] = analogRead(0); //Reads the value from analog pin 0 (A0), quantize it and save it as a real term.
    vImag[i] = 0; //Makes imaginary term 0 always

    /*remaining wait time between samples if necessary*/
    while(micros() < (microseconds + samplingPeriod))
    {
      //do nothing
    }
  }

  /*Perform FFT on samples*/
  FFT.Windowing(vReal, SAMPLES, FFT_WIN_TYP_HAMMING, FFT_FORWARD);
  FFT.Compute(vReal, vImag, SAMPLES, FFT_FORWARD);
  FFT.ComplexToMagnitude(vReal, vImag, SAMPLES);
}
```

Figure 2.7: Snippet of Arduino code that converts the signal into an understandable frequency

The Arduino and sound sensor both rely on the Raspberry Pi for their source of power and thus are ultimately controlled by the powering on and off of the Raspberry Pi. The miniature computer handles the data logging portion of the project as it pulls the data in real time from the serial monitor of the Arduino. The program that runs concurrently is called PuTTY and a snapshot of the parameters that can be modified can be seen in Figure 2.8. The current process collects data and creates a .CSV file with the log file name corresponding to the date and time that the build was occurring. This format will assist in the future organizational structure development of the data and help to maintain a simple methodology of nomenclature.

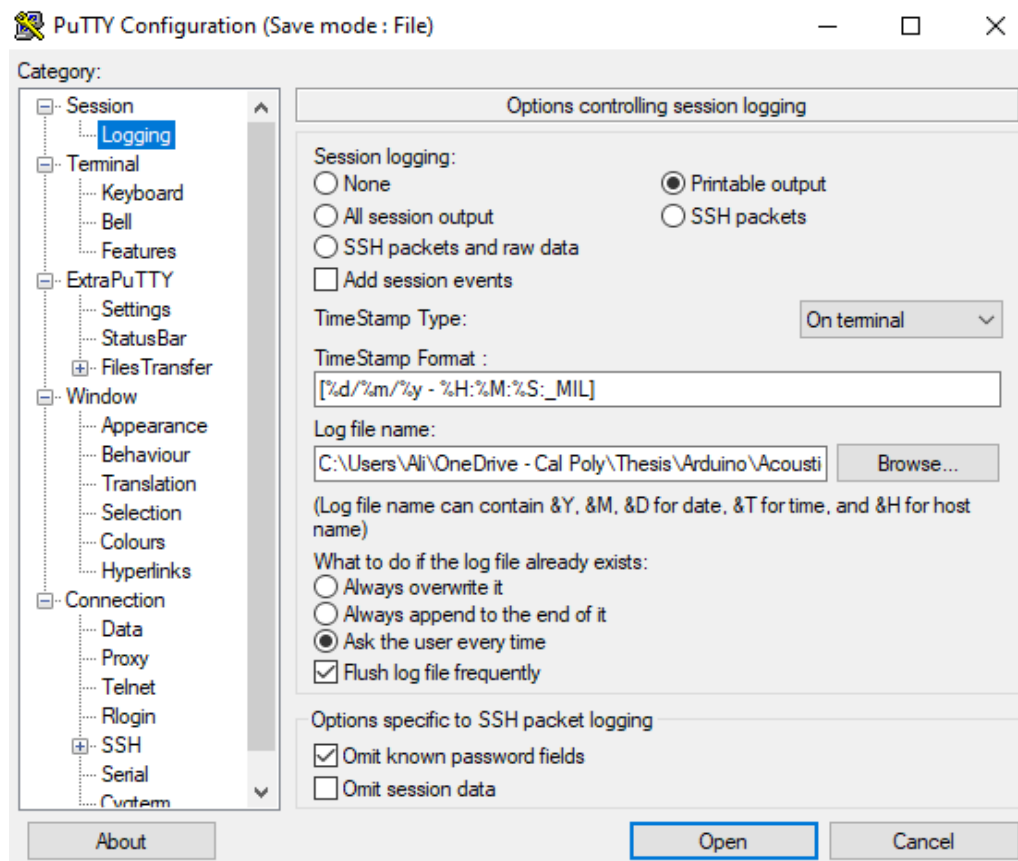


Figure 2.8: Datalogger that pulls all information output from the Arduino's serial monitor in real time

2.3 Cost Comparison of Systems

When comparing the different systems that exist in the field of in-situ monitoring, cost and applicability of data are two of the main factors that we assess. There are other factors that should also be taken into consideration such as compatibility within the given system and effective autonomy of the system to alert and divert potential issues. There are currently many competitors emerging in this new field of monitoring, with most stemming from SLS machine producers (OEMs), as seen in Table 2.1. (Everton 2016) Costs can stem from 30k for a light lean system with minimal data capture capabilities to over 150k for a full-fledged data capture system with cameras and appropriate softwares that can detect anomalies and issues within a build. Unfortunately these systems are not fully proven out yet and as they continue to advance there will need to be a significant amount of testing and development done on the consumer side to gain full confidence.

Table 2.1 Existing commercial AM in-situ monitoring systems

OEM Supplier	System Name	Failure Mode Monitored	Altered Parameter	Equipment
Arcam	LayerQam	Porosity	N/A	Camera
B6 Sigma	PrintRite3Dâ INSPECT	Unknown	N/A	Thermocouple & high-speed camera
Concept Laser	QM melt pool	Melt pool monitoring	Laser Power	High-speed CMOS camera
EOS	N/A	Unknown	N/A	Camera
SLM Solutions	LCS	Powder distribution	Recoater	Camera
SLM Solutions	MPM	Melt pool monitoring	N/A	Two photodiodes
DEMCON	LCC 100	Melt pool monitoring	Laser Power	Camera
DM3D Technology	closed-loop feedback system	Melt pool monitoring & build height	Laser Power	Dual-color pyrometer & three high-speed cameras
Laser Depth	LD-600	Depth measurement	Laser Power	Inline coherent imaging
Promotec	PD 2000	Melt pool monitoring	N/A	CMOS-camera
Promotec	PM 7000	Melt pool monitoring	N/A	1D photo detector
Stratonic	ThermaViz system	Melt pool temperature	Laser Power	Two-wavelength imaging pyrometer

The goal of this experiment is to produce a hardware solution that can provide a simple, yet effective insight into the overall quality of a build. By being a keeping the cost significantly lower than an original OEM solution, the potential ROI can be easily justified. With a sensor package that is simple to use, compact in nature, and universal among machines the possibilities can evolve with time and additional technology. The hardware cost for this experiment can be seen in Table 2.2.

Table 2.2 Cost Analysis for acoustic vibration setup

Item	Cost	Function	Supplier
Arduino Mega 2560 Rev3	\$50.00	Sound Sensor Signal Processing	https://www.amazon.co
Raspberry Pi 3 Model B	\$45.00	Data Collection/Storage	https://www.amazon.co
64 gb MicroSD	\$12.00	Data Collection/Storage	https://www.amazon.co
USB A male to USB B male	\$7.00	Link between Arduino and Raspberry Pi	https://www.amazon.co
Power switch for Rasp Pi	\$11.99	Power Switch for Setup	https://www.amazon.co
Wireless Mini Keyboard	\$25.99	Interface for manual adjustment to Raspberry Pi	https://www.amazon.co
Devmo Sound Sensor	\$13.99	Main Sound monitor	https://www.amazon.co
Male to Female Bread Board Jump	\$5.99	Cables to connect sound sensor to arduino	https://www.amazon.co
3D printed enclosures	\$0.00	Enclosures for sensor, Arduino, and Raspberry Pi	Cal Poly Machine Shop
HDMI Cable	\$0.00	Connection between Raspberry Pi and Monitor	Provided from home
10 ft Extension Cord	\$0.00	power supply for Raspberry Pi	Cal Poly Machine Shop
Velcro Strips	\$0.00	Mounting solution to SLM 125	Provided from home
Monitor	\$0.00	Monitor to view Raspberry Pi	Provided from home
Total	\$171.96		

In conjunction with a senior project conducted in 2017, a variety of sensors and a data acquisition module were procured to aide in the collection and monitoring of anomalies within the build chamber during a highly sensitive build. These sensors and module equated to over \$7500 and their cost breakdown can be seen in Figure 2.9. When comparing the parts purchased in 2017 with the parts used in this build, it is apparent that the quality of parts is comparable to the price point at which these items are at. In short, the accelerometers and sound sensors have a higher degree of confidence and fidelity when compared to parts purchased from Amazon. With further testing, this proves true as

these sensors are meant to collect data at a considerably higher sensitivity and accuracy. The purpose of this comparison is not to disprove the necessity for parts of this price point, but to attempt to replicate the results at a potentially lower confidence level by a system that may roughly end up costing 2% of the closest mid-range competitor. Although this may seem unnecessary for a company spending potentially millions of dollars on these types of products, the future application within a wider consumer base makes this product viable.

<u>Already Purchased</u>	<u>Anticipated Costs</u>
Sensors	Material for mounting sensors
Triaxial Accelerometer: \$1,715.00	Adhesive - \$75
Acoustic Emission Sensor: \$705.00	Metal Enclosure - \$50
Single-Axis Accelerometer: \$583.00	Extraneous - \$125
Sensor Equipment	Total Anticipated Cost: \$250
LabAmp: \$2,924.00	
Acoustic Emission Coupler: \$717.00	
Plug In Filter Set: \$329.00	
Triaxial Output Cable: \$253.00	
Connecting Cable: \$68.00	
Total Already Purchased: \$7,294.00	Total Overall Cost: \$7,544.00

Figure 2.9: Sensors/DAQ equipment purchased for a previous experiment to measure anomalies within the build chamber (Coria 2017)

2.4 Test Coupon Design and Print Parameters

This trial primarily focuses on using a variety of different coupons while maintaining parameter setups to gain a wide range of data that can be analyzed. The test coupons that were printed ranged from FDM calibration builds, thin-walled pressure vessels, and tensile coupons. The parameters that were used for the experiments stayed the primarily the same throughout the builds, apart from Build 3 (thin-walled pressure vessels). A summary of the chess parameters can be seen in Table 2.3. By preserving a uniform parameter set, the baseline accuracy could be established as the prints proved to

be stable. Once a stable enough dataset was developed, the opportunities for further expansion upon the capabilities of the system could be possible.

Table 2.3 Chess print parameters used in printing coupons for the majority of this experiment

Parameter	Chess	Units
Minimum Scanning Time	30	sec
Layer Height	0.03	mm
Build Plate Heater	On	-
Hatching Up-Skin	Off	-
Hatching Border Distance	0.09	mm
Border Power	60	watts
Border Speed	600	mm/s
Fill Contours	Off	-
Fill Contours Distance	-	mm
Number of Fill Contours	-	-
Hatching Outer Hull Distance	0.084	mm
Outer Hull Power	90	watts
Outer Hull Speed	600	mm/s
Fill Pattern	Chess	-
Field Size/Stripe Size	5	mm
Transition Contours	Off	
Transition Contour Distance	-	mm
Number of Transition Contours	-	

2.5 Original Testing Plan and Pivot

Originally, there was a planned design of experiments which incorporated a modified test coupon originally designed for a previous project. This coupon can be seen in Figure 2.10 and was designed to fail by cracking at the outlined red areas. The failure would be induced by a lack of efficient heat transfer due to the drastic diameter change. This failure would be catastrophic for the part and would produce an audible sound that would be picked up the sensors. The height of this failure could be controlled, and a test plan could be developed to correlate the failure with any triggers from the sensors. As

such, with a proper training algorithm a machine learning approach could be taken to properly teach a system what anomalies could look like. Unfortunately, this means that after each build the potential for damage to the machine was significantly higher than normal operation. The lack of control in how damaging these builds could have required us to pivot towards a safer approach to preserve the machine's quality and decrease the chance of taking the machine down for maintenance.

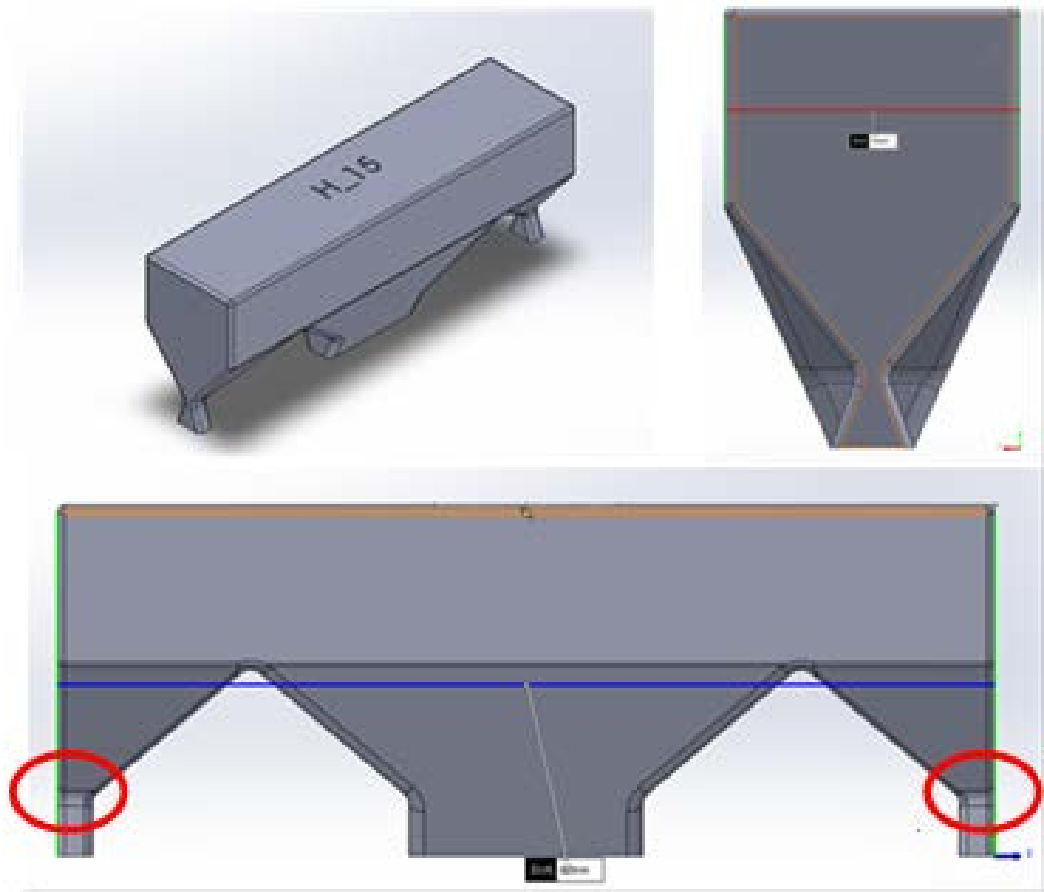


Figure 2.10: Modified DOE coupon, designed to fail at red outlined areas

3. Coupon Builds and Data Collection Analysis

The coupons designed and built during this experiment consisted of student projects and calibration builds. Builds 1-6 can be seen below along with a brief description of their purpose, which may help to outline the design considerations taken to create these parts. Overall, the printer faced a few minor setbacks and delays due to maintenance issues and reduced usage during the COVID-19 pandemic. As a result, the data was collected over the course of several months.

3.1 Build 1 and Build 2

The first two builds consisted of test parts for a research project being conducted. These initial builds were used to test the hardware/software for functionality and, as a result, minimal data was collected during these trials. The hardware worked well in its current orientation and settings; the code was calibrated to work with the stable noise environment that is created during a standard print. As these were initial test prints, there were no pictures taken of the builds; however, there was data collected which is presented in Figure 3.1 and Figure 3.2. This data was collected after tuning to the ambient room sound. The frequency hovers between 1750 and 2250 hz; however, this does not indicate the true frequency of the ambient environment as this is an estimate that has been collected by the sound sensor and was not fully calibrated to proper frequency recognition. Though, this does not impact the experiment as the main goal is to detect a frequency disturbance and can still be done even if the frequencies are not tuned exactly.

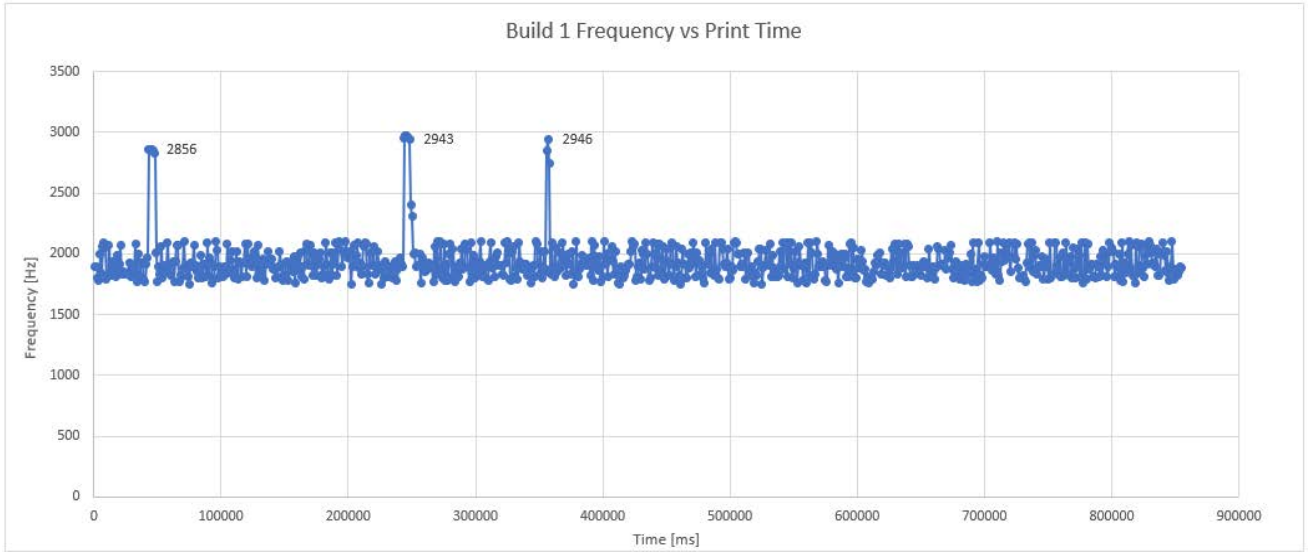


Figure 3.1: Build 1 frequency vs. print time plot (11-03-2021)

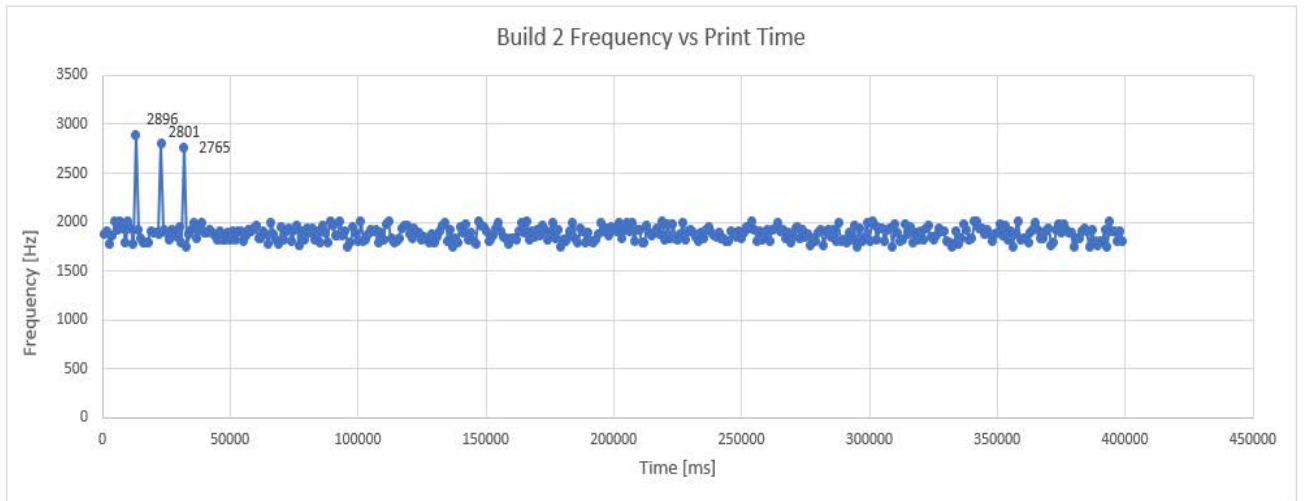


Figure 3.2: Build 2 frequency vs. print time plot (12-15-2021)

This preliminary data shows promising results as the system appears to identify deviation from the ambient decibel conditions surrounding a standard print. Although there are no images to support these anomalies, the frequency response from Build 1 and

Build 2 demonstrate that it is possible to isolate some type of natural sound, whether it is caused by the print or some outside variable, requires further validation and testing.

Using the Anderson-Darling normality test, seen in Figure 3.3 and Figure 3.4, we can reject the null hypothesis ($p < 0.005$), therefore, the data is not normally distributed. A 1-sample sign nonparametric test was then conducted to estimate the median of the population (Figure 3.5). According the 1-sample sign test, we are 95% confident that the median frequency falls between 1897 and 1909 Hz, any values that are more than 3 standard deviations from the median are significantly different. The same pattern is found in the statistical analysis of Build 2. These experiments yielded preliminary anomalous readings that may correlate to significant events within the build. Frequencies that exist above the original ambient measurements may indicate defects within the build. However, more data is required to fully confirm this

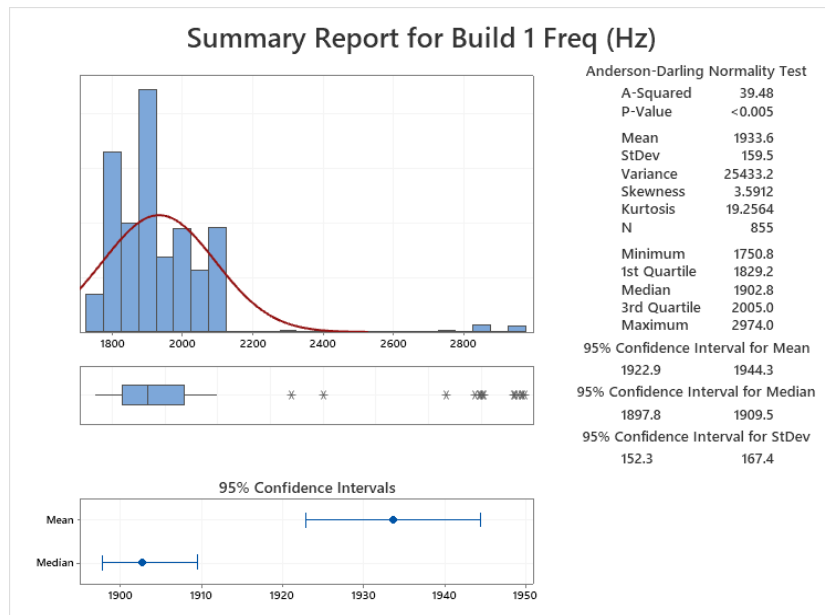


Figure 3.3: Descriptive statistical analysis for homemade system using Minitab - Build 1

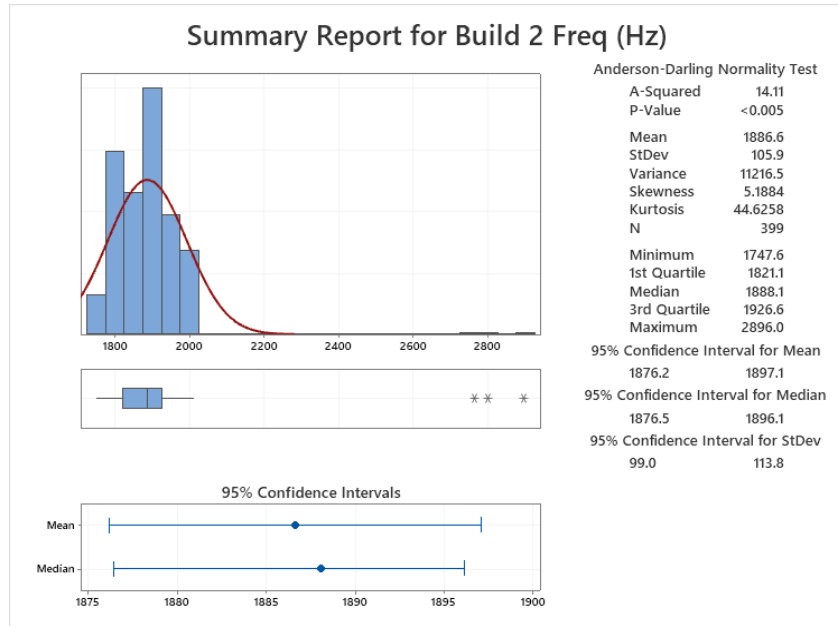


Figure 3.4: Descriptive statistical analysis for homemade system using Minitab - Build 2

Sign CI: Build 1 Freq (Hz)

Method

η : median of Build 1 Freq (Hz)

Descriptive Statistics

Sample	N	Median
Build 1 Freq (Hz)	855	1902.76

95% Confidence Interval for η

Sample	CI for η	Achieved Confidence Position
Build 1 Freq (Hz)	(1897.87, 1909.48)	94.45% (400, 456)
	(1897.83, 1909.48)	95.00% Interpolation
	(1897.81, 1909.48)	95.27% (399, 457)

Figure 3.5: 1 sample sign test using Minitab - Build 1

3.2 Build 3

Build 3 began as a starter build to build momentum for the print team as we began the quarter. The goal was to print a few items that were not particularly complicated, but still valuable in the context of building confidence in operation of the machine and verification of the parameters and material. This build consisted of standard “benchys” FDM stress test parts, orthogonally designed rings, and two AM welding flat coupons. The print was optimized to minimize difficult to reach internal support structures (Figure 3.6). From the figure below, the quality of the finished build appears good, with minimal discoloration and/or warpage. The sensor data was collected parallel to the removal of the build and was processed into a scatter plot (Figure 3.7). The sound sensor appears to pick up some sort of disturbance during the beginning of the build, which is indicated by the jumps in frequency values in what appears to be systematic increments. This timing roughly correlates to the rake’s movement between sessions.



Figure 3.6: Completed Build 3 with parts on build plate (Welding coupons, rings, and benchys)

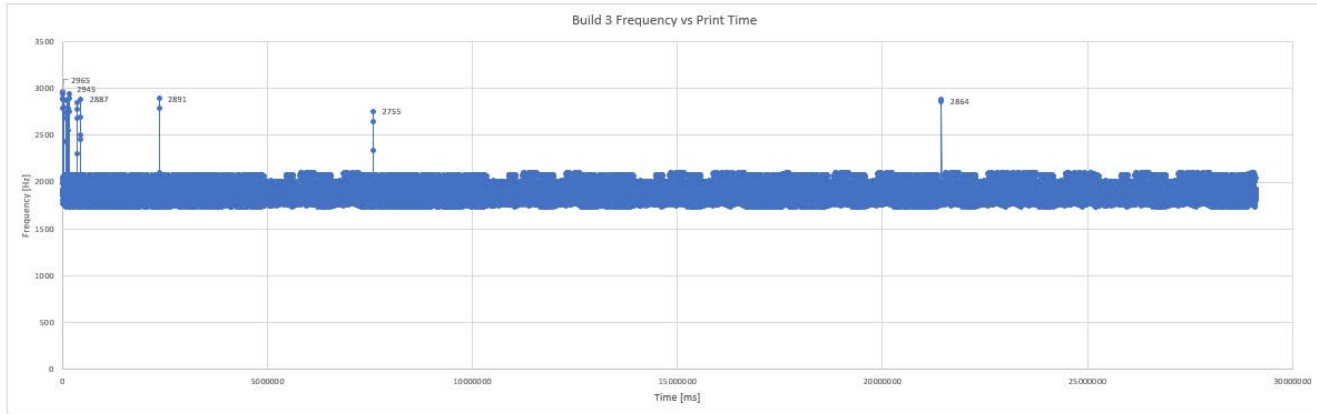


Figure 3.7: Build 3 frequency vs. print time lot (01-20-2022)

When the parts were examined, there were some visible adhesion issues between the welding coupons and the support structures at the edge of the part. This can be seen more clearly in Figure 3.8, and may indicate some issues with heat dissipation from the part to the build plate or a lack of powder in the mating surface between the part and support. Another potential hypothesis for edge separation is the lack of support structures present on the curvature of the part.



Figure 3.8: Enhanced image of welding coupons, emphasizing the delamination between the part and support structures

Upon further examination of the processed build file, it was determined that the file had overlapped STL files, causing the software to overexpose the support layers during the first 25 layers. This resulted in a buildup of material in a few areas. The original overlapped parts were corrected early in the print, but this initial correction did not seem to prevent issues as the parts grew in the Z-direction. Figure 3.9 shows this issue during the first few layers of the build; the streaks were later determined to be the main cause of the part's delamination. These physical observations led to a deeper analysis of the data provided by the acoustic sensor during the first 50 layers. The zoomed in version of the above plot can be seen in Figure 3.10. Initially it appears as though there is a consistent ping that occurs at similar intervals. These intervals occur every 40 seconds and likely correspond to the movement of the rake across the build platform. An interesting situation happens after several minutes as it appears that the sound disappears and then reappears. This can be attributed to a few possibilities as the introduction of powder flowability may contribute to a decrease in the amount of powder across the raised areas which would cause them to not interact with the rake. After the first few layers, the issue was corrected on the software and the program resumed without the overlapping support structures. This fixed the interference issue but continued to leave streaks in the powder as the rubber rake had already been sufficiently damaged.

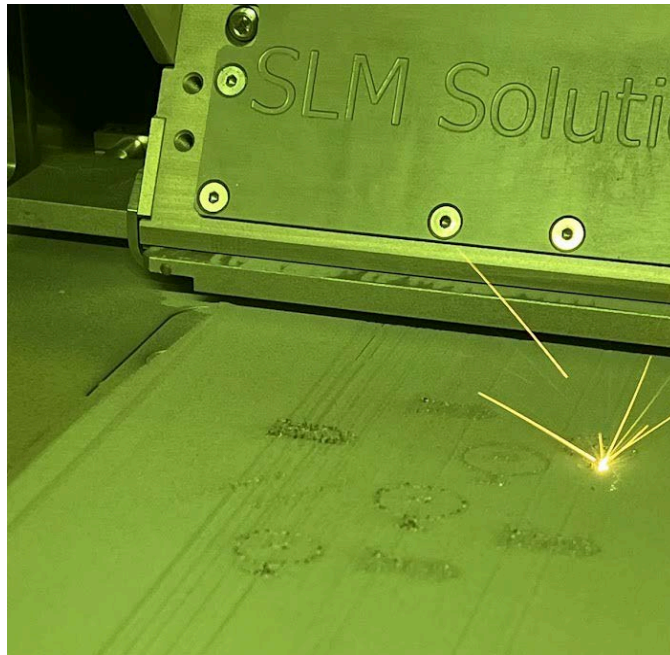


Figure 3.9: Image of the first few layers of build 3 in which the support structures in front of the welding coupons were overexposed due to an issue in preprocessing

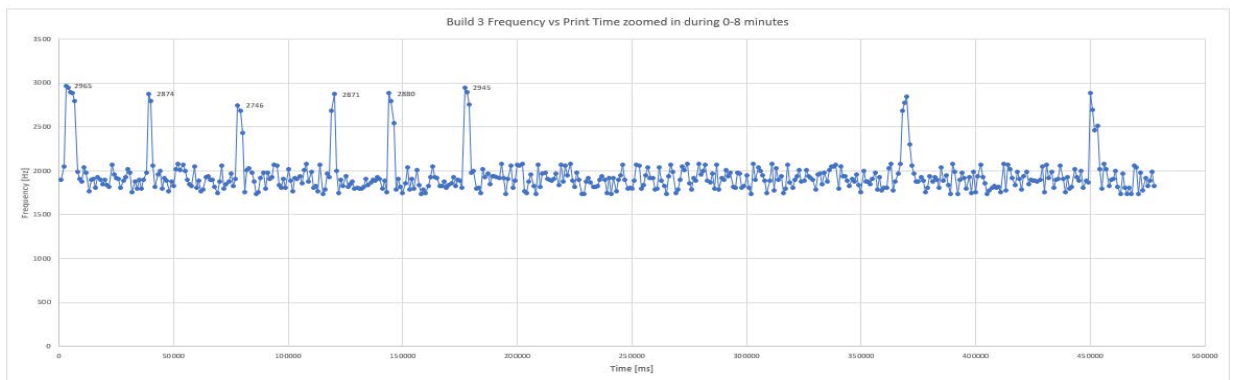


Figure 3.10: Build 3 frequency vs. print time zoomed in during 0-8 minutes (01-20-22)

By examining the frequency response of build 3, it can be inferred that there were a few anomalies that were recorded during the first few minutes of the build (Figure 3.10). From the initial normality test, it is clear the data is not normally distributed ($p < 0.005$), resulting in rejection of the null hypothesis (Figure 3.11). The nonparametric test provides a basis for the median of this data set within the 95 % confidence interval of

1891-1893 Hz (Figure 3.12). These values do not necessarily correlate to defects generated within the build but do open up the potential for further focused analysis into the layers where these acoustics were recorded. This evaluation provides a compelling argument for a proper process that can produce results in a repeatable fashion across different builds.

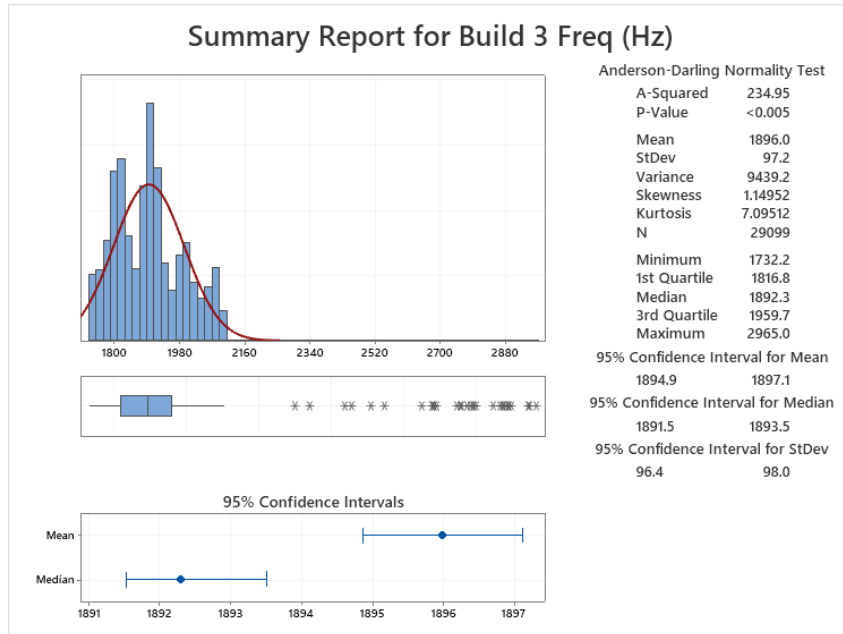


Figure 3.11: Descriptive statistical analysis for homemade system using Minitab - Build 3

Sign CI: Build 3 Freq (Hz)

Method

η : median of Build 3 Freq (Hz)

Descriptive Statistics

Sample	N	Median
Build 3 Freq (Hz)	29099	1892.29

95% Confidence Interval for η

Sample	CI for η	Achieved Confidence	Position
Build 3 Freq (Hz)	(1891.53, 1893.51)	94.98%	(14383, 14717)
	(1891.53, 1893.51)	95.00%	Interpolation
	(1891.53, 1893.51)	95.11%	(14382, 14718)

Figure 3.12: 1 sample sign test using Minitab - Build 3

3.3 Build 4

Build 4 consisted of several iterations of a thin walled pressure vessel. These vessels were designed to test the minimum wall thickness required to prevent leakage of air through the body of the part. As can be seen in Figure 3.13, the vessels were aligned in a staggered formation to prevent overpressure of the rake during powder spread. For the most part, the test specimens appear to be uniform in color and build. Upon further inspection, it can be seen that the intersection between the main body and the topmost hex mating surface shows signs of discoloration or lack of proper heat dissipation. This discoloration can potentially be a sign of delamination at this intersection, which could allow for leakage. The zoomed in image showing the discoloration up close can be seen in Figure 3.14. These parts took approximately 16 hours to print, during which data was collected using the sound sensor setup. The compiled data appears to provide some potential insight on the timing of anomalies that occurred and their correlation to the timing of the layers of interest.



Figure 3.13: Build 4 thin-walled pressure vessels test coupons



Figure 3.14: Zoomed in image on intersection between hex and main body showing discoloration and potential leak points

From the plot in Figure 3.15, there appear to be some irregularities at the beginning and at the end of the build. There is also a single trigger $\frac{3}{4}$ of the way through the build. This single irregularity was inspected further and deemed inconclusive as there were no visible surface defects on the parts, nor were there singular leakage issues that could be pinpointed to this layer. The sections that appear to have issues happen between 0-9 minutes and 830-860 minutes. By zooming in on these two time periods, it can be seen that there are definitive frequency fluctuations at these slice layers.

During the first 9 minutes of Build 4, a significant frequency change was recorded 3 separate times. These spikes in frequency could have been the result of potential cracks or breaks within the support layers in the first 20 layers (Figure 3.16). This can be common within the early layers depending on the support type chosen or the asymmetry of the powder distribution process. Another potential reason for these spikes could be that students or techs were in the room during this time and created metal on metal noise

which would be picked up by the sensor. This could be anything from removing parts off previous build plates or simply dropping items on the table. One of the main drawbacks to having the printer in an accessible space is the potential for noise pollution from the surrounding lab environment. Upon further inspection, it was noted that there were no issues within the support layers of this build.

Within the 830-860 minute timespan there are substantially more spikes in frequency. This series of events appears to correlate to the transition period between main body and the hex threaded section. In Figure 3.17, the signals seem to have some methodical rhythm as though they trigger in conjunction with the rake moving back and forth. A theory in correlation with this observation is that the laser is creating a slightly raised surface that is coming into contact with the recoater on the forward and reverse passes. This could be due to the lack of heat dissipation due to the large change in mass from the thin wall to the full thickness hex threaded area. The timing of this change in frequency correlates with the anomaly found on the parts, however, coincidence cannot be ruled out as a possibility.

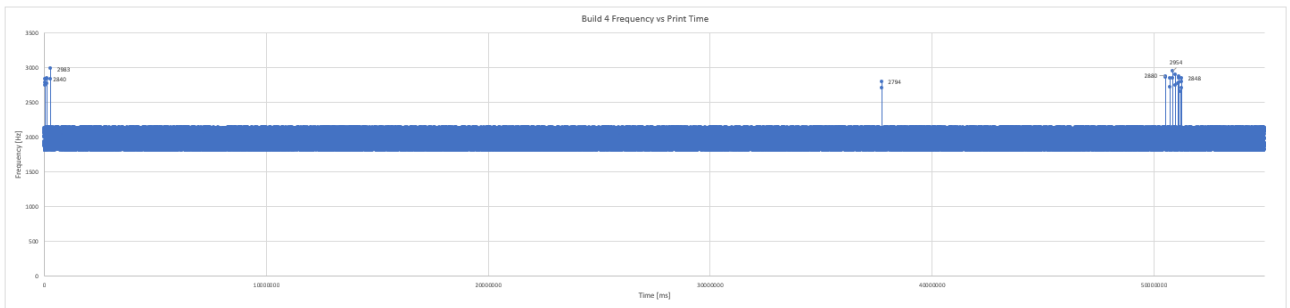


Figure 3.15: Build 4 frequency vs. print time plot (02-22-22)

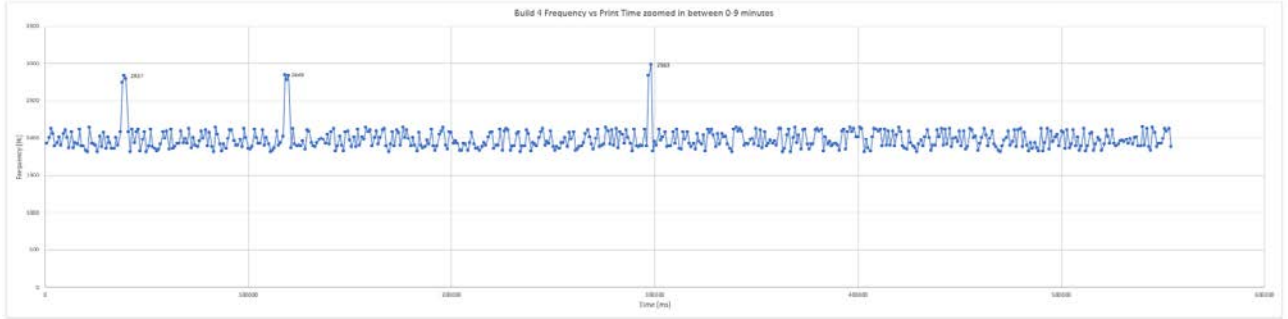


Figure 3.16: Build 4 frequency vs. print time zoomed in during 0-9 minutes (02-22-22)

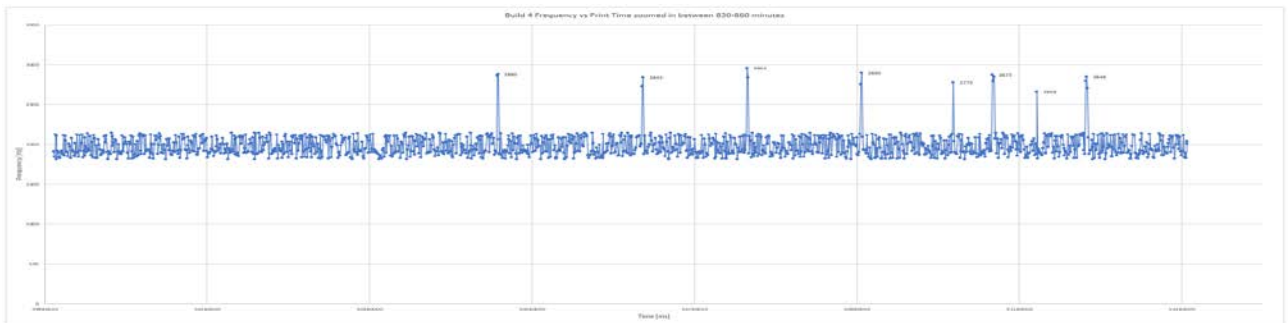


Figure 3.17: Build 4 frequency vs. print time zoomed in during 830-860 minutes (02-22-22)

The statistical analysis for Build 4 yielded similar results as the previous build; however, the distribution of data in this build began to represent more of a bimodal shape, as seen in Figure 3.18. Multiple peaks in distributions of frequency began to appear as builds became longer in length, as illustrated in future datasets. This phenomena could be due to multiple reasons, but one theory is that these peaks correspond to diameter changes during a build and the resulting stress relief that occurs naturally as these boundary layers cool. This hypothesis corresponds with the acoustic data that was collected near the layers that a significant change in diameter was present.

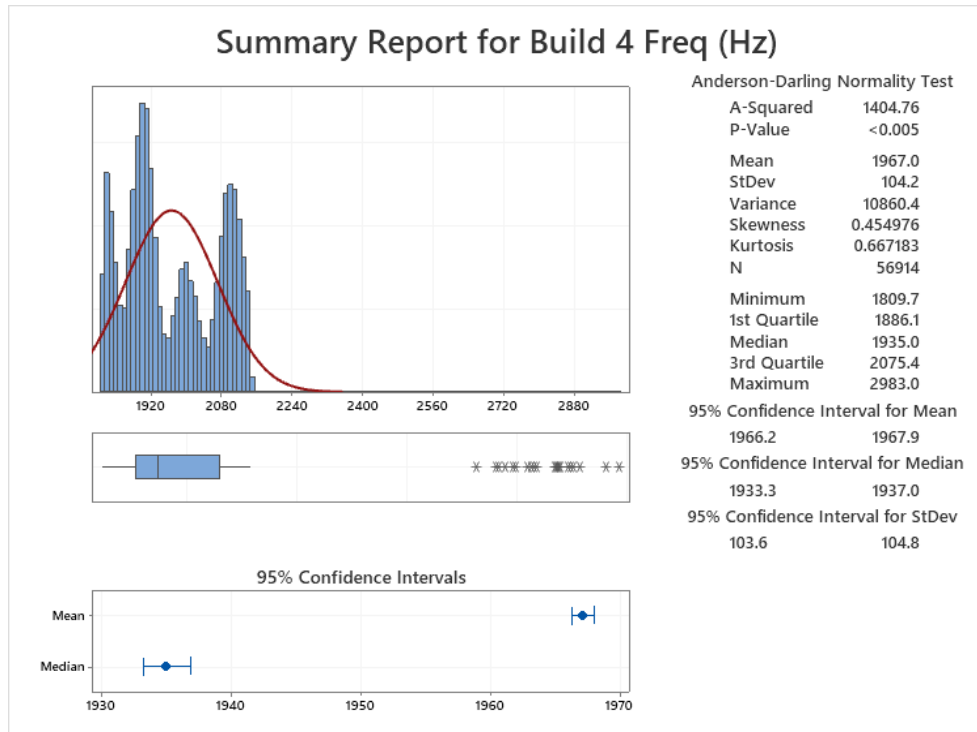


Figure 3.18: Descriptive statistical analysis for homemade system using Minitab - Build 4

3.4 Build 5

Build 5 involved producing standard ASTM Dogbone Tensile coupons at a 45° angle so that they could be tested in house. These coupons were used to determine the different downskin parameters that could be used. As such, they have no support structures within the main body of the coupon (smaller diameter middle section), as seen in Figure 3.19. These parts were unique in that on the surface they did not appear to have any visible defects or issues. The visual inspection deemed that these parts were satisfactory and may not have encountered any anomalous events during the build. According to the acoustic analysis there appeared to be a few events that were flagged for changes from baseline behavior. This analysis includes images gathered during the build as well as the acoustic data collected by the sensor system.

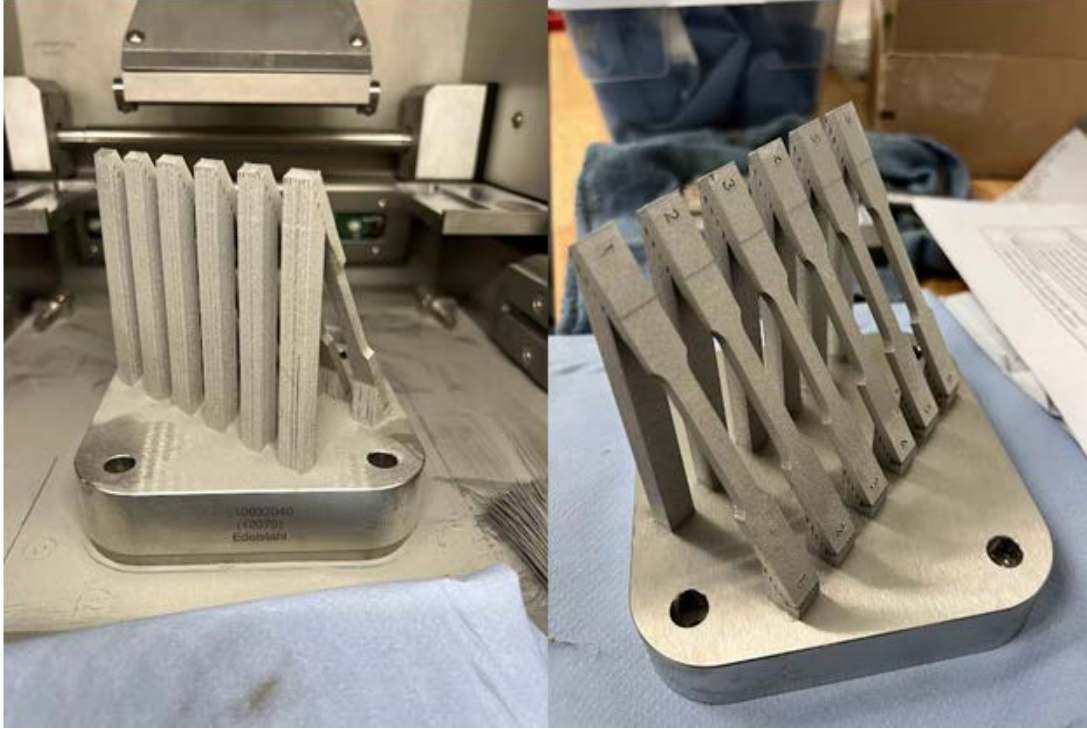


Figure 3.19: Build 5 tensile coupons printed at a 45° angle

The acoustic monitor was able to pick up distinct alerts at 3 separate time intervals from 0-27 minutes, 53-83 minutes, and 1397-1430 minutes. These intervals can be seen collectively in Figure 3.20 and correspond to layers 0-62, 113-177, and 2884-2954, respectively. These layers were pulled from the print log files by correlating the times with the layer height in the log. This method was also used to pull the images of the build, so that they could be compared with the acoustic analysis. Within these intervals, there are many potentials for an alarm to be raised as there could have been internal stresses, support structure movement, or crackage.

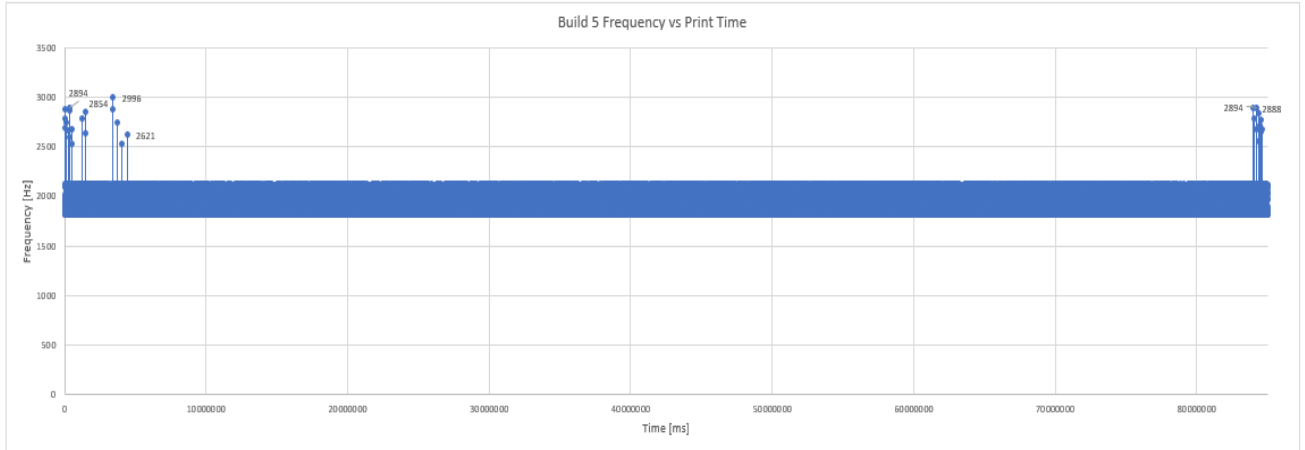


Figure 3.20: Build 5 frequency vs. print time plot (02-24-22)

When the plot was zoomed in to focus on the interval of 0-27 minutes, pictured in Figure 3.21, a few interesting points were observed. For one, the first few minutes seemed to have elicited a notable frequency response. These first few signals were most likely due to the initial exposure burn on the platen. These initial exposure burns are done to create a solid foundation for the parts to adhere properly and are often done with little powder on the bed, as seen in Figure 3.22. This limited powder creates a higher pitched noise than a regular powder-filled burn would and could explain the alerts generated during the first few minutes. Beginning around layer 17, a noticeable change in the appearance of the lasered images appears. As shown in Figure 3.23, seemingly sharp protrusions and darker shadows behind the parts start to appear. These protrusions are usually linked with damaging the recoater blade due to their height and naturally pointed structure. After a few layers, a visible line began to form on the left side of the build plate. Figure 3.24 outlines the streak formation in line with the third and fourth part from the right side of the plate. These streaks can lead to overall part failure as they increase in

size and spread throughout the recoater blade. It is apparent that the recoater has been damaged and will need to be replaced (Figure 3.25).

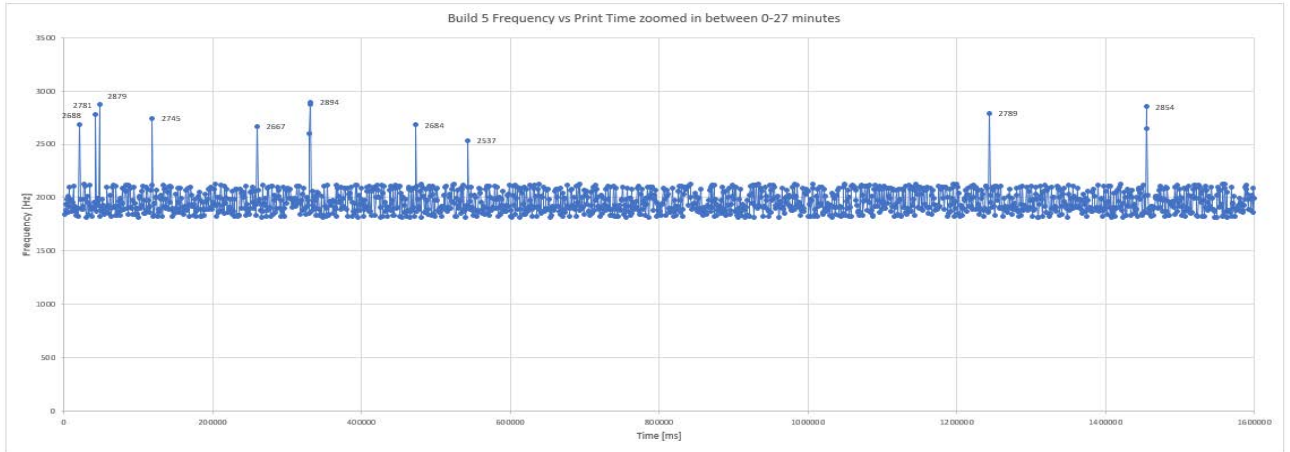


Figure 3.21: Build 5 frequency vs. print time zoomed in during 0-27 minutes (02-24-22)

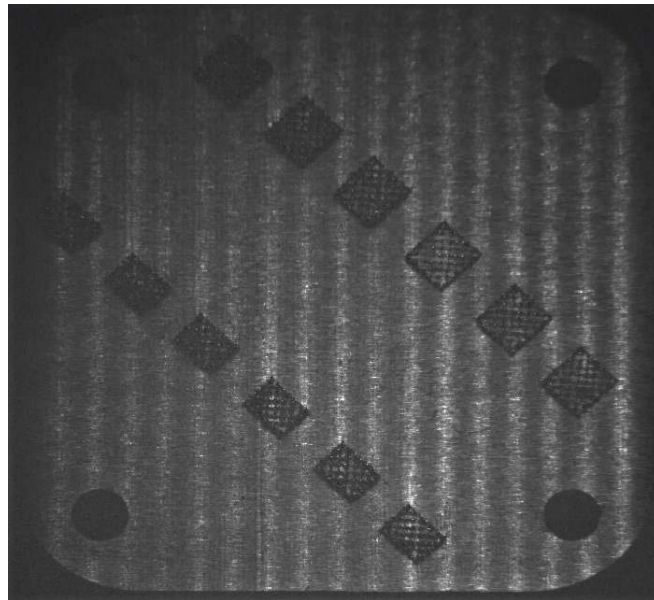


Figure 3.22: Build 5, Layer 5 Initial exposure burn with limited powder on bed

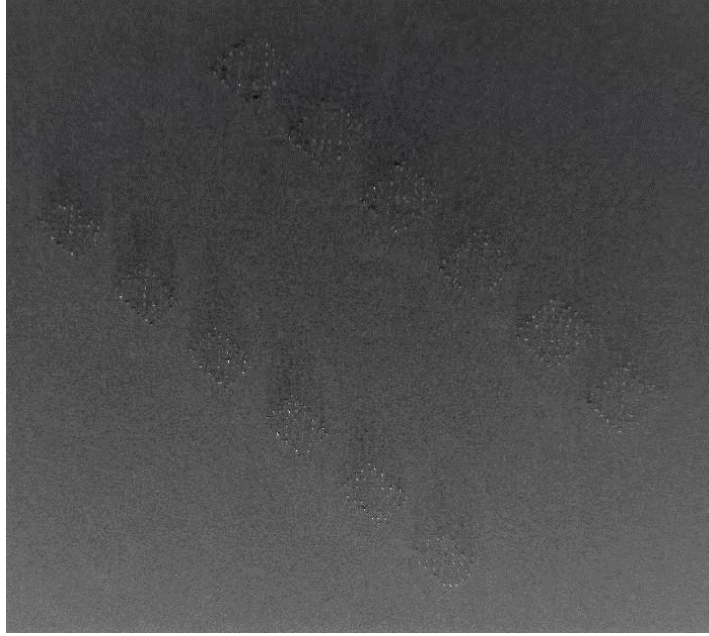


Figure 3.23: Build 5, Layer 17 sharp protrusions present creating shadows behind them

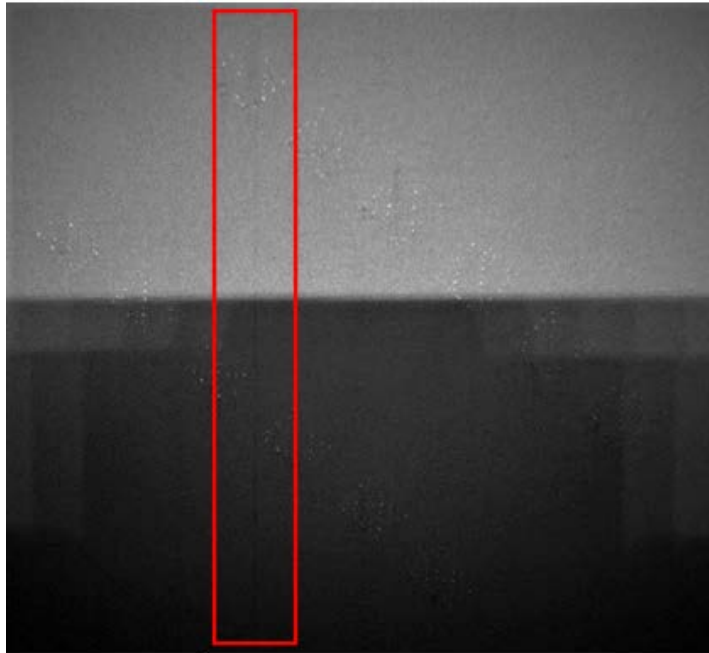


Figure 3.24: Build 5, Layer 36 first signs of rake deterioration with streak appearing

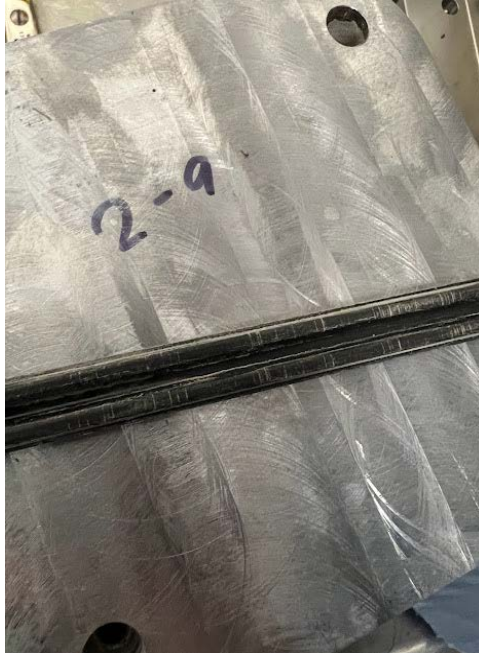


Figure 3.25: Damaged rubber recoater blade indicated by the lines filled with powder

Another interval that triggered a few responses was between the times of 53-83 minutes equating to layers 113-177. These layers were during the actual build of the parts with some sections still building support structures. From Figure 3.26, it can be deduced that there were a few notable pings that were registered within the software. When coupled with the images taken during this time, there are noticeable streaks that appear throughout the build plate, as seen in Figure 3.27. These streaks could have triggered some frequency response if an elongated support structure caused damage to the recoater blade and the underlying metal. In Figure 3.28, a few sections are highlighted to illustrate their change in height compared to the surrounding areas. These spots appear to be higher since they cast a faint shadow behind them on the powder. This intriguing phenomena is difficult to replicate as over time it sometimes self corrects these issues, potentially due to the particle grain distribution and natural flowability around the parts.

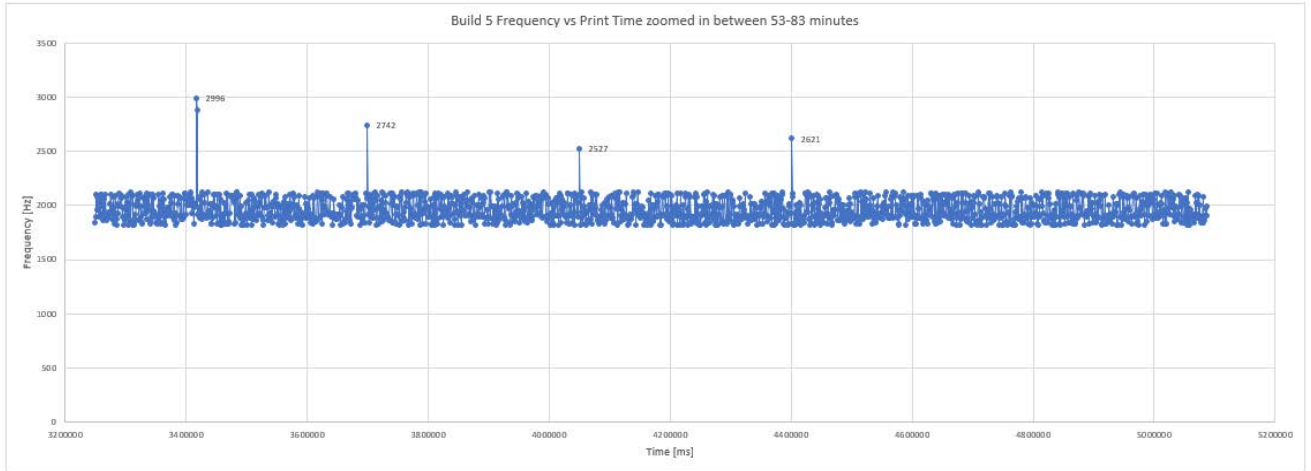


Figure 3.26: Build 5 frequency vs. print time zoomed in during 53-83 minutes (02-24-22)

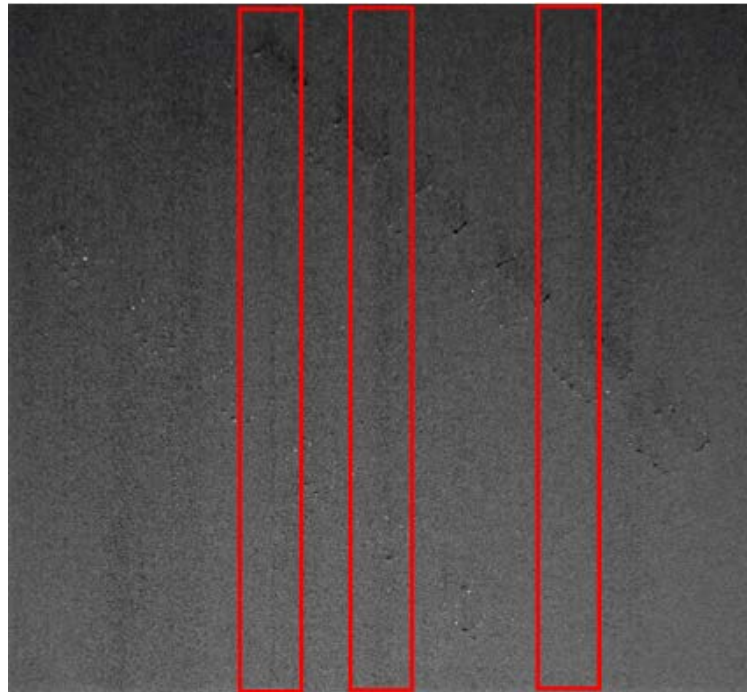


Figure 3.27: Build 5, Layer 131 multiple streaks present outlined in red showing locations that the recoated blade has been damaged

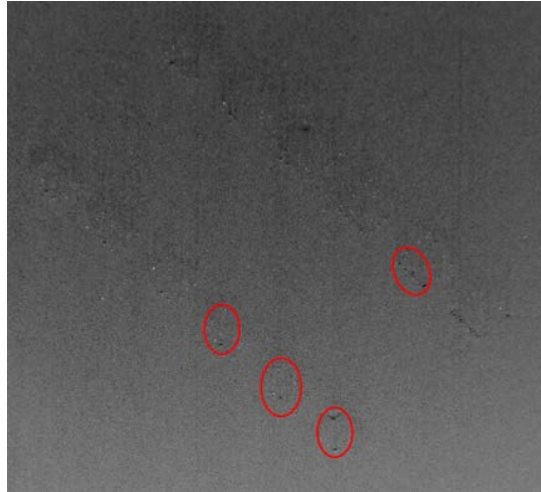


Figure 3.28: Build 5, Layer 153 distinct protrusions present near areas of streaking

The final period that was of notable interest occurred between 1397-1430 minutes. This particular section alerted more frequently than the previous segments and can be seen in Figure 3.29. By comparing the images taken, it was recorded that there were obvious signs of streaking on the build plate. These streaks were visible without much image enhancement in lighting or contrast. The image in Figure 3.30 highlights the various sized streaks as well as the shiny dots of what appears to be fused material projecting out of the powder layer. These dots most likely perpetuated the continual destruction of the recoater blade, as seen in Figure 3.25 previously.

Overall, this build seemed to complete properly without any visible surface defects or issues. From the side profile seen in Figure 3.31, minor discoloration can be seen from the transitional section between the upper radius and lower main body section. This is to be expected as the part goes from a larger mass to a smaller cross sectional area. The dissipation of heat can cause discoloration and, in this case, the discoloration is minor.

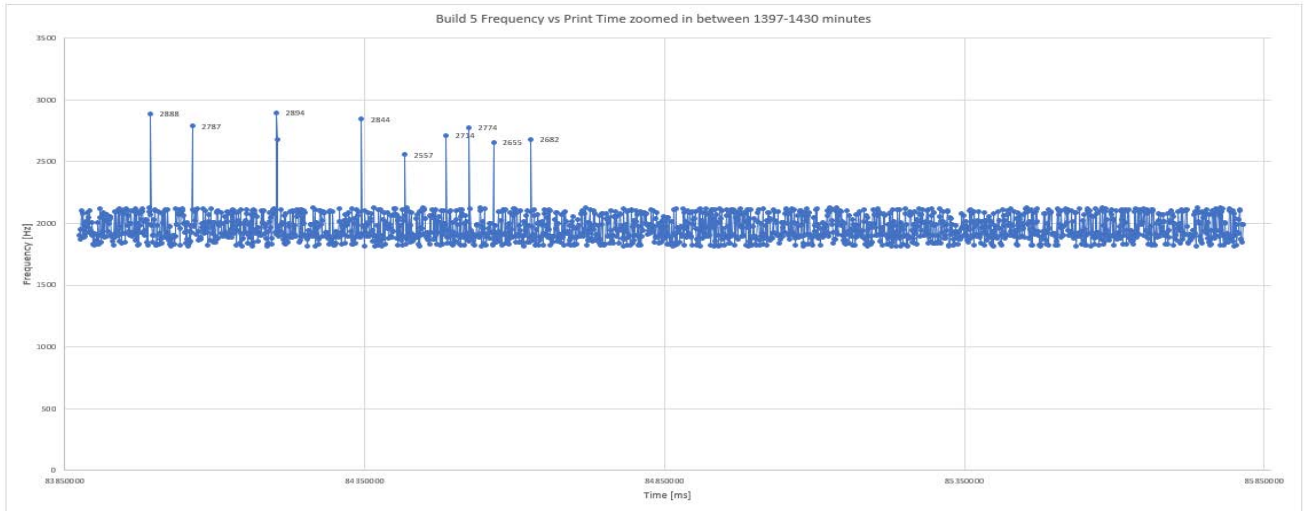


Figure 3.29: Build 5 frequency vs. print time zoomed in during 1397-1430 minutes (02-24-22)

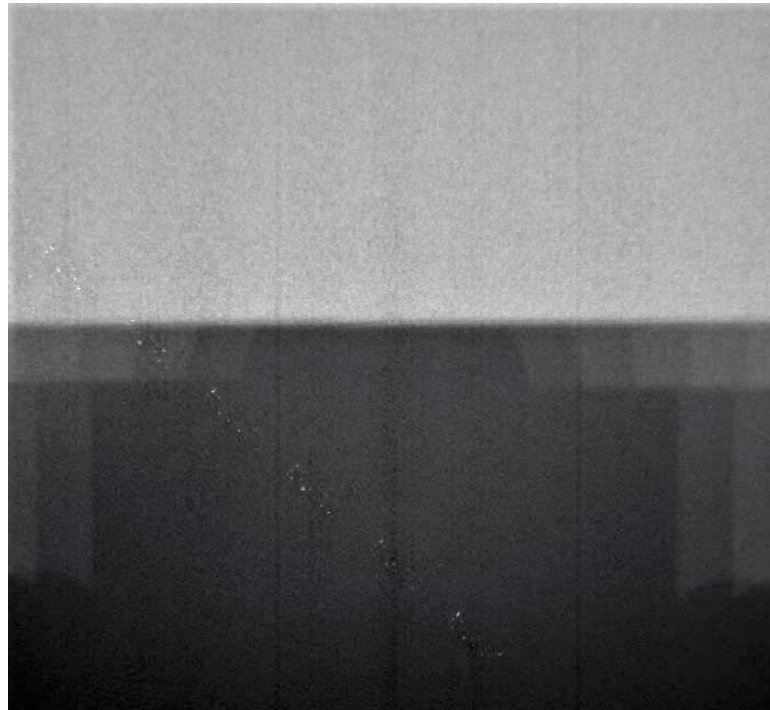


Figure 3.30: Build 5, Layer 2289 evident streaking and melted material protrusion from build plate



Figure 3.31: Side shot of Build 5 highlighting quality of build with minor discoloration at overhang

Statistical analysis was performed on Build 5's frequency response data. The resulting summary in Figure 3.33 helps solidify the interpretation of statistically significant events being recorded by the system. The continued twin peak data set can be seen well within this build and also correlates to the theory of stress relief during changes in diameter within the build. The frequency values that are above the standard deviation appear to be spread across a frequency range of 300 Hz. This may signify that there are different types of events occurring at these separate frequencies and it could be possible to dissect the parts and learn more from the internal microstructure correlating to the layers where these events took place.

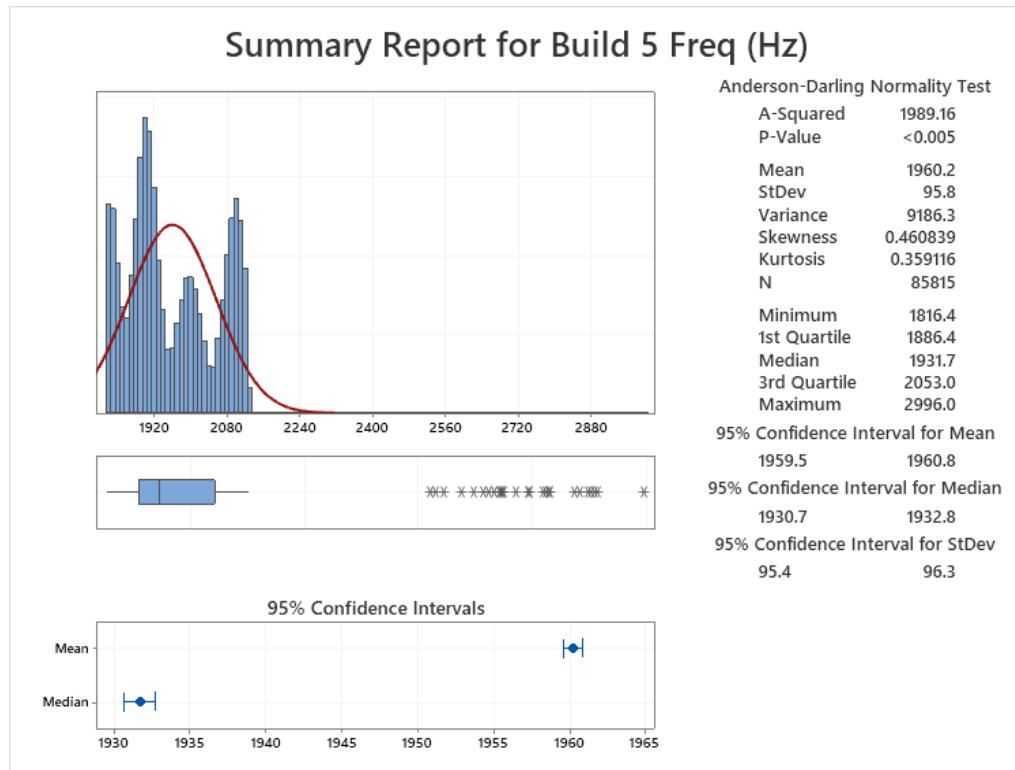


Figure 3.32: Descriptive statistical analysis for homemade system - Build 5 using Minitab

3.5 Build 6

It was deemed beneficial to the project to establish a baseline using a separate, independent acoustic monitoring system. The Kistler Lab-Amp 5165A4 system was chosen by a senior project group for an earlier project and has been mounted on the SLM 125 base plate in a strategic location seen in Figure 3.33. This system can provide very high sample rates (625 kSps) at input frequencies of up to 100 kHz. This system incorporates a Piezotron AE sensor as well as multiple accelerometers and has a built in data acquisition setup with real time statistics capabilities. Overall, this system is ideal for this type of data collection; however, the price tag makes this product an investment rather than a quick check solution.



Figure 3.33: Kistler DAQ system (Left), Mounting location under build plate for accelerometers and sound monitor (Right)

Build 6 was a repeat build using the same file as Build 3, excluding the welding coupons and the overlapped part files. This file was chosen as it previously printed well and was overall a short build that demonstrated many different stress tests for the LPBF process. The completed build can be seen in Figure 3.34 and illustrates the unique shapes and challenges that can be studied. After the parts were removed from the build plate it was observed that the benchys had major sagging issues on the unsupported overhangs (Figure 3.35). The intentional exclusion of support structures was intended to ease removal and turnover of the parts on the plate. The benchys were built on a 45° angle, but unfortunately this was not enough to maintain optimal part quality. This defect is particularly interesting as it is not something that the acoustic sensors would normally have the ability to detect. Unfortunately, with the setup used, it is unclear whether the sensors were able to distinctly identify the defect propagation using AE alone.

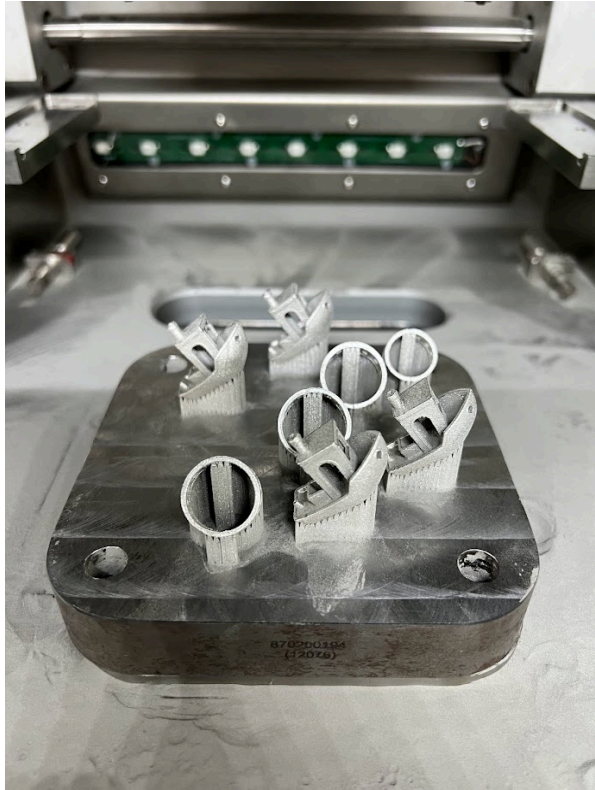


Figure 3.34: Build 6 benchys and rings comparison with Kistler System (3-14-22)

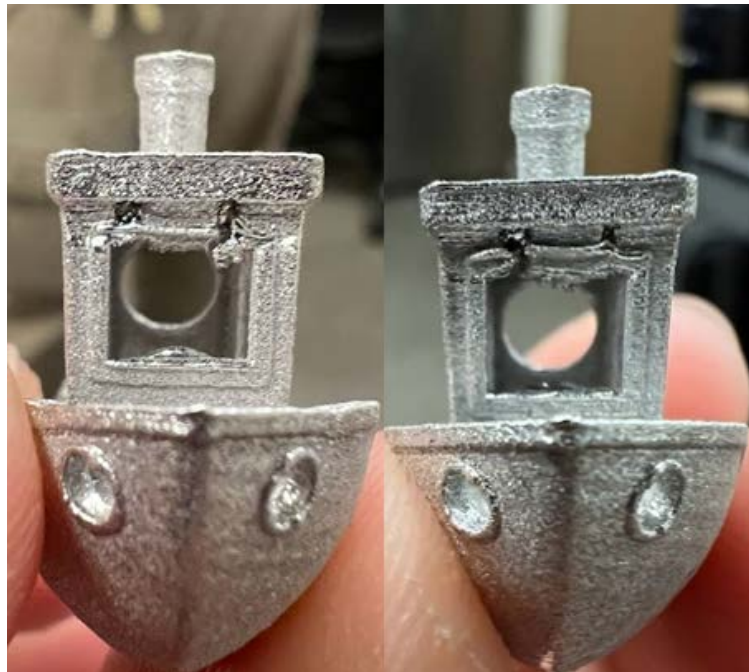


Figure 3.35: Picture of overhang failure on non-supported roof

Looking at the sensor plot in Figure 3.36, only a few instances are flagged for anomalous behavior. The first happens around 42 minutes and correlates with layers 91 and 92. This is near the top of the main support layers and may be an indication of support issues. This was compared with the Kistler data; however, it was inconclusive in determining if there was a similar response due to the noise present (Figure 3.37). As for the other two points that were also flagged in the original system, the Kistler Lab Amp also produced acceleration values that were higher than normal in those sections, but it cannot be attributed to detection of an anomaly due to the present noise within the sensitivity data. It is hard to compare the fidelity of the original system in this scenario, but it does show promise that the homemade system was able to pick up data points that are significantly different as compared to the competitor system. This could be due to lack of proper calibration of the Kistler system or the higher sensitivity response causing noise to be picked up much more easily. The two datasets that were collected occurred at 373 and 380 minutes, which corresponded to layers 790/791 and layers 812/813, respectively. These layers appear to be around the overhang issue that was seen in the previous images. To further validate the information gathered from the sound sensors, the in-situ images were pulled for this build and cross referenced with the time stamps of these points of interest.

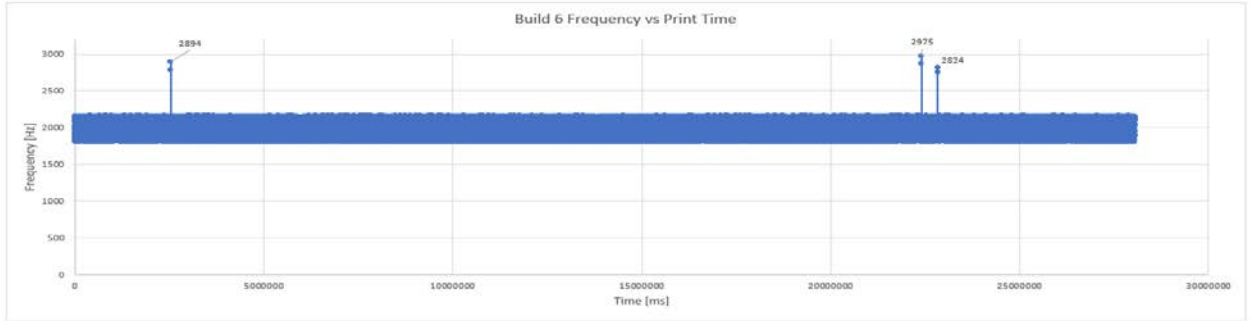


Figure 3.36: Build 6 frequency vs. print time plot (03-14-22)

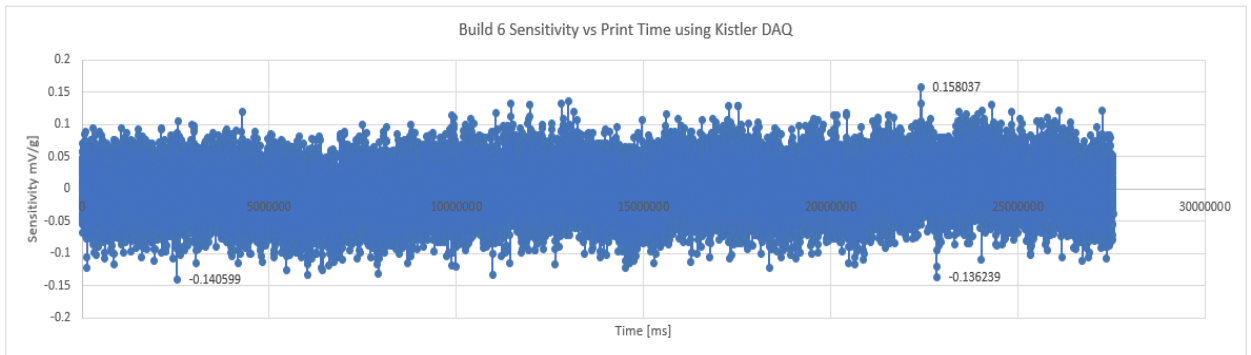


Figure 3.37: Build 6 sensitivity vs. print time plot (03-14-22)

As the acoustic data was compared to the images taken, a few critical anomalies were detected within the build. Starting off with Figure 3.38, this image was taken near the beginning of the build. This issue was not picked up by the acoustic sensors, but it was noticed when examining the images post-build. There is obvious streaking occurring and what appears to be solidified material extending above the powder layer, indicating impending damage to the recoater blade. The first noticeable acoustic event occurred at layers 91 and 92 and can be seen in Figure 3.39. In these images, there are multiple streaks present which appear to be causing deep troughs on the powder bed. This is also true in Figure 3.40, which displays layers 790 and 791 during the 373rd minute of the build. The next point is interesting in nature as it appears as though the streaking begins

to minimize and even out, as seen in Figure 3.41. This is recorded in the sensor system by reading a lower frequency ping for these particular layers.

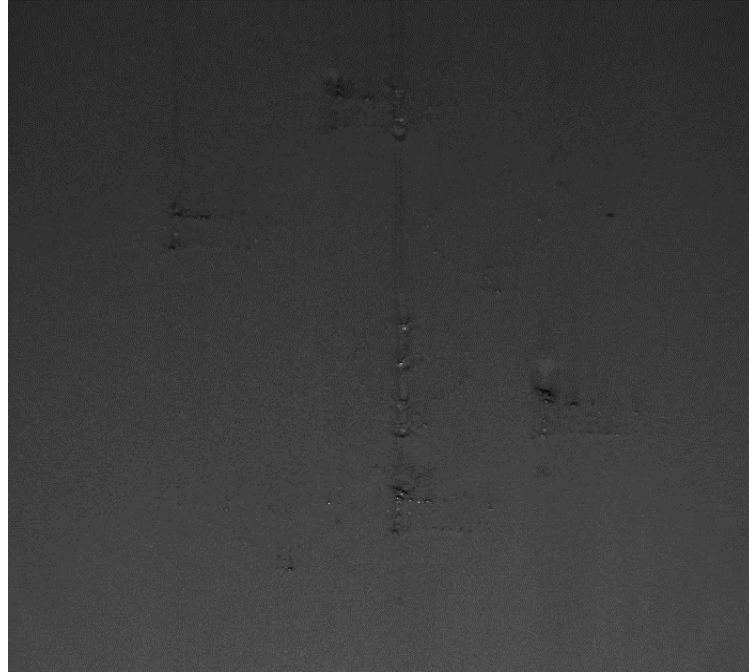


Figure 3.38: Build 6, Layer 47 prominent streaking visible in the middle of build plate

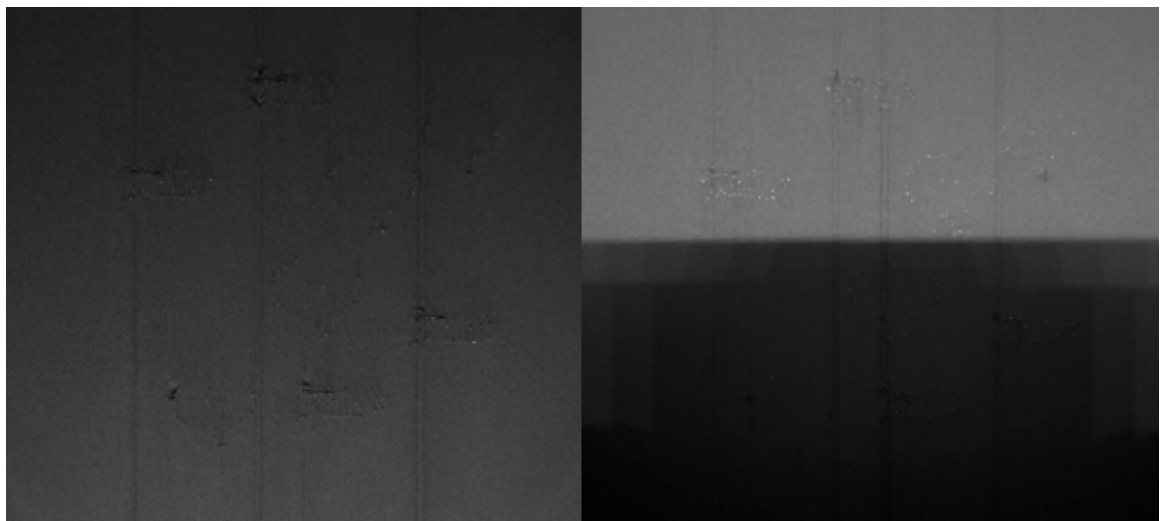


Figure 3.39: Build 6, Layers 91 and 92 illustrating streaking in multiple areas of the build as well as material protrusions from the powder

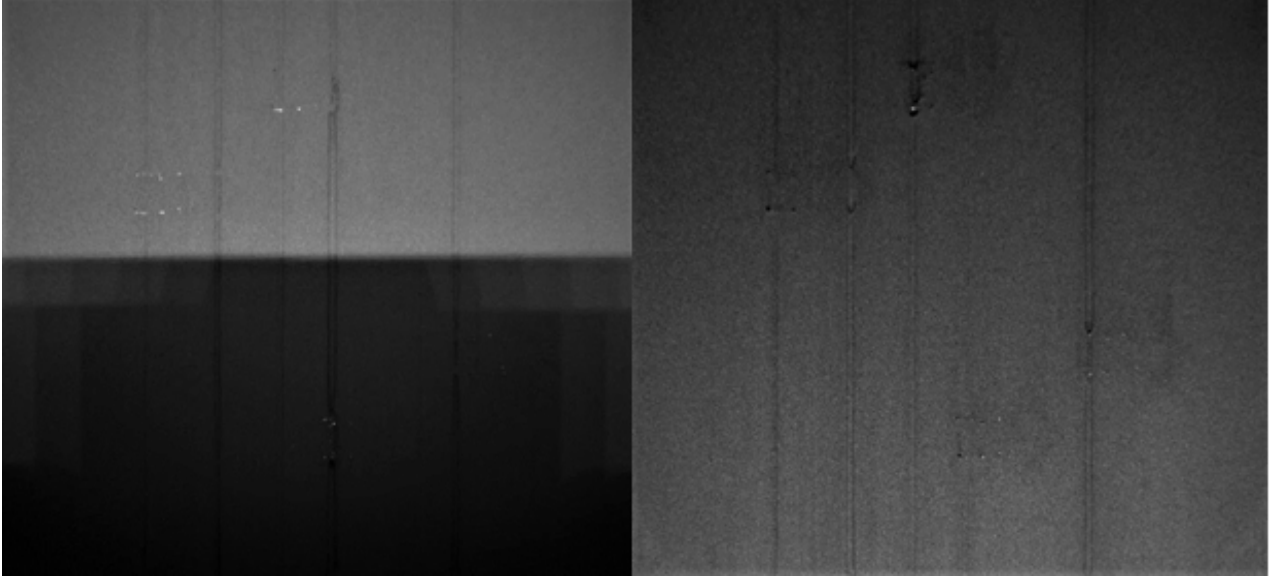


Figure 3.40: Build 6. Layers 790 and 791 streaks are more uniform in size and spread out throughout the build, there appears to be more areas of material protrusion

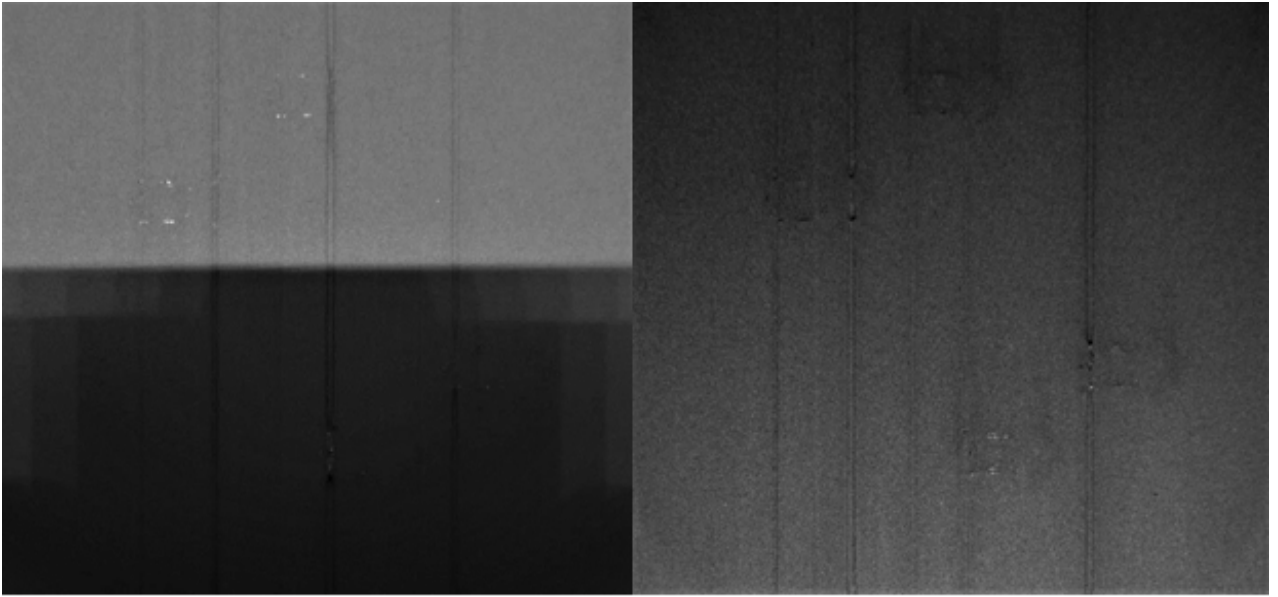


Figure 3.41: Build 6, Layers 812-813 minor anomaly detected, these layers appear to be the lower end of the benchy roof

The Kistler data was first converted into a frequency response so that it could be properly compared with the homemade system's original output. The frequencies for Build 6 were analyzed in Minitab to compare the descriptive statistics of the datasets from both the homemade and industrial systems, seen in Figure 3.42 and Figure 3.43. The frequency response for the Kistler system appears to be riddled with noise, which makes it difficult to draw meaningful conclusions from the statistical analysis. Nevertheless, the data was still analyzed, and since both datasets were not normally distributed, a Mann-Whitney nonparametric test was done to compare the differences between these independent datasets (Figure 3.44). The median for the Kistler system was 50 Hz and the median for the homemade system was 1931 Hz. Significant data outliers were found in both systems but at different frequency values. The data collected from the Kistler system suggests that the true frequency values were at least a magnitude lower than the values calculated by the homemade system. Although the homemade system may not be outputting the correct frequency values, this could be due to lack of proper tuning of the built-in potentiometer or calculation errors within the code.

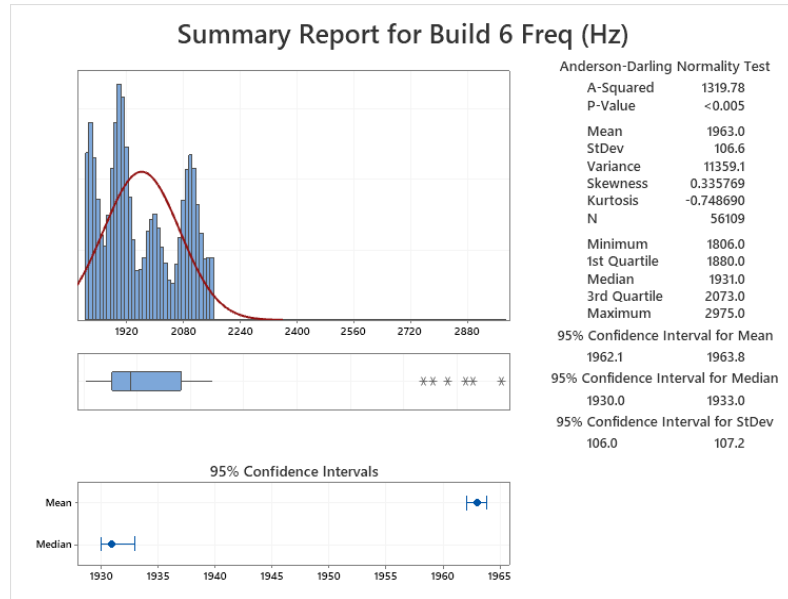


Figure 3.42: Descriptive statistical analysis for homemade system - Build 6 using Minitab

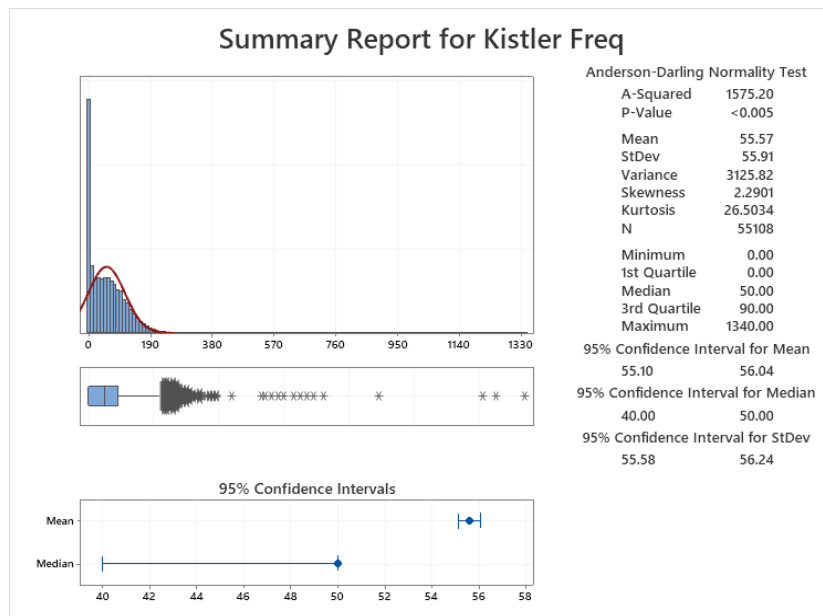


Figure 3.43: Descriptive statistical analysis for Kistler system - Build 6 using Minitab

Mann-Whitney: Build 6 Freq (Hz), Kistler Freq

Method

η_1 : median of Build 6 Freq (Hz)

η_2 : median of Kistler Freq

Difference: $\eta_1 - \eta_2$

Descriptive Statistics

Sample	N	Median
Build 6 Freq (Hz)	55108	1931
Kistler Freq	55108	50

Estimation for Difference

Difference	CI for Difference	Achieved Confidence
1895	(1894, 1896)	95.00%

Test

Null hypothesis $H_0: \eta_1 - \eta_2 = 0$

Alternative hypothesis $H_a: \eta_1 - \eta_2 \neq 0$

Method	W-Value	P-Value
Not adjusted for ties	4.55537E+09	0.0000
Adjusted for ties	4.55537E+09	0.0000

Figure 3.44: Mann-Whitney nonparametric test - Build 6 using Minitab

4. Defect Detection Analysis

4.1 Calibration Builds

To begin collecting viable data, a baseline was needed to establish the acoustics within the room during operation. The initial calibration builds helped to develop a baseline for the acoustics in the room. Although the accuracy of the system was still unknown, the baseline calibration builds helped shape the continued improvement of the system and its necessary user options. With the data generated, a reasonable baseline standard frequency was established between 1750-2100 Hz during normal operating procedures. Slight deviations were observed while things were being moved around in the room and when metal objects were struck together in the nearby vicinity. By understanding the operational conditions of a particular room, a system similar to this can be calibrated and tuned to minimize the range of frequencies that are analyzed and to improve the capability of the hardware.

4.2 Acoustic Analysis

After a build was completed, the acoustic data was collected and uploaded to a cloud server. This server has the potential to be automated to pull the data and run it through an analysis algorithm that would notice any anomalies within the build and be able to alert the user in real time. Currently, this is beyond the scope of this project and therefore has not been fully implemented. However, the current acoustic analysis was optimally completed by using excel macros that can take data and prepopulate it into a form that creates a visual graph.

To compare the Kistler data to the Arduino signal processing, the data needed to be processed using Discrete Fourier transform. This was accomplished using an Excel plugin that enabled handling of large datasets. The resulting frequencies were then plotted using Minitab to generate the frequency response plot seen in Figure 4.1, which was representative of the response provided by the Kistler system. From the chart, a main peak can be seen at a value near zero indicating no significant frequency response for a majority of the build. Another peak is also present at a value near 60-75 Hz, which may indicate the natural resting frequency of the SLM printer. The frequencies registered by the Kistler system were much lower than the homemade system and it can be presumed that the homemade system was not fully calibrated to proper frequency. Instead, it was baselined with the standard potentiometer settings provided by the Devmo supplier.

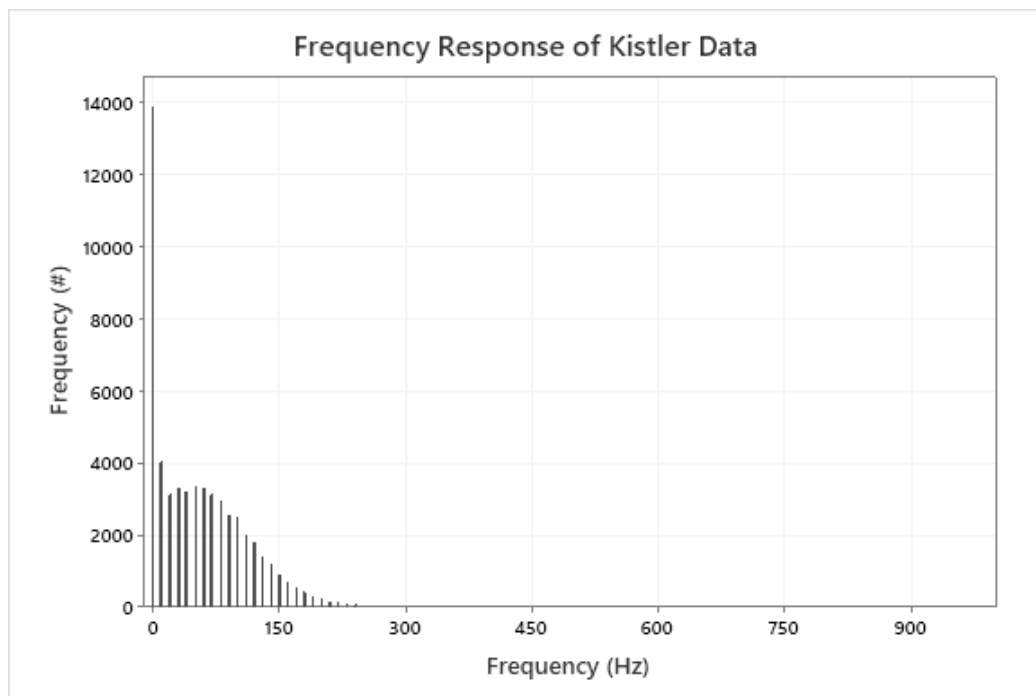


Figure 4.1: Frequency response plot using Discrete Fourier Transform analysis

Once the data was processed a statistical analysis was performed to determine the significance of the data differences in acoustic frequency values. As the data was processed in Minitab, its p-value, shape, and standard deviation were evaluated for statistical significance, patterns, and similarities, respectively. The p-value ($p < 0.005$) for each analysis was found to be statistically significant, which means that the data was not normally distributed, so a nonparametric analysis was conducted. The standard deviation remained very similar within the builds on the homemade system between 90-110 Hz, while the Kistler system's standard deviation was near 56 Hz. The flagged anomalies were each at least 3 standard deviations higher in frequency than the baseline. These values were found to have some correlation with layer count at which an anomaly occurred, but not necessarily the exact layer that it was first seen. Unfortunately, this does not yield a successful detection because the inability to accurately pinpoint a potential defect leaves much to be understood. A correlation analysis was performed between the Kistler system and the homemade system. Although the data was visually similar, the magnitude difference resulted in no linear correlation between the two systems. Therefore, a comparable baseline could not be established without more tuning of the original system so that it may correlate to the Kistler product properly.

4.3 Image Analysis

Along with the acoustic data collected, a few builds had images taken throughout the 3D printing process. These images were used to confirm the accuracy of any anomaly detections alerted by the sensor system. This two-factor point of reference increases confidence in the data being recorded. The image analysis methodology can be automated and optimized; however, in this experiment it was only used as a complement to the acoustic data collection. The in-situ images helped to provide an in-depth visual of the build plate as the anomalies were being detected, which significantly aided in the interpretation of the data post-build.

4.4 Experimental Setup Evaluation

The design of the experimental hardware considered the many complexities of a laser bed fusion machine; however, there were many complications that were unavoidable. Although the ambient room noise level was expected, the overall location of the machine allowed outside noise pollution to potentially interfere with the experiment. There were also many drawbacks to not fully automating the system; for example, it would collect data well past the build end time, which required further processing to trim the data back down to within the limitations of the build. Overall, the homemade sensor system operated well near the door, and its location did not interfere with the printer's normal operating procedures.

5. Conclusion

5.1 Analysis Summary

By comparing the different analysis methodologies conducted, a difference was found between the homemade and purchased system. This differentiation is due to the fidelity of the purchased system, as it was much more sensitive in detecting the slightest changes in frequency. However, they could not be compared on their effectiveness in detecting anomalies. The homemade system was able to detect potential anomalies within a build, but since the Kistler system has a much finer resolution, it detected more noise. When first analyzing the frequency responses of the builds, the Kistler data did not appear to have a significant peak past 0 Hz. Upon further investigation, a peak could be seen near the 60 Hz range, indicating that this could be a possible baseline value that correlates with the electrical frequency of the SLM. Overall, the other builds demonstrated multiple peaks within their statistical analysis, which may coincide with electrical ambient noise, the movement of the recoater blade, the initialization of the laser, or background noise pertaining to the location of the sensors. The FFT analysis is a breakthrough in signal processing and allows in-situ monitoring to become feasible on a larger scale. The real time processing of data can functionally be done on a small scale using a homemade system. However, the Kistler system requires much more back end processing power which may deter the effectiveness of the increased overall fidelity of this system.

5.2 Future Recommendations

Any good experiment should be continuously improved upon and adapted for different use cases. This system was designed with continuous improvement in mind through the use of off-the-shelf equipment and parts. The open-source code is simple to manipulate and calibrate. Future iterations of this experiment would benefit from adding different types of sensors, changing mounting locations, and incorporating machine learning.

First off, the system can be improved by using higher quality microphones or increasing the number of sensors available to take data during the build. By increasing the number of sensors, the chance of detecting anomalies increases, but the complexity of the system also increases. Incorporating a variety of different sensors, such as vapor, vibration, or spectrometry, may also increase analysis potential which could be beneficial to the overall understanding of the parts being produced. A decision would need to be made to determine whether the added complexity would be beneficial to the consumer and how it can be automated to self-regulate and calibrate each sensor.

Secondly, there could be improvements to how the sensors are mounted to the machine. They currently sit on the outside of the machine and are limited in their operation potential due to the obstruction of a door between the build chamber and the sensor. If there could be a way to mount the sensors inside of the build chamber through wireless methods while still maintaining the precision required to detect issues within a build, this would be great improvement to this system.

Finally, the incorporation of neural network or machine learning approaches would greatly increase the speed and fidelity of this overall process. To do this properly, first a baseline of good and bad parts each with examples of acceptable and nonacceptable defects needs to be created. To do this, a single part incorporating many different types of defects at different levels will need to be developed. After gathering data from multiple builds (25-50), an algorithm can be trained to decipher between allowable and rejectable defects. Future studies could attempt to incorporate feed forward or feedback modification of the build to correct potential issues during a build or apply corrective actions to fix an impending issue.

5.3 Conclusion

This experiment provided a large amount of insight into the different nuances of in-situ monitoring techniques. Currently, the standard does not exist for this new and emerging technology. Therefore, there will continue to be advancements and growth in this field. For an industry to continue to create and innovate, they will need to grow and adapt to processes that also learn and grow with them. Cost-effective solutions may not be necessary in equipment used in multi-million-dollar operations, but as they begin to trickle down into the consumer field, there will be a need for more affordable, modular systems for defect detection. The emphasis of this project was to develop a user-friendly, cost-effective alternative to image analysis methods that can be adaptable for a multitude of technologies and equipment. To be viable in a large-scale consumer base, the technology must not only be cost-effective, but also modular to fit the continued advancements in the small-scale machinery. Steps were taken to create a system that can

function on a much more complex machine as well as transfer to a smaller, less complex device.

One of the main findings from this experiment was that AE monitoring technology appears to be more fitting for situations of monitoring qualitative characteristics, such as surface quality and roughness, as opposed to image analysis. It can be deduced that when a build was operating smoothly, the sensors maintained a baseline frequency range, which correlated with a good quality surface roughness. For situations in which high fidelity and confidence is required in a build, there are much better alternatives such as thermal and optical tomography. The main drawbacks to these systems continue to be the large amount of data produced and their overall costs. If a simple system is required for quick validation or immediate operator alerts, the aforementioned sensor suite can be modified to fit many different types of applications not only in the additive manufacturing industry, but also in most other manufacturing settings.

References

- Avnet. (2021). Piezoelectric pressure sensors. Avnet Abacus. Retrieved February 21, 2022, from <https://www.avnet.com/wps/portal/abacus/solutions/technologies/sensors/pressure-sensors/core-technologies/piezoelectric/>
- Carter, L. N., Martin, C., Withers, P. J., & Attallah, M. M. (2014). The influence of the laser scan strategy on grain structure and cracking behaviour in SLM powder-bed fabricated nickel superalloy. *Journal of Alloys and Compounds*, 615, 338-347. doi:10.1016/j.jallcom.2014.06.172
- Comparing MEMS and Electret condenser (ECM) microphones. CUI Devices. (2019, January 8). Retrieved February 21, 2022, from <https://www.cuidevices.com/blog/comparing-mems-and-electret-condenser-microphones#electret-condenser-microphone-basics>
- Condenser microphone. Teach Me Audio. (2022). Retrieved February 21, 2022, from <https://www.teachmeaudio.com/recording/microphones/condenser-microphone#:~:text=Condenser%20microphones%20operate%20on%20an,plates%20to%20help%20generate%20sound.&text=When%20a%20sound%20wave%20hits,an%20electrical%20characteristic%20called%20capacitance>
- Coria, A., Whipple, J., & Grant, S. (2017, June 10). Additive Manufacturing Part Failure Detection. digitalcommons.calpoly.edu. Retrieved May 15, 2022, from

<https://digitalcommons.calpoly.edu/cgi/viewcontent.cgi?article=1420&context=mesp>

Craeghs, T., Clijsters, S., Kruth, J., Bechmann, F., & Ebert, M. (2012). Detection of Process Failures in Layerwise Laser Melting with Optical Process Monitoring. *Physics Procedia*, 39, 753-759. doi:10.1016/j.phpro.2012.10.097

Dynamic microphone. Teach Me Audio. (2022). Retrieved February 21, 2022, from <https://www.teachmeaudio.com/recording/microphones/dynamic-microphone>

EOS. (2021). 3D printing software for monitoring and Quality Assurance. 3D printing software for monitoring and quality assurance. Retrieved February 21, 2022, from <https://www.eos.info/en/additive-manufacturing/software-3d-printing/monitoring-software>

Everton, S., Hirsch, M., Stravroulakis, P., Leach, R., and Clare, A., "Review of In-Situ Process Monitoring and In-Situ Metrology for Metal Additive Manufacturing," *Materials and Design*, no. 95, pp. 431-445, 2016.

Grans, S. (2020). Visualizing point clouds with RViz2 and python. Visualizing point clouds with RViz2 and Python – Sebastian Grans – The curious chemist & computer scientist. Retrieved February 21, 2022, from <http://sebastiangrans.github.io/Visualizing-PCD-with-RViz/>

Grasso, M., & Colosimo, B. M. (2017). Process defects and in situ monitoring methods in metal powder bed fusion: A review. *Measurement Science and Technology*, 28, 4th

ser. Retrieved November 3, 2020, from

<https://iopscience.iop.org/article/10.1088/1361-6501/aa5c4f/meta>

Khanzadeh, M., Tian, W., Yadollahi, A., Doude, H. R., Tschopp, M. A., & Bian, L.

(2018). Dual process monitoring of metal-based additive manufacturing using tensor decomposition of thermal image streams. *Additive Manufacturing*, 23, 443-456. doi:10.1016/j.addma.2018.08.014

Ko, H., Witherell, P., Lu, Y., Kim, S., & Rosen, D. W. (2020). Machine Learning and Knowledge Graph based Design Rule Construction for Additive Manufacturing.

Additive Manufacturing, 101620. doi:10.1016/j.addma.2020.101620

Koeppe, A., Padilla, C. A., Voshage, M., Schleifenbaum, J. H., & Markert, B. (2018).

Efficient numerical modeling of 3D-printed lattice-cell structures using neural networks. *Manufacturing Letters*, 15, 147-150. doi:10.1016/j.mfglet.2018.01.002

Li Z, Liu X, Wen S, He P, Zhong K, Wei Q, Shi Y, Liu S. In Situ 3D Monitoring of

Geometric Signatures in the Powder-Bed-Fusion Additive Manufacturing Process via Vision Sensing Methods. *Sensors*. 2018; 18(4):1180.

<https://doi.org/10.3390/s18041180>

McCann, R., Obeidi, M. A., Hughes, C., McCarthy, É., Egan, D. S., Vijayaraghavan, R.

K., Joshi, A. M., Acinas Garzon, V., Dowling, D. P., McNally, P. J., & Brabazon, D. (2021). In-situ sensing, process monitoring and machine control in Laser

Powder Bed Fusion: A Review. *Additive Manufacturing*, 45, 102058.

<https://doi.org/10.1016/j.addma.2021.102058>

Razvi, S. S., Feng, S., Narayanan, A., Lee, Y. T., & Witherell, P. (2019). A Review of Machine Learning Applications in Additive Manufacturing. *Volume 1: 39th Computers and Information in Engineering Conference*. doi:10.1115/detc2019-98415

Renken, V., Albinger, S., Goch, G., Neef, A., & Emmelmann, C. (2017). Development of an adaptive, self-learning control concept for an additive manufacturing process. *CIRP Journal of Manufacturing Science and Technology*, 19, 57-61. doi:10.1016/j.cirpj.2017.05.002

Sadowsky, J. (1994). THE CONTINUOUS WAVELET TRANSFORM: A TOOL FOR SIGNAL INVESTIGATION AND UNDERSTANDING. *Johns Hopkins APL Technical Digest*, 306-318. Retrieved November 3, 2020, from https://www.researchgate.net/publication/2437352_The_Continuous_Wavelet_Transform_and_Variable_Resolution_Time-Frequency_Analysis

Shevchik, S., Kenel, C., Leinenbach, C., & Wasmer, K. (2018). Acoustic emission for in situ quality monitoring in additive manufacturing using spectral convolutional neural networks. *Additive Manufacturing*, 21, 598-604. doi:10.1016/j.addma.2017.11.012

- Shevchik, S. A., Masinelli, G., Kenel, C., Leinenbach, C., & Wasmer, K. (2019). Deep Learning for In Situ and Real-Time Quality Monitoring in Additive Manufacturing Using Acoustic Emission. *IEEE Transactions on Industrial Informatics*, 15(9), 5194-5203. doi:10.1109/tii.2019.2910524
- Strantza, M., Hemelrijck, D. V., Guillaume, P., & Aggelis, D. G. (2017). Acoustic emission monitoring of crack propagation in additively manufactured and conventional titanium components. *Mechanics Research Communications*, 84, 8-13. doi:10.1016/j.mechrescom.2017.05.009
- Swartz, P. "Evaluation of Tensile Properties for Selective Laser Melted 316L Stainless Steel and the Influence of Inherent Process Features on Static Performance," 2019.
- Twilight-Global. (2022). What is powder bed fusion? process definition and advantages. TWI. Retrieved February 21, 2022, from <https://www.twi-global.com/technical-knowledge/faqs/what-is-powder-bed-fusion>
- Wang, T., Kwok, T., Zhou, C., & Vader, S. (2018). In-situ droplet inspection and closed-loop control system using machine learning for liquid metal jet printing. *Journal of Manufacturing Systems*, 47, 83-92. doi:10.1016/j.jmsy.2018.04.003
- Zhang, W., Mehta, A., Desai, P. S., & Higgs, C. (2017, August). Machine learning enabled powder spreading process map for metal additive manufacturing (AM). In *Int. Solid Free Form Fabr. Symp.* Austin, TX (pp. 1235-1249).

Zhu, Z., Ferreira, K., Anwer, N., Mathieu, L., Guo, K., & Qiao, L. (2020). Convolutional Neural Network for geometric deviation prediction in Additive Manufacturing.

Procedia CIRP, 91, 534-539. doi:10.1016/j.procir.2020.03.108

Wang, X. Cal Poly AMUG 2019 Presentation, 2019.

Wanhammar, L. (2007, September 2). Digital Signal Processing. DSP Integrated Circuits.

Retrieved May 25, 2022, from

<https://www.sciencedirect.com/science/article/pii/B9780127345307500039>

12 acoustic sensors. National Tsing Hua University. (n.d.). Retrieved February 21, 2022,

from <http://mx.nthu.edu.tw/~yucsu/3271/p08.pdf>

Appendix A. Arduino Code

```
/*  
File/Sketch Name: AudioFrequencyDetectorV2.0  
  
Version No.: v2.0 Created September 6, 2021  
  
Description: This code/sketch makes displays the approximate frequency of the loudest  
sound detected by a sound detection module. For this project, the analog output from the  
sound module detector sends the analog audio signal detected to A0 of the Arduino Uno.  
The analog signal is sampled and quantized(digitized). A Fast Fourier Transform (FFT) is  
then performed on the digitized data. The FFT converts the digital data from the  
approximate discrete-time domain result. The maximum frequency of the approximate  
discrete-time domain result is then determined and displayed via the Arduino IDE Serial  
Monitor.  
  
Preface: The arduinoFFT.h library needs to be added to the Arduino IDE before  
compiling and uploading this script/sketch to an Arduino.  
  
*/  
  
#include "arduinoFFT.h"  
  
#define SAMPLES 128 //SAMPLES-pt FFT. Must be a base 2 number.  
#define SAMPLING_FREQUENCY 4000 //Ts = Based on Nyquist, must be 2 times the  
highest expected frequency.  
  
arduinoFFT FFT = arduinoFFT();  
  
unsigned int samplingPeriod;  
unsigned long microSeconds;  
unsigned long myTime;  
  
double vReal[SAMPLES]; //create vector of size SAMPLES to hold real values  
double vImag[SAMPLES]; //create vector of size SAMPLES to hold imaginary values  
  
void setup()  
{  
  Serial.begin(115200); //Baud rate for the Serial Monitor  
  samplingPeriod = round(1000000*(1.0/SAMPLING_FREQUENCY)); //Period in  
  microseconds  
}  
void loop()
```

```

{
  /*Sample SAMPLES times*/
  for(int i=0; i<SAMPLES; i++)
  {
    microSeconds = micros(); //Returns the number of microseconds since the
    Arduino board began running the current script.

    vReal[i] = analogRead(0); //Reads the value from analog pin 0 (A0), quantize it and
    save it as a real term.
    vImag[i] = 0; //Makes imaginary term 0 always

    /*remaining wait time between samples if necessary*/
    while(micros() < (microSeconds + samplingPeriod))
    {

    }
  }

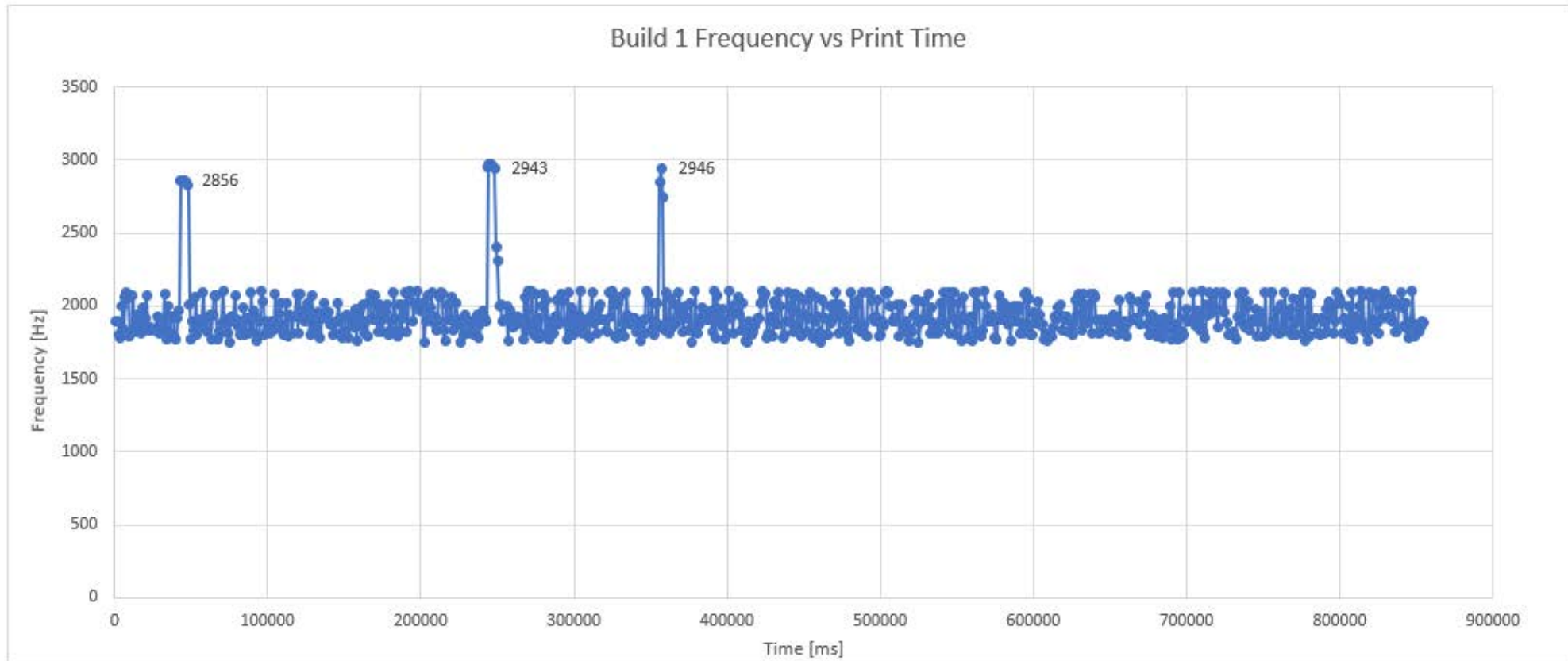
  /*Perform FFT on samples*/
  FFT.Windowing(vReal, SAMPLES, FFT_WIN_TYP_HAMMING,
  FFT_FORWARD);
  FFT.Compute(vReal, vImag, SAMPLES, FFT_FORWARD);
  FFT.ComplexToMagnitude(vReal, vImag, SAMPLES);

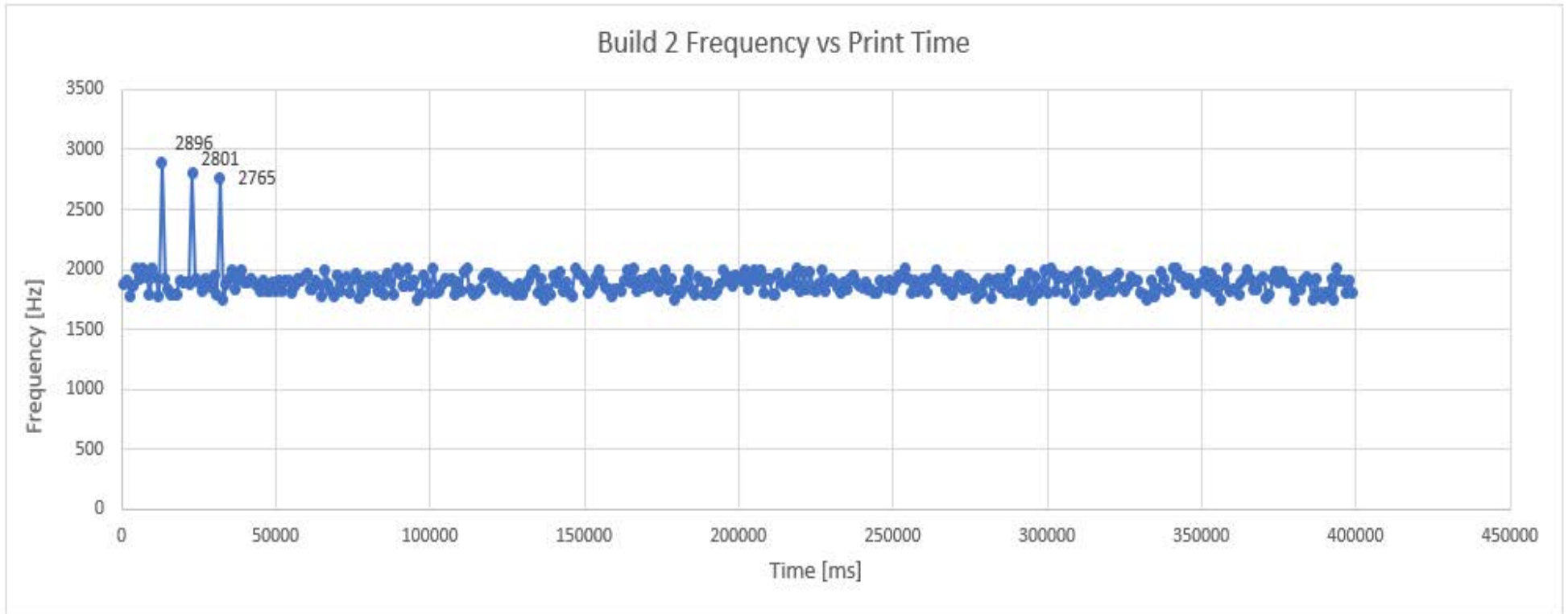
  /*Find peak frequency and print peak*/
  double peak = FFT.MajorPeak(vReal, SAMPLES, SAMPLING_FREQUENCY);

  //Print out the most dominant frequency.
  myTime = millis();
  Serial.print("Time:");
  Serial.print(myTime);
  Serial.print(":");
  Serial.print("Freq:");
  Serial.println(peak);
}

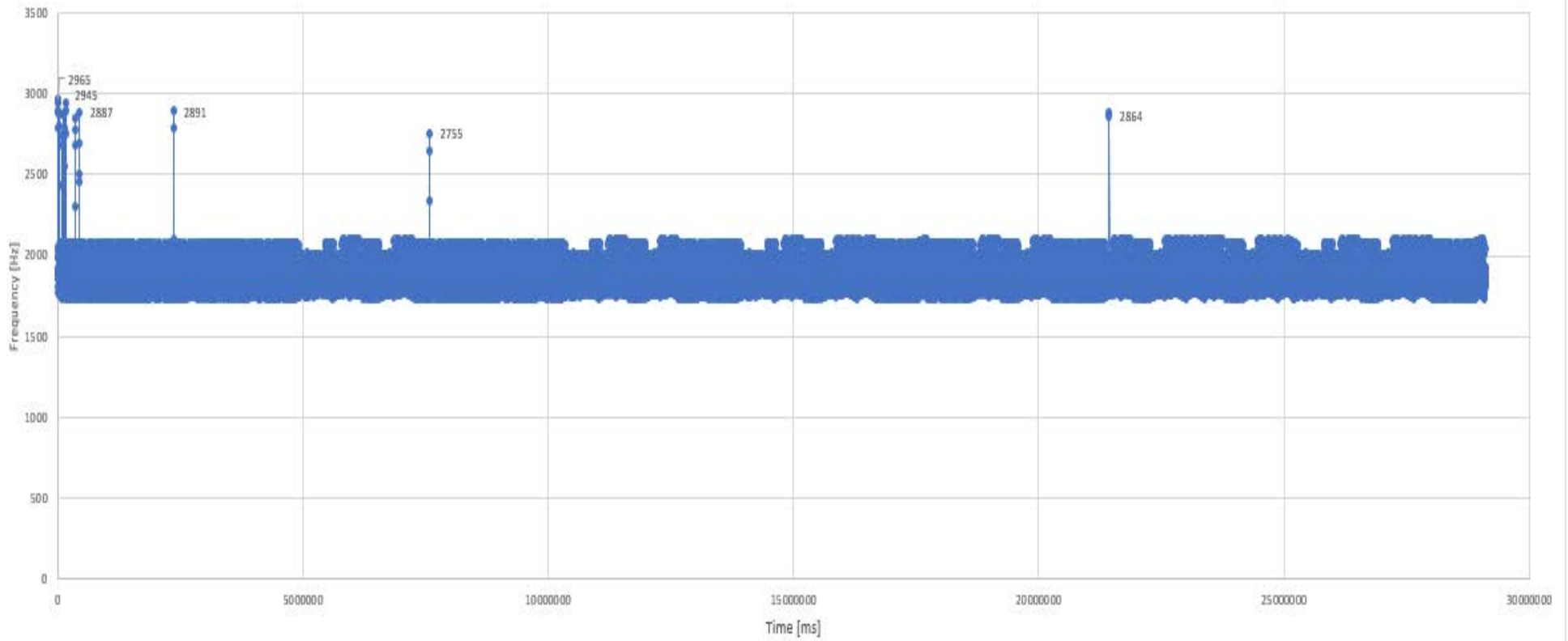
```

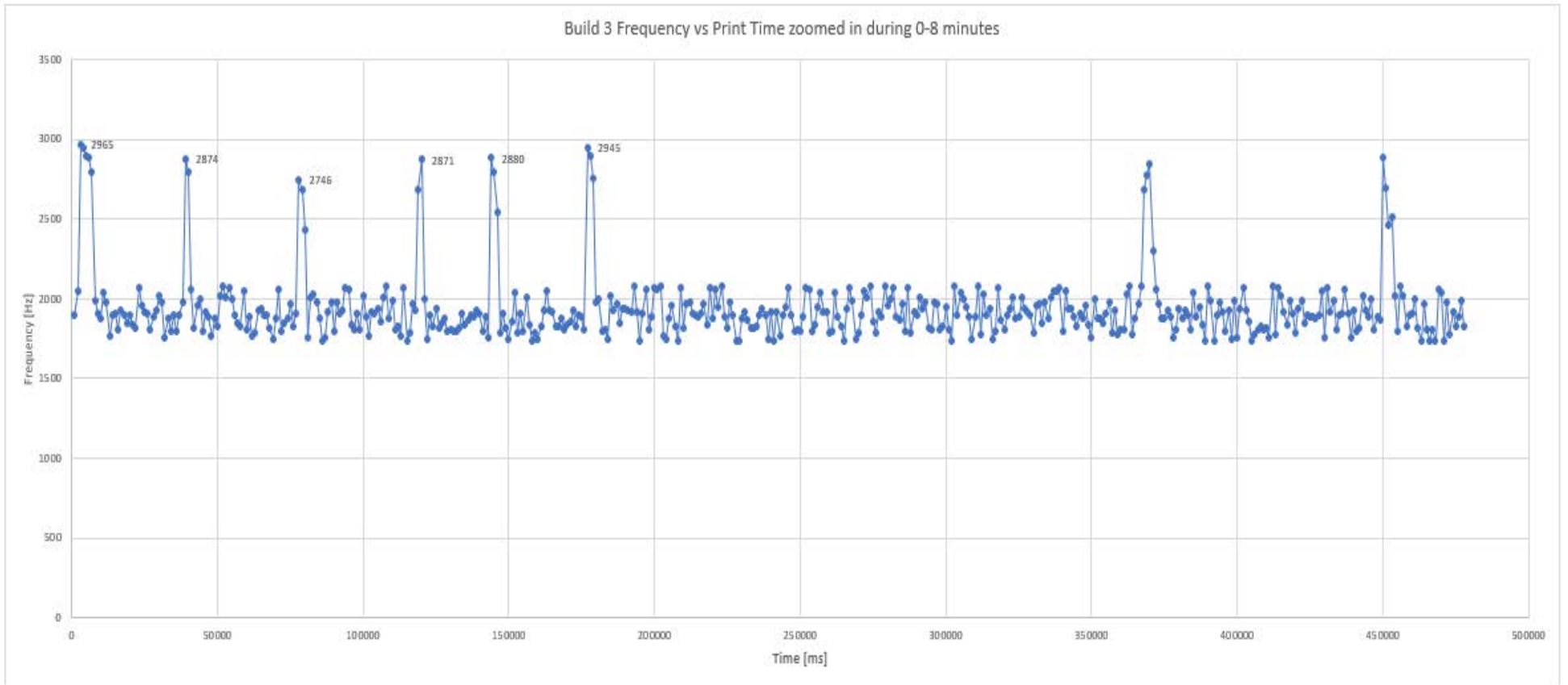
Appendix B. Full Size Images of Frequency Plots

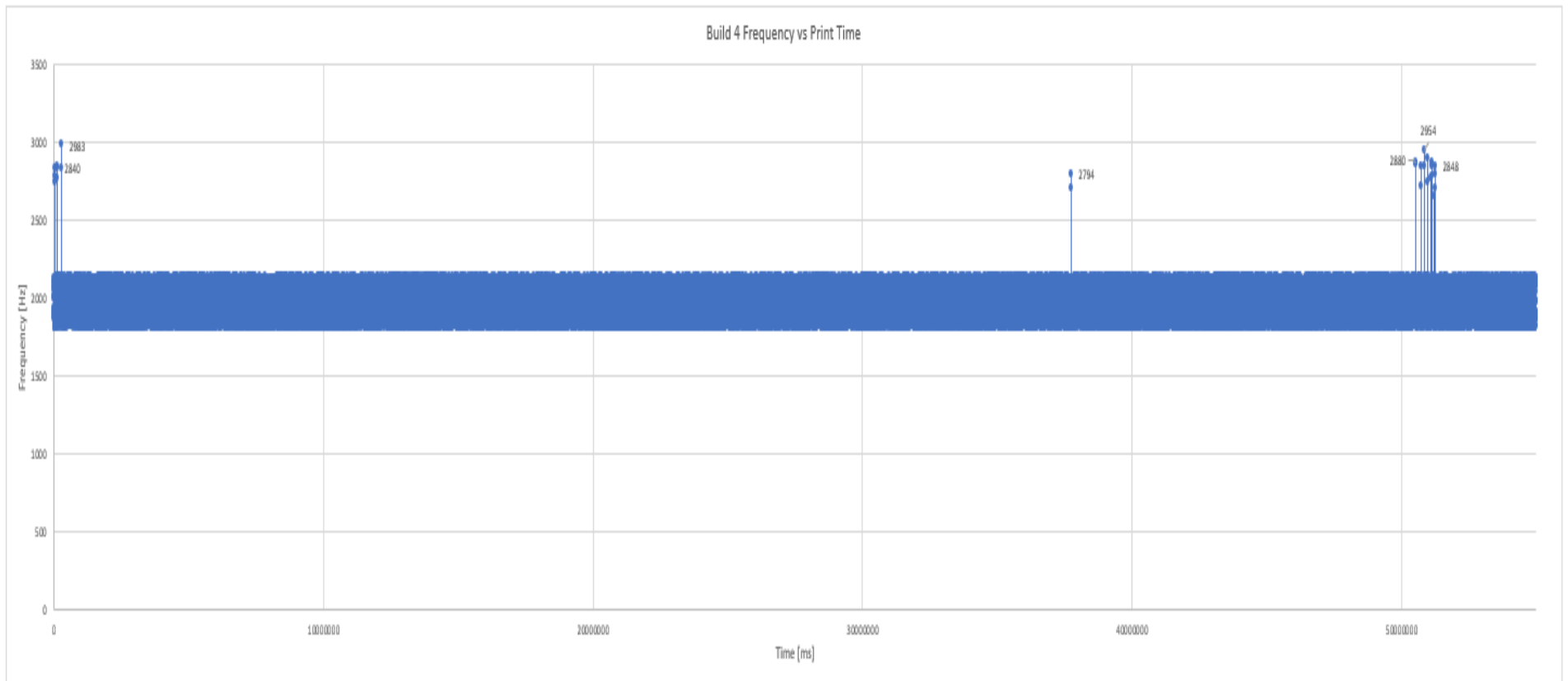




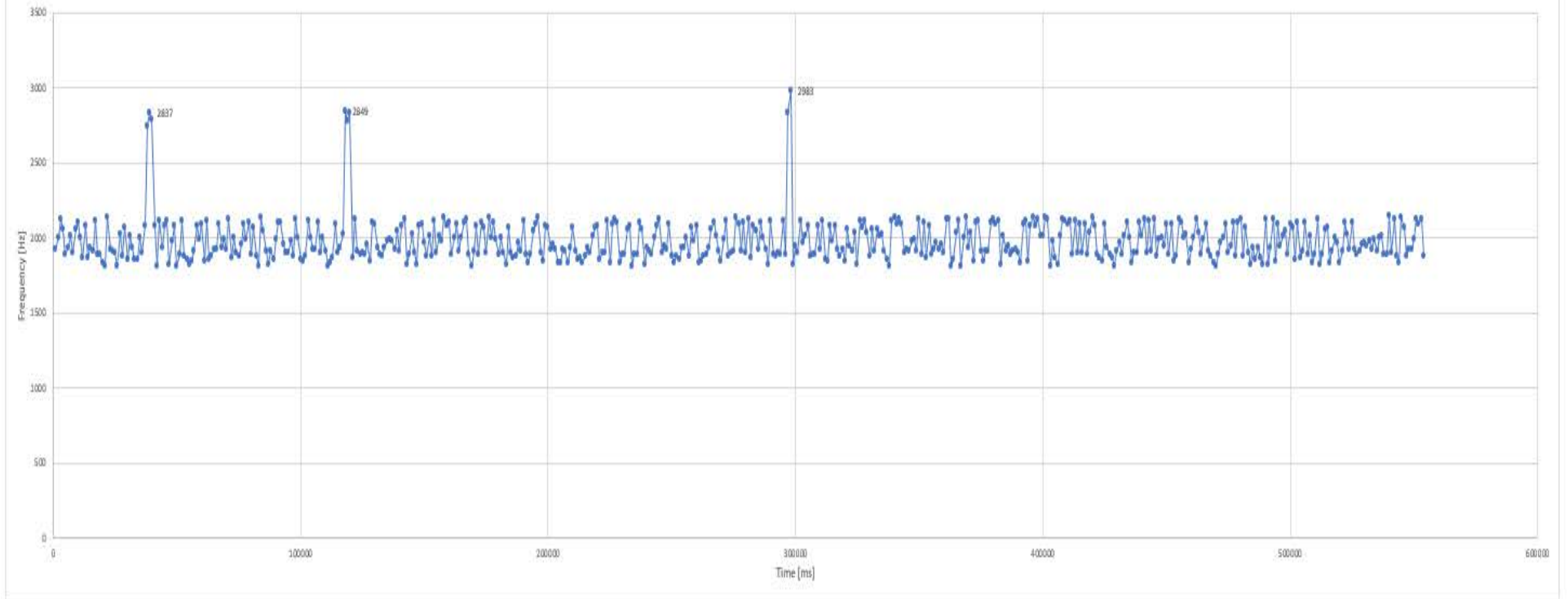
Build 3 Frequency vs Print Time

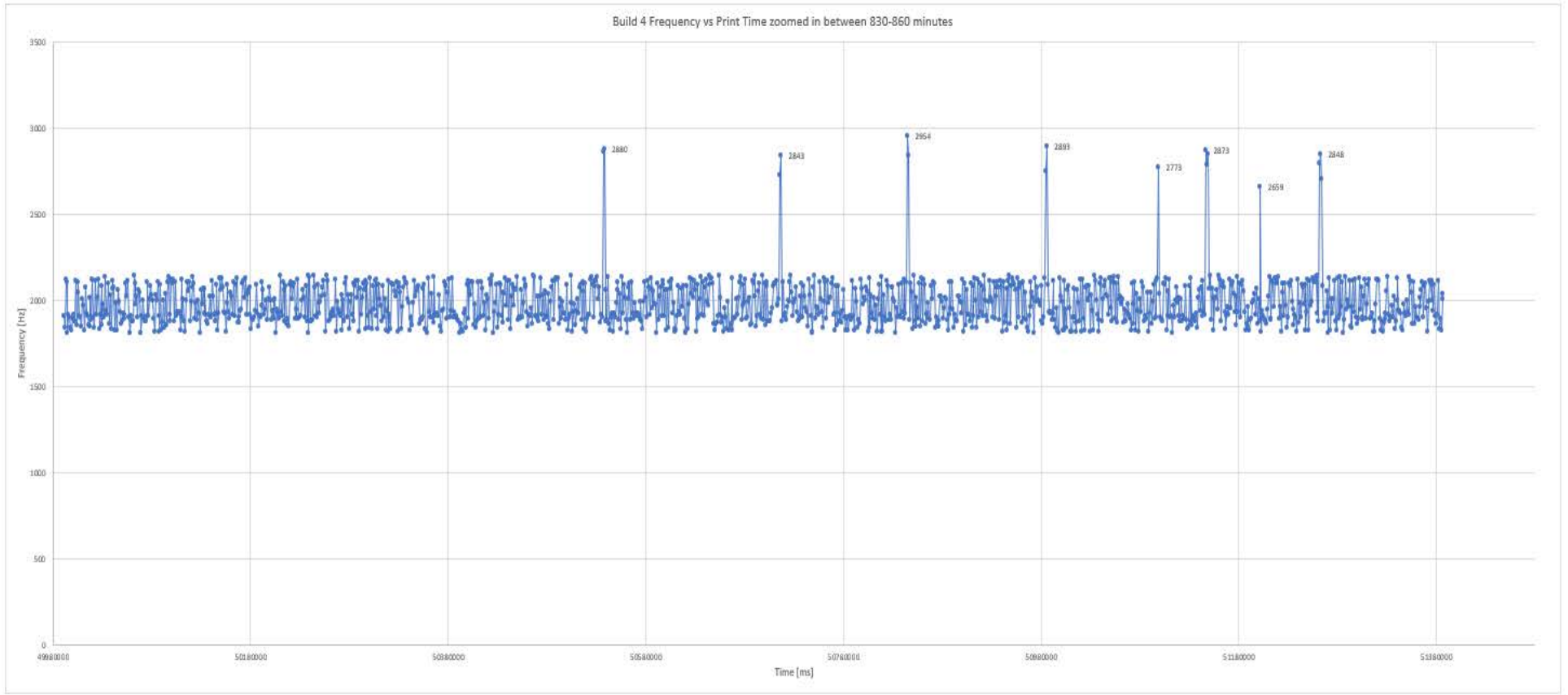




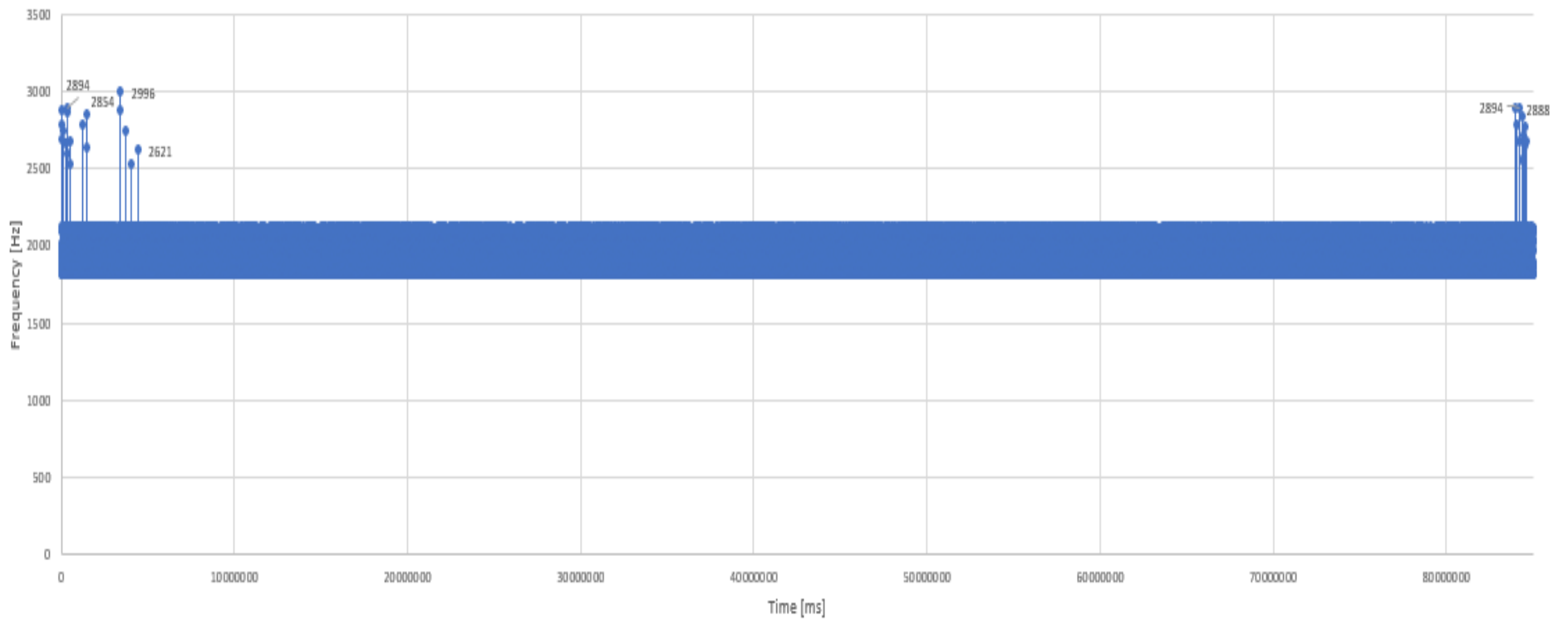


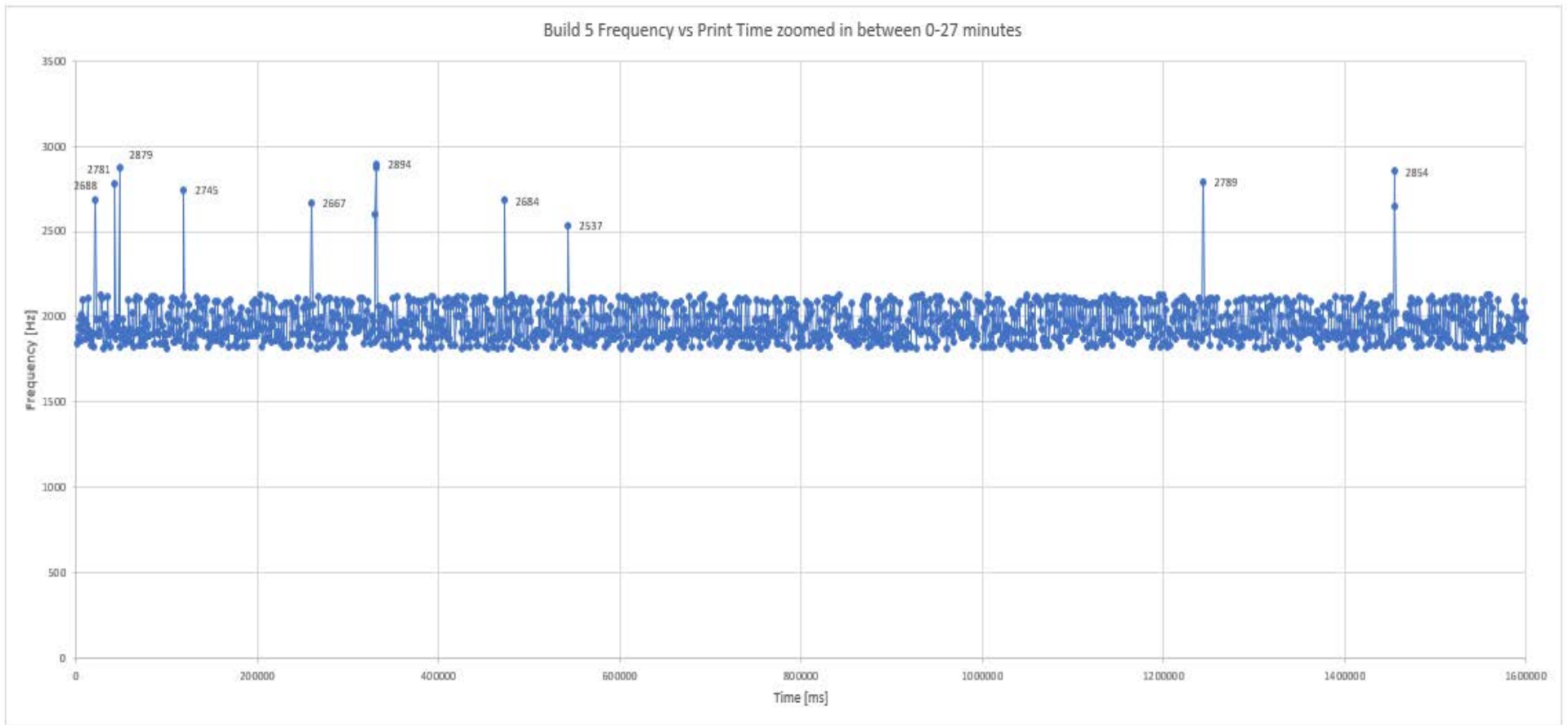
Build 4 Frequency vs Print Time zoomed in between 0-9 minutes



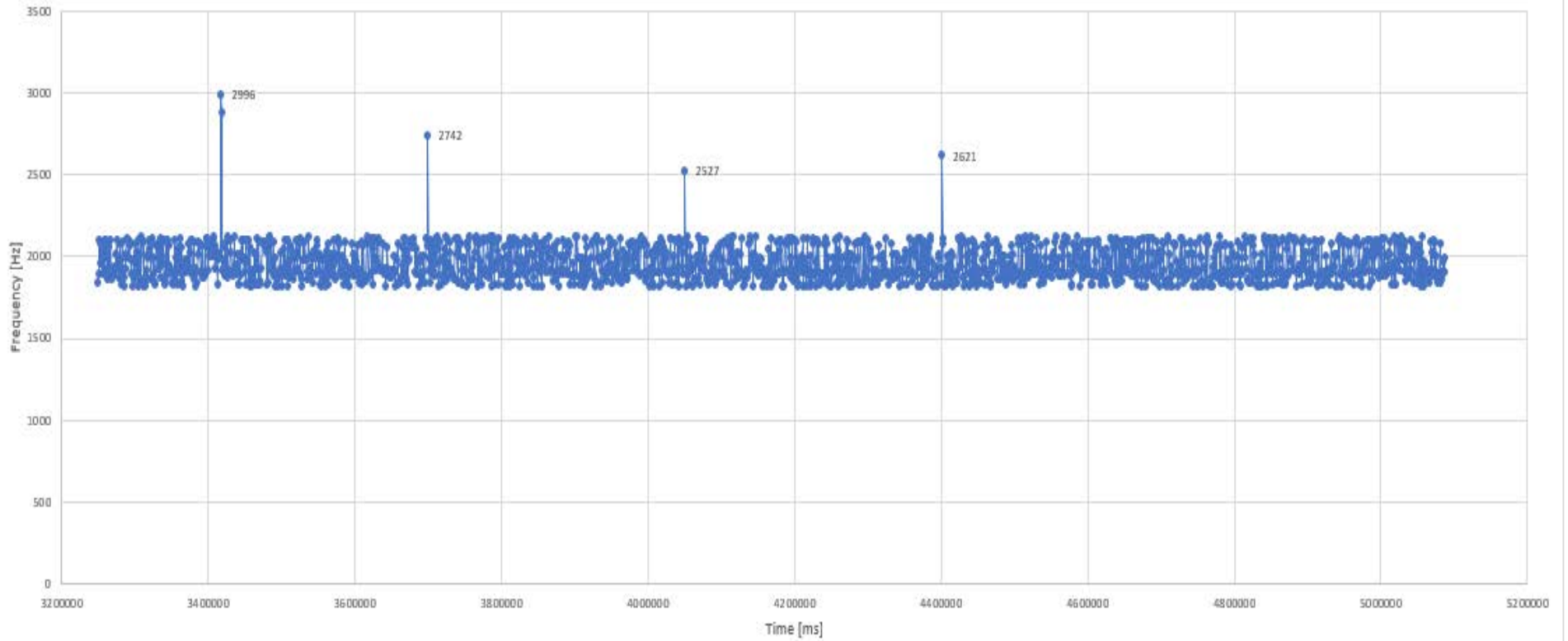


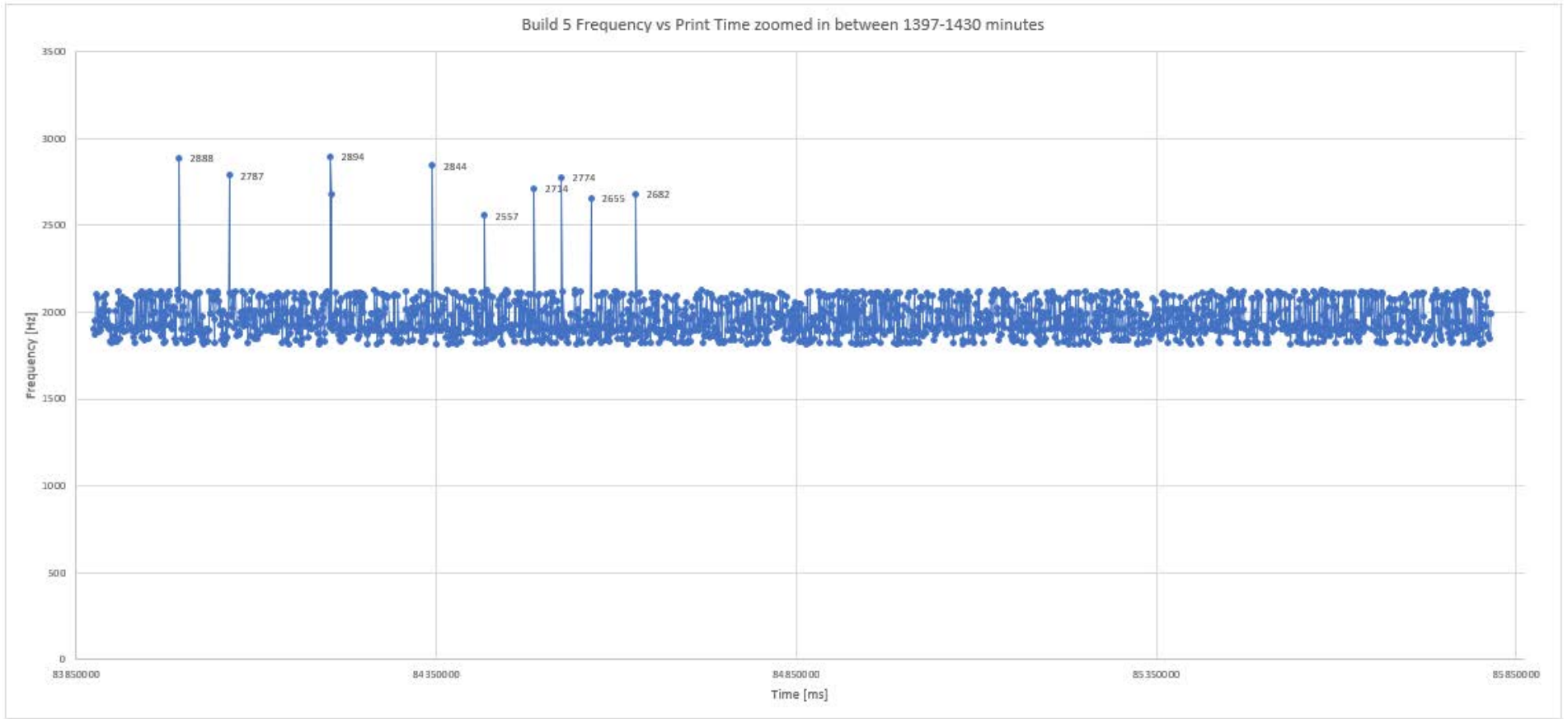
Build 5 Frequency vs Print Time



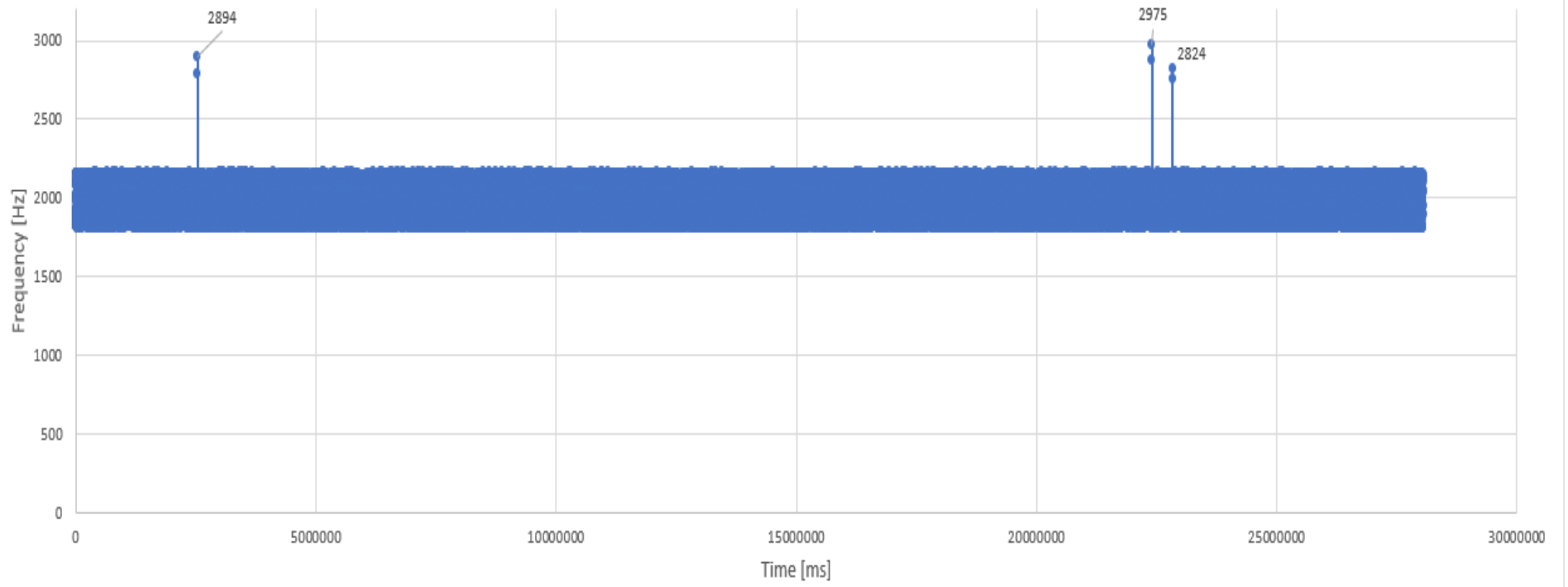


Build 5 Frequency vs Print Time zoomed in between 53-83 minutes





Build 6 Frequency vs Print Time



Build 6 Sensitivity vs Print Time using Kistler DAQ

